Department of Chemical Engineering

University of Cape Town

The Hydrated Lime Dissolution Kinetics in Acid Mine Drainage Neutralization

Dissertation submitted in fulfilment of the requirements for the degree of Master of Science in Chemical Engineering

Prepared by: Senzo Mntukhona Mgabhi

Prepared for: Department of Chemical Engineering

Main Supervisors: Jochen Petersen,

Co - Supervisors: Alison Lewis and Tokoloho Rampai

February 2020

Plagiarism Declaration

I understand that plagiarism is a serious academic violation; I hereby declare that all the work in this document was produced by myself (Senzo Mntukhona Mgabhi) except the information (including figures and tables) from the sources that are properly referenced.

Signature Signed by candidate Date: _____**10/02/2020**_____

Abstract

Hydrated lime, $Ca(OH)_2$, has been rediscovered as an environmentally sustainable product, which could be of help in the remediation of acid mine drainage (AMD), especially in the AMD neutralization process. This is due to its ease of acquisition, affordable price and unique versatile properties such as reactivity and neutralization efficiency. AMD is an acidic wastewater containing high concentrations of sulphates and dissolved heavy metals mainly ferrous iron. The dissolution of $Ca(OH)_2$ in aqueous solution is complex, which make its kinetics in AMD neutralization difficult to understand. The aim of this study was therefore to understand the $Ca(OH)_2$ kinetics in simplified solutions such as de-ionized water and CH_3COOH.

The neutralization process is an acid-base reaction; therefore, pH was used as a critical parameter determining $Ca(OH)_2$ dissolution rate. The determination of the dissolution rate was attempted in two ways – measurement of dissolved calcium and determining change of particle size distribution. Two methods of determining calcium assays were investigated, EDTA-EBT titration method and OCPC spectrophotometric method. Both methods worked successfully for a $Ca(OH)_2$-H_2O system. The EDTA-EBT titration method worked better even at higher concentrations of calcium (up to 100 ppm) while the complexometric spectrophotometric method was consistent with Beer-Lambert Law for a narrow calcium concentration range of 1 to 2 ppm, when a small amount of magnesium was introduced. However, both methods failed in the presence of appreciable quantities of magnesium, sulphates and ferric ion. The investigation for particle characterization found that image analysis of SEM images was a better particle-size characterization option than laser diffraction measurement, which tended to cause blinding of the instrument window, but still yielded only qualitative results.

There were four reactor configurations used, that is batch reactor for determining the effect of the hydrodynamics (stirring rate and powder addition) and three types of slurry CSTRs. The jacketed chemostat was found to be optimal reactor configuration while the other two were used base cases. The $Ca(OH)_2$ dissolution rate in de-ionized water decreased from 4.0×10^{-5} to 1.6×10^{-5} $mol\cdot L^{-1}\cdot s^{-1}$ when the temperature was increased from 26 °C to 42 °C. Correspondingly, the pH decreased with $Ca(OH)_2$ dissolution rate from 11.89 to 11.6. The dissolution rate expression was first order and consistent with the Nernst-Brunner Equation,

with the dissolution rate constant of 2.34×10^{-3} s^{-1} and the activation energy of 18.1 kJ mol^{-1} respectively.

The overall $Ca(OH)_2$ dissolution rate in CH_3COOH solution decreased from 2.6×10^{-4} to 1.7×10^{-4} $mol\cdot L^{-1}\cdot s^{-1}$ when the temperature was increased from 25 °C to 44 °C. At constant ambient temperature (22°C), the $Ca(OH)_2$ dissolution rate increases with the decrease in pH from 12.1 to 4.38, then decreases with the decrease in pH from 4.38 to 3.5. Using pH to correlate dissolved calcium data and then to determine the rate of reaction, it was found that the dissolution rate is zeroth-order to hydrogen proton and first-order with respect to calcium concentration with the dissolution rate constant of 1.2×10^{-2} s^{-1} and the activation energy of 5.7kJ mol^{-1} respectively.

These results confirmed that the dissolution of $Ca(OH)_2$ in DI water and the acetic acid solution is complex. The lower values of the activation energies (5.7 – 18.1 kJ mol^{-1}), signifies that the kinetics of the $Ca(OH)_2$ dissolution are mass transfer controlled. Furthermore, these results were confirmed by the weak dependence of the dissolution rate to temperature. However, it was found that slurry CSTR is an efficient reactor system to study the effect of pH on the kinetics of hydrated lime at steady-state conditions.

Acknowledgements

I would like to thank God, furthermore I would like to deeply thank the following people of which this thesis would not be possible; my main supervisor Prof. Jochen Petersen for financial and constant support and taking a chance with me when it was not even favourable to do so.

I would like reserve a special gratitude to Julian Baring Scholarship Fund, Angela and Mary Hilton for graciously granting me an opportunity to pursue my dream.

I would like to extend my endless gratitude to my supervising team (Professor Jochen Petersen, Professor Alison Lewis and Miss Tokoloho Rampai) for their wise guidance, tireless support and generously sharing their expertise with me. Professor Alison Lewis hosted me as part of Crystallization and Precipitation Research Unit family. Miss Tokoloho Rampai support went beyond just academic guidance to financial assistance and moral support including assistance with rotating disk apparatus. Mechanical Workshop for their assistance with rig assembling and impellor modifications, reactor baffles, lime tanks, rotating disk welding. Mrs Hayley Battle-Mckrill for almost everything, friendship, financial assistance, moral support and other things I might be forgetting.

Mr Jemitias Chivavava for free sharing his love for science, mentorship and research guidance.

The Late Professor Dee Bradshaw (The Living Gold) for giving me a chance to find myself and integrate my social life to one force for the good and betterment of humankind through mineral beneficiation.

Neill H Ridgley and Irabien for their assistance and advice even though they did not know me or even abridged to do so.

The Hydrometallurgy team for their support during seminars, lending me lab equipment, their expertise, transport to and from pizza-nights and fun writing weekends away.

Mr Zaeem Najaar and CPU family for birthdays and fun activities.

The Minerals to Metal for constantly reminding me why it was important to have people in mind as I go about my life and my project, Thursday forum, for helping meet inspiring people including government officials.

Minions in the lab; these includes but not limited to Lisa October who helped me with EBT-EDTA titrations and OCPC, experiments; Debora for helping me in the lab. Fernanda Yamoto for helping me in the lab and with SEM and Image analysis.

My friends for praying with me and encouraging me to carry on when I felt like giving up Theophilus Dzingai, Flora Kurasha, Primrose Kurasha, Henry and Joyce Munyanduki, Champion Mtileni, Simanga Prince Ngcobo, Victor Takunda Chivhidze, Anthony Rapulani, Vukosi Khoza, Godfrey, Rendani, Ishmael Chicco, Sanele Mazibuko, Brother Papy Ndalamba, Nicole Uys, Omer Ngoy, sis Nomps, Sis Yokai, Sis Connie and mukoma Tatenda, Phindile Xaba; Lihle Ellen Maseko, my spiritual parents Bishop Tshalo and Pastor Beatrice Katshunga, members of Gospel Ramah Church especially intercession team.

My family for serving as a constant encouragement and a reminder especially Sanele, Mdala, Nokuthula, Thabani, Mlotshwa and my dad uMnumu Mziwenkonzo Mgabhi.

My uncles; Mduduzi Betheul Mthiyane, Phila and Khanyi Mthiyane.

The UCT Interlibrary Loan Team, Knowledge Commons and Research Commons Staff.

Table of Contents

List of Figures

List of Tables

Glossary

Term	Definition
Quicklime	Calcium oxide
Hydrated lime	Calcium hydroxide
Calcite	Calcium carbonate
Ferric	Trivalent iron cation
Ferrous	Divalent iron cation
Acid strength	Acid concentration
Colloids	Very tiny particles, sub-microns particles (or ultra-fines)
hydroxyl	Hydroxide molecule or branch
Solid density	Solid concentration
Milk of lime	$Ca(OH)_2$ suspension with solid concentration ranging from 1 to 20% quicklime
Eriochrome black T ($C_{20}H_{12}N_3NaO_7S$)	sodium;(4Z)-4-[(1-hydroxynaphthalen-2-yl)hydrazinylidene]-7-nitro-3-oxonaphthalene-1-sulfonate (Pub Chem, 2018)
o-Cresolphthalein complexone ($C_{32}H_{32}N_2O_{12}$)	2-[[5-[1-[3-[[bis(carboxymethyl)amino]methyl]-4-hydroxy-5-methylphenyl]-3-oxo-2-benzofuran-1-yl]-2-hydroxy-3-methylphenyl]methyl-(carboxymethyl)amino]acetic acid
Eriochrome black T ($C_{20}H_{12}N_3NaO_7S$)	l-(l-hydroxy-2-naphthylazo)-2-hydroxy-5-nitro-4-naphthalenesulphonic acid
o-Cresolphthalein complexone ($C_{32}H_{32}N_2O_{12}$)	2 : 6-xylenolphthalein-α : α'- bis(amino)diacetic acid
Hydroxyapatite $\{Ca_{10}(PO_4)_6(OH)_2\}$	Calcium phosphate

Nomenclature

Symbol	Definition
t	Time
T	Temperature
τ	Residence time
X_{A0}	Conversion of compound or chemical A at time t = 0,
X_A	Conversion of compound or chemical A at time t,
r_A	Reaction rate in terms of species
V	The volume of the reactor content at time t,
V_0	The volume of the reactor content at time t = 0,
k	Reaction rate constant
k_d	Mass transfer constant
ρ_C	Density of substance C
C_{A0}	Concentration of compound or chemical A at time t = 0,
C_A	Concentration of compound or chemical A at time t,
x	Mole fraction
E	Activation energy
ΔT_t	Temperature is rise (or change) at time t
ΔT_f	Final temperature change
r_0	Initial mean size
F_{A0}	Inlet flowrate of A
ω	the stirring rate in the reactor
v	kinematic viscosity of water
S	dissolution rate
m_C	Mass of substance C
N_s	Dissolution rate of calcium
$D_{Ca(OH)_2}$	Diffusion coefficient of calcium hydroxide
$CaCO_3$	Calcium carbonate
$Ca(OH)_2$	Calcium hydroxide or $Ca(OH)_2$
CaO	Calcium oxide or quicklime
CO_2	Carbon dioxide

OH^-	Hydroxide ion
$CaOH^+$	Calcium hydroxide cation
Ca^{2+}	Calcium cation
H^+	Hydrogen cation or proton
$[Ca]_{sat}$	Concentration of calcium at saturation
AMD	Acid mine drainage
SEM	Scanning electron microscopy
RDM	Rotating disk method
TGA	Thermogravimetric analysis
XRD	X-ray diffraction
PSD	Particle size distribution
RD	Rotating disk
φ	$Ca(OH)_2$ solid density or solid particle concentration

Chapter 1: Introduction

The aim of this section is to detail the relevance of this study in the context of South African and global acid mine drainage treatment and its necessity in recovering value metals and its potential role in handling water scarcity issues. It further covers the aim, scope and the thesis outline.

1.1 Background

Climate Change and growing population put stress on the water demand in South Africa and most parts of the world. This compels researchers, policy makers and all stakeholders to look for innovative ways of meeting water demands. According to United Nations (2017a) projections, the world is likely to face a 40% shortfall in water availability by 2030, should it continue its current attitude toward water; this would affect at least 1.8 billion people. In September 2015, United Nations Countries including South Africa, agreed on 17 global sustainable development goals (SDGs) which are aimed at ending extreme poverty, inequality and climate change. Among these goals; goal 6 deals with water and sanitation. The United Nations (2017b) reported that in 2015, 6.6 billion people, which is about 91 per cent of the global population, used an improved drinking water source, against 82% reported in 2000. Despite the 9 percent increase, an estimated 663 million people were still using unimproved water sources or surface water, and it is reported that most of these people are from Africa (United Nations, 2017b). In order to meet these demands, alternative sources of water need to be considered. This includes recycling waste streams and even looking at abandoned mines as water sources.

Acid mine drainage (AMD) is the major environmental concern in South Africa and other countries such as Australia, Canada, United State of America and Germany (Mjimba, et al., 2017). AMD contains high concentrations of dissolved heavy metals and anions such as sulphates. Due to these concentrations, AMD has pH values as low as 2.5 (Maree & van Tonder, 2000). According to Maree and van Tonder (2000), effluent wastewater with pH values lower than 5.5 can be toxic to plants and aquatic life. It is therefore important to treat acidic effluents before they are discharged to environment. The treatment of AMD involves a neutralization process where the AMD is reacted with basic material or solution such as lime

solutions to adjust pH to within acceptable environmental standards. The acid neutralisation process is an essential process in industrial waste water treatment and industrial acidic effluent treatment. Amongst many various chemical and biological technologies that are currently applied in acid mine drainage (AMD) and waste water treatment, lime neutralisation remains the most widely used and cost-effective treatment method (Aube, 2005).

A range of alkaline solutions are used to neutralise acidic streams. These include sodium hydroxide (NaOH), calcium oxide (lime, quicklime or CaO), slaked lime ($Ca(OH)_2$), limestone ($CaCO_3$), soda ash (Na_2CO_3) and other bases. NaOH is the most expensive while limestone is the least expensive (Lewis & Boynton, 1999; Maree & van Tonder, 2000). However, limestone is not preferred due to low dissolution rate and associated armouring or scaling problems (Maree & van Tonder, 2000; Hammarstrom et al., 2003). According to Lewis and Boynton (1999), lime was widely used as a neutralising agent even before environmental institutions increased pressure on chemical industries to treat acidic effluent streams. This therefore justifies its adoption in treating of AMD and other acidic effluents. It is desired in the chemical and metallurgical industry to neutralize AMD using economically viable neutralization processes. The viability of a process is determined by factors such as cost, availability and the capacity of a base to bring acidic solution (or vice versa) to a required pH. Lime neutralization is currently applied on plant effluents, as well as in waste and wastewater treatment (Aube, 2003; Aldaco, et al., 2007 and Tai, 1999).

A simplified lime neutralisation process involves two preparatory steps: hydration or slaking of lime to form $Ca(OH)_2$ and its subsequent dissolution. It has been established that during $Ca(OH)_2$ neutralisation, calcium cations react with sulphates in AMD forming insoluble calcium sulphate compounds. Furthermore, dissolved ferric and ferrous cations react with hydroxides forming a range of hard-to-characterise, water-retaining, amorphous ferric oxides; ferric oxy-hydroxides and ferric sulphate hydroxides sludges, which are notoriously difficult to de-water (Aube, 2005; Stefanakis, et al., 2014). To improve dewatering capacity while recovering value metals, it is desired to fully characterise this sludge. This is where this study comes in; the approach is, if the sludge formation process is understood not just in terms of its final stable state but in terms of the individual steps, and the rate at which these steps occur, it would become easier to solving this problem.

There are many reactions involved in AMD-lime neutralization because of the metals and anions in AMD. In unpacking the overall process, many reactions are considered. This study

focuses on developing a thorough understanding of the dissolution of $Ca(OH)_2$ to release hydroxide ions which then react with metals and calcium ions which react with balance anions especially sulphates. In contrast with the general understanding of 'lime' as an umbrella term for quicklime, $Ca(OH)_2$ or even limestone, the commonly adopted approach is to exclude limestone, and therefore limit the definition of lime to only quicklime and $Ca(OH)_2$. The slaking of quicklime process is also considered separately from dissolution of $Ca(OH)_2$ because a lot of work has been done on the mechanisms, parameters and factors affecting slaking or hydration of lime. However, limited studies have been conducted on the mechanism and kinetics of dissolution of $Ca(OH)_2$ in water as a separate process, let alone in the context of AMD neutralisation. This study therefore seeks to understand dissolution of $Ca(OH)_2$ as an essential preliminary step of the sludge formation during AMD neutralization.

1.2 Project aim and scope

The main aim of this study was to determine the rate at which calcium hydroxide, $Ca(OH)_2$, dissolution occurs in a simplified synthetic AMD solution. The synthetic AMD was simplified by focusing only on the influence of major components (of typical South African AMD streams) on the rate of $Ca(OH)_2$ dissolution. These components were ferric ion (Fe^{3+}), sulphates (SO_4^{2-}) and magnesium (Mg^{2+}), selected to adequately appreciate the effect of each species on the rate of dissolution of $Ca(OH)_2$ particles (without the influence of other species). Due to the predictable complexities (such as precipitation of gypsum and metal hydroxides) that the selected species introduce to the dissolution solution, deionized water, acetic acid and perchloric acid were used instead of the synthetic AMD.

This was achieved in two reactor systems, a batch system and continuous stirred tank reactor (CSTR) system under controlled conditions to simulate industrial conditions. A jacketed CSTR (or chemostat) method was adopted to control pH, temperature and reactor content. This thesis, therefore, focussed on the development of the methodologies to measure hydrated lime dissolution primarily tested these with respect to the effect of pH and temperature.

1.3 Thesis outline

This thesis comprises seven chapters. Chapter 2 covers the basic theory of acid-base neutralization, solid-liquid reaction, dissolution kinetics models, continuous stirred tank reactor, lime circle or lime production, lime hydration or slaking, AMD generation and AMD treatment. The focus of this chapter is to cover all the fundamentals that are directly or likely to affect the dissolution of $Ca(OH)_2$ in AMD neutralization. Chapter 3 discusses the relevant literature on the factors or parameters that affect the dissolution of lime in AMD. The methodology and equipment used for experimental work are outlined in Chapter 4; experimental design, set-up and procedure are also included. The experimental results and discussion are provided in Chapter 5. Key findings and conclusions are in Chapter 6, eventually recommendations for future work are proposed in Chapter 7.

Chapter 2: Literature review

The aim of this literature review is to provide an informed review of the literature in the context of lime neutralisation of acid mine drainage, based on the accessed body of literature.

2.1 Acid rock or mine drainage treatment

Acid mine (or rock) drainage (AMD or ARD) is a very acidic wastewater containing high concentrations of sulphates and dissolved heavy metals, mostly ferrous iron (Mujuru, et al., 2017). The terms ARD and AMD are often used interchangeably; however, ARD is a less commonly used term referring to the naturally occurring process during weathering of sulphide surface rocks while AMD specifically refers to the complicated process due to existing and abandoned mining activities (Geller, et al., 1998; Mujuru, et al., 2017; Naidoo, 2017; Mjimba, et al., 2017). According to Global Acid Rock Drainage Guide (GARD Guide), AMD or ARD result when rock surfaces containing sulfide minerals are exposed to water and air; chemical reactions can occur, resulting in soluble oxidation by-products which, when they dissolved in water, can acidify water. The acidification process is catalyzed by a bacteria, primarily members of the *Acidithiobacilli* (The International Network for Acid Prevention, 2014). A lot of research work has been done on generation and mitigation of AMD for the past 50 years and more (Mujuru, et al., 2017).

2.1.1 AMD generation

AMD formation is complex; it differs depending on various parameters, such as geology of the mining area (existing ores), the quality of water in that area, weather conditions (prevailing temperatures) and micro-organisms (Mujuru, et al., 2017). A common chemical generation of AMD through pyrite oxidation is shown in Figure 2.1.

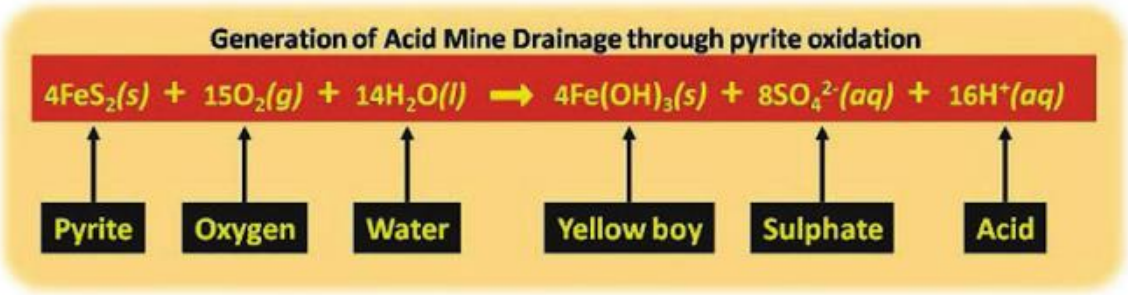

Figure 2.1 Chemical generation of AMD through pyrite oxidation (Mjimba, et al., 2017)

As shown in Figure 2.1 and Table 2-1, AMD generation is predominantly through pyrite and marcasite; other possible sulphide minerals, as discussed in Mujuru et al. (2017), are given in Table 2-1; the AMD generation is not limited to metal sulfides presented in Table 2-1, the composition is largely dependant on the region and ore that is being processed (Johnson & Hallberg, 2005). Some sulphide minerals incorporate more than two metals, such as pyrrhotite {$(Fe,Ni,Co)_{1-x}S$ } which has cobalt and nickel (Minerals.net, 2014).

Table 2-1: Common minerals that are involved in AMD generation

Ore (Metal sulphide)	Chemical formula
Pyrite	FeS_2
Marcasite	FeS_2
Pyrrhotite	$Fe_{1-x}S$ (x ranges from 0.0 to 0.2)
Chalcocite	Cu_2S
Covelite	CuS
Chalcopyrite	$CuFeS_2$
Molybdenite	MoS_2
Millerite	NiS
Galena	PbS
Sphalerite	ZnS
Arsenopyrite	FeAsS

2.1.2 AMD neutralisation

During neutralisation process, AMD is reacted with basic material or basic solution to adjust pH to be within acceptable environmental standards. There is a range of bases used to to neutralise acidic effluent streams; the most common ones include sodium hydroxide (NaOH), quicklime or $Ca(OH)_2$, limestone and soda ash. Sodium hydroxide is the most efficient but also most expensive, limestone is the least expensive, however not prefered due to its slow dissolution rate and associated amouring or scaling problems. Soda ash is cheaper than sodium hydroxide, but relatively more expensive than lime and limestone.

Lime has been the most widely used neutralizing agent long before environmental institutions increased the pressure on chemical industries to treat acidic effluent streams (Lewis & Boynton, 1999). Lime is adopted because it reacts readily with all types of acids, from the strongest to weakest of both organic and inorganic type (Boynton, 1980).

2.1.3 Metals recovery through precipitation

One of the main reasons lime netralization is adopted is because hydroxide ions are used to precipitate out undesired metals (such as iron and other heavy metals) through hydrolysis and precipitation. The hydrolysis process is a strong fuction of pH, it is a well researched phenomenon on how metals, especially heavy metals such as iron, precipitate along the pH scale. This phenomenon has been investigated for stage-wise removal of metals with a view of selective recovery (Johnson & Hallberg, 2005).

In the context acid mine drainage neutralisation (with $Ca(OH)_2$), dissolved metals, including ferric and ferrous cations, react with hydroxides, forming a range of hard-to-characterise, water-retaining, amorphous metal hydroxides which are dominated by ferric oxides; ferric oxy-hydroxides and ferric sulphate hydroxides sludge. Furthermore, other metals or cations including calcium (from lime dissolution) react with sulphates (in AMD) forming insoluble calcium sulphates and other metal sulphate compounds (Zinck, 2006).

2.1.4 Neutralisation treatment methods (AMD treatment methods)

There are two remedial options of AMD treatment, which are abiotic and biological treatment. There are many ongoing research improvements in biological treatment, some developments are cited in cited in Tereke & Kamika (2016). As shown As shown in Figure 2.2, lime neutralisation falls under abiotic treatments, and it is used in active chemical treatment systems (Johnson & Hallberg, 2005).

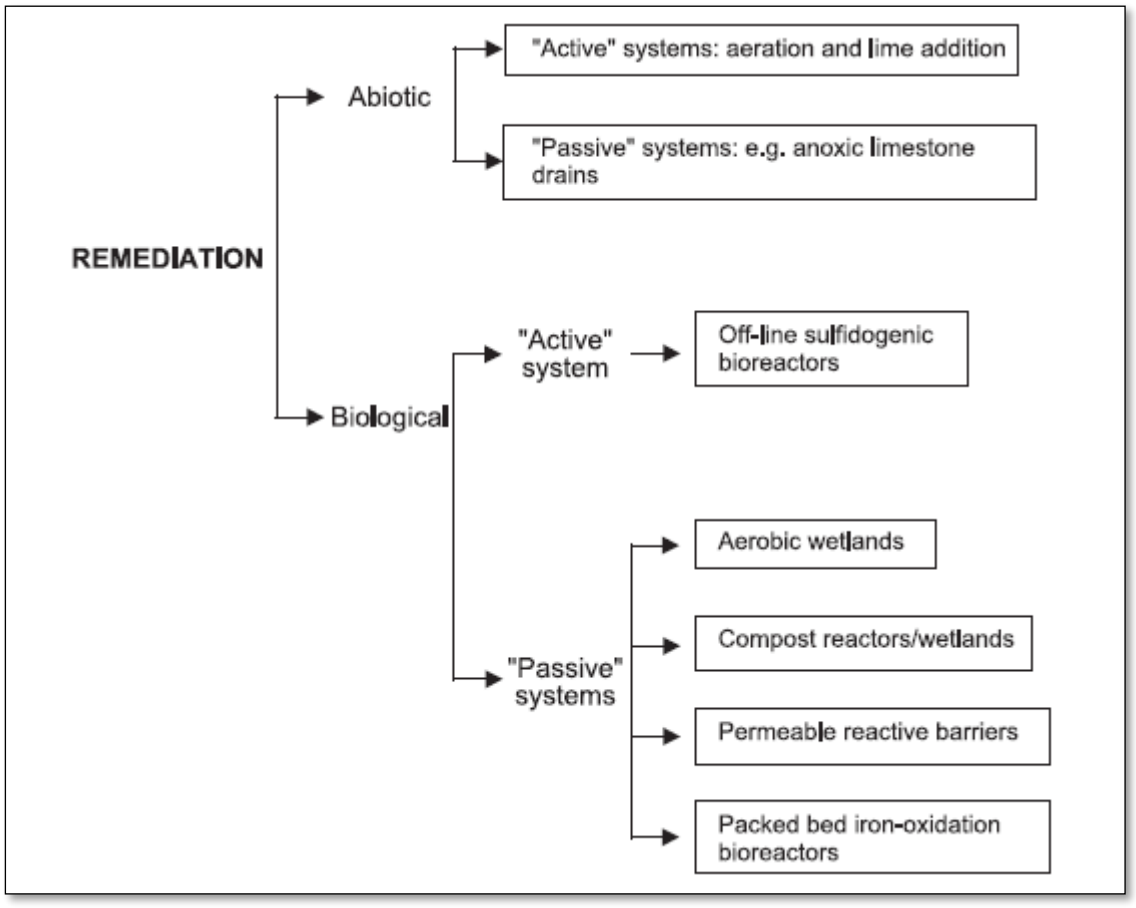

Figure 2.2: Biological and abiotic strategies as detailed by Johnson and Hallberg (2005).

2.2 Lime: Chemistry and Production

The production of lime usually refers to the manufacturing of quicklime (CaO) and $Ca(OH)_2$ {$Ca(OH)_2$ } especially for commercial use. The production of $Ca(OH)_2$ cannot be looked at separately from quicklime. Likewise, the production of CaO cannot be separated from the

production of limestone ($CaCO_3$). All three chemicals are interconnected, and this is referred to as the lime cycle.

2.2.1 Limestone

Limestone is a sedimentary rock comprised mainly of calcium carbonate and varying impurities depending on the original mechanism of its formation. The formation or sedimentation of $CaCO_3$ follows two principal pathways; organic and inorganic. The organic route is the sedimentary deposition of calcium carbonate by a biochemical reaction of dissolved calcium cations and CO_2 facilitated by micro-organisms. The inorganic route is the direct precipitation (or crystallisation) of carbonate. According to Oates (1998), most of the commercially viable deposits of limestone were formed by the organic route. The details on the mechanism (or rate) of formation, physical and chemical properties, types of limestones and micro-organisms invloved in its frormation are discussed thoroughly in Boynton (1980) and Oates (1998).

2.2.2 Quicklime (CaO)

Quicklime (or calcium oxide or CaO) is produced by calcination (thermal decomposition) of limestone ($CaCO_3$). This is achieved in a reactor or furnace called kiln. The thermal decomposition of limestone (calcite) proceeds as shown in Equation 2.1.

$$CaCO_3\ (s) + Q_d \rightarrow CaO\ (s) + CO_2\ (g) \qquad \ldots: 2.1$$

At the reference temperature of 25°C and 1 atm pressure, the value of the heat of decomposition or dissociation; Q_d is in following range; $2.91\frac{MJ}{kg} of\ CaO \leq Q_d \leq 3.49\frac{MJ}{kg} of\ CaO$. This has been reported by many authors. This means that 100g of $CaCO_3$ will produce 56g of CaO and 44g of CO_2. Boynton (1980) used the average value of 3.22 MJ/kg while Oates (1998) selected the value of 3.18 MJ/kg CaO. It has been established that the

impurities in the parent $CaCO_3$ will carry over to the produced CaO and subsequent products of CaO such as $Ca(OH)_2$ and other possible products. The impurities in $CaCO_3$ affect the reactivity of CaO and hence $Ca(OH)_2$.

2.2.3 Hydrated Lime ($Ca(OH)_2$)

$Ca(OH)_2$ is produced through the slaking of quicklime (reaction of $Ca(OH)_2$ with water). Equation 2.2 shows the progression of this reversible reaction; the forward exothermic reaction is favoured at temperatures below 350°C, the heat released is approximately 1.14 MJ/kg high-calcium CaO reacted (Boynton, 1980). Oates (1998) reported the value of 1.15 MJ/kg high-calcium CaO reacted.

$$CaO\ (s) + H_2O\ (l) \leftrightarrow Ca(OH)_2\ (s) + Heat \quad \text{...: 2.2}$$

At temperatures higher than 350 °C the reverse reaction (Equation 2.2) occurs (Oates, 1998). At elevated temperatures, depending on the amount of water available, the heat liberated is absorbed by available water, causing it to evaporate. Above 350 °C, the corresponding liberated heat is used to evaporate solvent water, including free and chemically combined moisture in the pores of particles and hence decomposes $Ca(OH)_2$ to quicklime while water is lost to the atmosphere.

$$Ca(OH)_2\ (s) + Heat \leftrightarrow CaO\ (s) + H_2O\ (g) \quad \text{...: 2.3}$$

2.2.4 Lime cycle

From Section 2.2.2 limestone (which is mostly calcium carbonate) thermally decomposes to quicklime (calcium oxide) and carbon dioxide (CO_2). Quicklime reacts readily with water, forming $Ca(OH)_2$ according to Equation 2.2. $Ca(OH)_2$ reacts readily with CO_2, re-forming calcium carbonate. At standard condition (STP), quicklime (due to its hygroscopicity) can completely or partially react with atmospheric moisture, forming $Ca(OH)_2$, which then reacts

with CO_2 forming calcium carbonate which is the most stable form of the three lime compounds. This phenomenon is known as the lime cycle.

2.3 Theory of lime hydration

Hydration of lime refers to the reaction of quicklime with water forming $Ca(OH)_2$ or slaked lime. The terms 'hydration' and 'slaking' are technically used interchangeably. However, to be strict with definitions, or for the sake of differentiation, hydration is reacting quicklime (lumps or powder) with controlled excess amount of water, hence forming dry-powdered $Ca(OH)_2$ product. Slaking on the other hand refers to the reaction of quicklime with water forming wet or suspended $Ca(OH)_2$ product such as $Ca(OH)_2$ suspension (lime slurry and milk of lime) and lime putty. In other words, slaking is wet hydration or hydration is dry slaking.

2.3.1 Lime hydrates

$Ca(OH)_2$ has become synonymous with powdered $Ca(OH)_2$ product. However, as discussed above, there are different forms of $Ca(OH)_2$ s; these includes dry-powdered $Ca(OH)_2$, lime putty, milk of lime, lime slurry and saturated $Ca(OH)_2$ solution (lime water). The difference between the forms of hydrates is characterised by ratio of quicklime to free water.

Powdered $Ca(OH)_2$

This is one of the most common forms of $Ca(OH)_2$. It is widely used in pharmaceuticals as a precursor of other medical chemicals and laboratories as reagent grade product. Generally, powdered hydrates are dry, with less than 1% of unreacted water or moisture (Oates, 1998). According to Boynton (1980), commercial powdered hydrates contain 72–74 % quicklime lime solids, 23-27% chemically combined moisture and the balance percentage is shared between free water and impurities.

Lime slurry

This is one of the most stable forms of hydrates. It is a colloidal suspension with 25-35% quicklime solid content and 60-73% free water (Boynton, 1980). According to Boynton (1980), lime slurry can be easily prepared by adding excess of water when quicklime is slaked, one-part quicklime to about two-part water by mass basis. The advantage of using slurry is that it can be pumped using a viscous liquid pump.

Milk of lime

Milk of lime is an aqueous colloidal suspension with qualities resembling that of whole milk. It is significantly thinner than slurry, and it is easier to pump with a viscosity as low as that of water. The other noticeable difference between lime slurry and milk-of-lime is the ratio of quicklime to water; which is 1:3 to 1:4.5 (Boynton, 1980). Furthermore, as cited in Boynton (1980), milk of lime solid concentration ranges from 1 to 20% quicklime. Apart from being the most stable form of $Ca(OH)_2$, it is also highly reactive due to relatively higher specific surface area because of the size of the particles (Oates, 1998). There are various ways of preparing milk of lime; for example: Similarly, to lime slurry preparation, it can be easily prepared by adding excess of water when quicklime is slaked. The slaking temperatures for this method is 65.5-82 °C (Boynton, 1980). The easiest and most common method of preparation is by diluting lime slurry to desired solid concentration.

Lime water

Lime water is the solid-free saturated or under-saturated aqueous solution of $Ca(OH)_2$. It is prepared by filtering the lime slurry or milk of lime to about 1.4 grams of quicklime equivalent of $Ca(OH)_2$ in a litre of saturated solution (Boynton, 1980). The solubility of $Ca(OH)_2$ in water decreases with rising temperature, an increase in temperature will cause calcium hydrate particles to re-precipitates out of the hydroxide solution as solid sediments or colloids. Contrary, a decrease in temperature will dissolves relatively more particles in a supersaturated solution, thereby increasing the $Ca(OH)_2$ concentration.

2.3.2 Lime addition

Lime is usually added in industrial processes as the milk of lime or lime slurry. This is due to the milk of lime stability and reactivity. Furthermore, it is very compatible with continuous processes because of its low viscosity which eases pumping.

2.4 Lime dissolution kinetics

$Ca(OH)_2$ dissolution in aqueous solution kinetics is relevant in a wide range of applications. This includes in the formation of hydroxyapatite $\{Ca_{10}(PO_4)_6(OH)_2\}$, water and wastewater softening, off-gas or stack gas cleaning and metal recovery in acidic mine effluent (Bernard, et al., 2000).

Most literature such as Dutta and Shirai (1980), Irabien *et al.* (1989), Ritchie and Xu (1990) and Bernard *et al*. (2000) studied $Ca(OH)_2$ kinetics and its mechanisms as part of the slaking reaction, but there are very few papers that look at the dissolution of $Ca(OH)_2$ as a separate reaction (Giles, et al., 1993; Johannsen & Rademacher, 1999; Robinson & Burnham, 2001). These papers argue that, in a mass transfer-controlled system, the slaking reaction is the fastest, provided quicklime readily reacts with water. This means that the dissolution of the formed $Ca(OH)_2$ in the aqueous solution will be the slowest step, considering that $Ca(OH)_2$ is sparingly soluble in water. However, this argument would only hold if the particles were of the same size with uniform shape and without impurities, which is highly unlikely. It has been established that impurities in the parent limestone affect the slaking reaction and hence dissolution of the formed $Ca(OH)_2$. Furthermore, most of the papers report that calcination conditions of precursor limestone such as the temperature and the type of a kiln, affect the reactivity of the formed quicklime and hence subsequent $Ca(OH)_2$. Calcination of limestone is an adequately researched topic and hence optimum or desired conditions are achievable.

2.5 Mechanism of $Ca(OH)_2$ dissolution

The mechanism of $Ca(OH)_2$ dissolution during slaking can be effectively broken down as follows (Ritchie & Xu, 1990; Giles, et al., 1993; Whittington, 1996; Bernard, et al., 2000).

$$\mathrm{CaO\ (s) + H_2O \xrightarrow{k_1} Ca(OH)_2\ (s) \xrightarrow{k_2} 2OH^-(aq, surface) + Ca^{2+}(aq, surface) \xrightarrow{k_3} 2OH^-(aq, bulk) + Ca^{2+}(aq, bulk)} \quad \text{...: 2.4}$$

The mechanism represented in Equation 2.4 is according to Whittington (1996); this review accounted the mechanism according to Ritchie and Xu (1990) findings. Ritchie and Xu (1990) found that dissolution of $Ca(OH)_2$ is the slowest step. Giles et al. (1993) confirmed that diffusion of the calcium ions and hydroxide ions from the surface (of a rotating disk surface) to the bulk solution at moderate stirring rate is consistent with findings by Ritchie and Xu (1990). In a highly controlled hydration process (stoichiometric reaction of quicklime with water), the hydration (k_1) proceeds to completion, before the surface dissolution of a formed $Ca(OH)_2$ (k_2). The same cannot be said during the slaking process, because when water is in excess and starting with quicklime, the hydration reaction will occur nearly simultaneously with the dissolution of $Ca(OH)_2$ at the surface. Due to this, it may be better to study the kinetics of $Ca(OH)_2$ dissolution independently. Even though this may not be a perfect solution due to hygroscopic nature of $Ca(OH)_2$ and other contributing factors such as its propensity of reacting with atmospheric CO_2 to form $CaCO_3$.

It is noted from literature sources on $Ca(OH)_2$ dissolution mechanisms, such as Ritchie & Xu (1990) and Giles *et al.* (1993), that during $Ca(OH)_2$ dissolution, an intermediate species $CaOH^+$ is formed. This means that $Ca(OH)_2$ will first lose one hydroxide ion, then eventually a complete surface dissociation will occur. In Equation 2.4, this is represented by k_2. Equation 2.5 – 2.7 is the simplified breakdown of the $Ca(OH)_2$ dissolution route as proposed by Ritchie & Xu (1990) and Giles *et al.* (1993).

$$\mathrm{Ca(OH)_2\ (s) \rightarrow CaOH^+\ (aq, surface) + OH^-\ (aq, surface)} \quad \text{...: 2.5}$$

$$\mathrm{CaOH^+\ (aq, surface) \rightarrow OH^-\ (aq, surface) + Ca^{2+}(aq, surface)} \quad \text{...: 2.6}$$

$$\mathrm{CaOH^+\ (aq, surface) \rightarrow CaOH^+\ (aq, solution)} \quad \text{...: 2.7}$$

$$\mathrm{OH^-\ (aq, surf.) + Ca^{2+}(aq, surf.) \rightarrow OH^-\ (aq, bulk) + Ca^{2+}(aq, bulk)} \quad \text{...: 2.8}$$

Ritchie and Xu (1990), using a rotating disk found that at the surface of $Ca(OH)_2$, the calculated pH is relatively lower than in the bulk solution. The authors claim that this is because the concentration of hydroxyl ions at surface is lower because of the species $CaOH^+$. This means that the diffusion of $CaOH^+$ from surface to the bulk solution is neglible. Using a rotating disk approach , Ritchie and Xu (1990), and Giles *et al.* (1993) concluded that on the surface of compressed $Ca(OH)_2$, or liquid-solid interface, there is thin film or layer where $CaOH^+$, OH^- and Ca^{2+} linger before they diffuse to the bulk solution, and this is the slowest step. The above explanation is true for the $Ca(OH)_2 – H_2O$ system, however, the mechanism may differ when other anions or cations are present in the system. A realistic $Ca(OH)_2$ – AMD system has dissolved metals and salts present, therefore the presence of various ions is inevitable.

2.6 Limitations in factors influencing $Ca(OH)_2$ dissolution

Apart from the calcination conditions of limestone, factors such as the temperature of the system, particle sizes and their distribution, concentration of the reactants or species in the system, pH and other properties such as agitation rate affect the dissolution of $Ca(OH)_2$. On the other hand, dissolution is measured using factors such as concentration, particle size and particle size distribution. For example, Johannsen and Rademacher (1999) claimed that it is impossible to predict the dissolution of $Ca(OH)_2$ using its concentration, particle diameter and temperature. Johannsen and Rademacher (1999), used conductivity of calcium cation in a H_2O - $Ca(OH)_2$ system in a batch reactor to trace the dissolution rate of 8 different types from different sources of $Ca(OH)_2$ samples.

2.6.1 Effect of particle size on $Ca(OH)_2$ dissolution

As discussed above, dissolution of a solid particle is particle size dependent, however this remains a vague statement unless a thourough investigation of this effect is investigated. According to Patterson et al. (2004) particles size is one of the major factors in reaction rate determination of solid-liquid reactions. Experimental work should therefore be developed in

such a way that it determines the effect of particle size and separate dissolution kinetics from chemical kinetics. Patterson et al. (2004), argue that true chemical kinetics must be established by initially using a saturated solution and then the overall reaction rate be evaluated for dissolution limitations. Ritchie and Xu (1990), successfully controlled the effect of particle size in slaking reaction by using a rotating disc method (RDM), which is a well established hydrometallurgical method of investigating kinetics of both homogeneous solution reactions and heterogeneous electrochemical reaction systems (Marsden & House, 2006). Apart from being widely used in hydrometallurgical operations, in RDM experiments the hydrodynamics of solution flow caused by rotation have been modelled and mass transfer rate can be calculated directly from measurements obtained. Furthermore, as reported by Marsden and House (2006), RDM experiments provide effective control of thermodynamics for mass transport or (electro-) chemically controlled reactions. Ritchie and Xu (1990) formulated the Levich Equation (Equation 2.9) for $Ca(OH)_2$ dissolution as follows:

$$S = 0.62\ D_{Ca(OH)_2}^{2/3} v^{-1/6} \omega^{1/2} [Ca(OH)_2]_s \quad \text{...: 2.9}$$

Where,

- S = dissolution rate in $mol \cdot L^{-1} \cdot s^{-1}$;
- $D_{Ca(OH)_2}$ = is the diffusion coefficient of $Ca(OH)_2$ in $m^2 \cdot s^{-1}$;
- v = kinematic viscosity of water $m^2 \cdot s^{-1}$;
- $[Ca(OH)_2]_s$ = concentration of a saturated solution of $Ca(OH)_2$ at the reacting surface in $mol \cdot L^{-1}$.
- ω = rotation speed in $rad \cdot s^{-1}$.

Since the zero-order rate constant is the same as the rate of zero-order reaction, therefore $S = k_0$. Substituting k_0 in the Equation 2.9; and let $k = k_0/\omega^{1/2}$ then rate equation become:

$$k = 0.62\ D_{Ca(OH)_2}^{2/3} v^{-1/6} [Ca(OH)_2]_s \quad \text{...: 2.10}$$

In Equation 2.10, v was taken from the Weast's Handbook of Chemistry and Physics as cited by Ritchie and Xu (1990) (Weast, 1984), k was then determined by estimating the values of $D_{Ca(OH)_2}$. The detailed RDM mass transfer correlation can be found in Ritchie and Xu (1990) and the corrected version in Giles *et al.* (1993).

Ritchie and Xu (1990) used scanning electron micrograph (SEM) and X-ray powder diffraction pattern of the quicklime to estimate the particle size range of 2 to 5 micrometers. However, this estimation was based on visual judgement that the small rough particles on the surface of the quicklime disc, after being immersed in water, were $Ca(OH)_2$. Giles et al. (1993) used the same methods as Ritchie and Xu (1990) except that instead of quicklime, $Ca(OH)_2$ was used.

2.6.2 Rotating disk versus the powder suspension on the effect $Ca(OH)_2$ dissolution

In the industrial operations such as Bayer process and waste water treatment, quicklime is slaked before it is introduced in the process (Whittington, 1996). This means that lime is added in a suspension form (the milk of lime or lime slurry). However, it is difficult to measure the lime suspension PSD due to its affinity to CO_2 which then forms a more stable and insoluble calcium carbonate. Formed calcium carbonate in a suspension coats glassware including those of the measuring devices such as laser diffraction scatter window in laser diffractometric devices. On the other hand, in the rotating disk method it is easy to control and minimize both the surface area and permeability of the solid (Wang, et al., 1998). The disadvantage of RDM is that it is difficult to prepare and test $Ca(OH)_2$ discs, including tests such as thermogravimetric (TGA) dehydration test, surface polishing, water content and chemical composition. These tests are done to make sure that the $Ca(OH)_2$ disc, chemical and physical properties resemble those of a $Ca(OH)_2$ powder. Wang, et al. (1998) claimed that it takes approximately 80% of the project time to prepare a $Ca(OH)_2$ disc and then 20% to do the main dissolution tests.

2.6.3 Particle size distribution on $Ca(OH)_2$ dissolution

One of the most important parameters or variables in determining the kinetics of a solid liquid suspension system is particle size distribution (PSD), particularly in the dissolution. It is expected that the smaller particles dissolve faster, provided all other properties remain the same. Therefore, the wider the particle size range, the harder it is to determine the kinetics as a function of a particle size. Giles et al. (1993) reported the initial particle size of their sample to be in the range of 45 to 63 micrometers, determined by an X-ray diffraction (XRD) method, which is quite coarse. The limitation of XRD is that small structures or particles are undetectable (Johnson, 2018); according to Oates (1998) saturated $Ca(OH)_2$ suspension has a tendency to re-precipitate, forming smaller particles or microcrystalline particles. Bernard et al. (2000) used the particle size range of 40 to 60 micrometers, these results were determined by a laser sizer. Kelly and Etzler (2005) report that even though laser sizer is a preferred PSD analysis method due to its ease of use and proven precision, it has several disadvantages such as follow: it is based on limited assumptions, the reported distribution can be skewed toward the smaller range, the results varies with optical parameters, the software used for calculation of results cannot be validated independently and the accuracy of measurements for non-spherical particles is inconsistent with equivalent spherical particles (Kelly & Etzler, 2005). Further details on these limitations are reported in Snorek et al. (2007) and Eshel et al. (2004). Robinson and Burnham (2001) used screens from 100 (149 micrometers) to 400 (37 micrometers) mesh to analyse PSD of seven different $Ca(OH)_2$s from different parts of United States. There are two challenges with this approach of using screens, one being the difficulty of preventing the interference of CO_2 from air on the powdered $Ca(OH)_2$ during screening. The dissolution of powdered $Ca(OH)_2$ that was exposed to CO_2 is compromised due to the complete or partial formation of calcium carbonate (Boynton, 1980; Whittington, 1996 and Oates, 1998). The second one, is the inefficiency of the screens in determining the PSD (Lawinska & Modrzewski, 2017). It is reported by Lawinska and Modrzewski (2017) that the efficiency of the vibrating screens is significantly reduced by the clogging of the holes by the particles or grains of varying sizes and geometries. This occurs as particles of varying sizes and geometries compete for a single hole. Consistent with the findings of Lawinska and Modrzewski (2017), preliminary studies of this work proved that this phenomenon further promotes aggregation.

2.6.4 Effect of solid concentration in $Ca(OH)_2$ dissolution

It is reported by different authors and institutions such as National Lime Association (NLA) that milk of lime is the most convenient form to use in industrial applications (Oates, 1998; Lewis & Boynton, 1999). According to Boynton (1980), milk-of-lime is thinner than the typical lime slurry; it flows readily as water and its solid concentration ranges from 1 to 20% (see chapter 2). The additional advantages of adding lime as milk-of-lime are as follows; it is easy to handle and store, it disperses well in aqueous systems and it has high chemical reactivity (Boynton, 1980; Lewis & Boynton, 1999). From Lewis and Boynton (1999), it is reported that particle size and its distribution (PSD) are one of the most important parameters in acid neutralisation with lime. However, particle size and PSD cannot be studied in isolation of solid concentration or solid density, as commonly referred to by most of the authors. The study by Robinson and Burnham (2001) is the only one that directly investigated the effect solid density on the reactivity of $Ca(OH)_2$ in suspended form in DI water (DI water). The authors investigated three levels of concentration; the lowest being 2% slurry, the medium level of 5% and the highest level which was 10%. This was done by comparing the reaction times of the highly reactive lime using a videotape to trace the progress of reaction by measuring turbidity and by calculating the percentage of undissolved $Ca(OH)_2$ particles. Robinson and Burnham (2001) found that in about five seconds, approximately 80% of 2% slurry had dissolved, about 50% of the 10% slurry had dissolved; in contrast only 21% of the 5% slurry had dissolved which was unexpected, and there is currently no convincing explanation for this. There was no significant difference between 5% and 10% slurry from five seconds to about eight seconds, however all different slurries approach saturation after 10 seconds. The 2% slurry was found to be the most reactive system; this is due to the availability of hydrogen ions from self-ionization of water. According to Lewis and Boynton (1999) the reactivity is proportional to the available hydrogen ions. Fundamentally, DI water in this case acts as a conjugate acid, converting hydroxyl ions from the solid-liquid interface around the surface of the particles to water molecules. This argument still holds for 5% and 10% slurry, considering that in 10% slurry experiments, the volume of DI water had to be adjusted from (200 ml used in 2% and 5%) to 400 ml because of the minimum deliverable volume of the adjusted pipette. The details supporting this argument can be found in Robinson and Burnham (2001).

2.7 Effect of the impellor rotation speed on $Ca(OH)_2$ dissolution

Mixing is very essential in chemical engineering reaction science, according to Shah et al. (2012), mixing and apparent reaction rate are intrinsically related. For reaction rate to be chemically controlled, mixing must be adequately fast to overcome diffusion or mass transport contribution to the reaction rate. This is dependent on various factors such as stirrer speed, nature of the system (homogeneous or heterogeneous system), impellor type, impellor size and type of reactor in use. It is desired to eliminate mass transfer influences on the rate of $Ca(OH)_2$ dissolution, hence the critical rate to be investigated is the chemical reaction rate.

Using RDM, Ritchie and Xu (1990) found the slaking reaction (of quicklime) to be a strong function of disc rotation speed. They established that at lower rotation speed, the pseudo-zero order reaction rate is controlled by the diffusion of OH^- and Ca^{2+} from the oxide surface to the bulk solution. Giles et al. (1993) confirmed the findings of Ritchie and Xu (1990) for independent dissolution of $Ca(OH)_2$. Giles et al. (1993) argued that, consistent with slaking of quicklime, the independent dissolution of $Ca(OH)_2$ is diffusion controlled below 250 rpm. However above 250 rpm, dissolution reaction rate was found to be independent of the disc rotation speed. Even though the dissolution reaction rate of $Ca(OH)_2$ was found to be approximately 40% less than that of slaking reaction rate of quicklime, Giles et al. (1993) were convinced that the consistency in the results is because both systems share a common chemically-controlled region.

In order to solidify this claim, Giles et al. (1993) studied the surface of the disc under different rotation speeds using X-ray diffraction. They found that between 100 and 200 rpm, the disc had small rough crystals. The small crystals are attributed to the redisposition or re-precipitation of $Ca(OH)_2$ crystals due to the supersaturated interface or layer between the disc and the solution (Oates, 1998). The small crystals diminished significantly between 400 and 600 rpm. This is because at higher rotation speed the saturation layer between the disc surface and solution is reduced significantly. The agitation rate of 400 rpm is relatively close to 370 rpm used by Bernard et al. (2000), even though Bernard et al. (2000) used an agitated $Ca(OH)_2$ suspension instead of the rotating disc. It is also acknowledged that rotation speed in and of itself is not a meaningful parameter and needs to be translated into a corresponding Reynolds or Froude Number. Bernard et al. (2000) used two levels of agitation, the lower level (370 rpm) and higher level (470 rpm). The mixing times at the experimental agitation rates (370-470 rpm) were compared favourably to the calculated mixing times determined by mixing theory.

Furthermore, using the calculated concentration of calcium in the bulk solution, Bernard et al. (2000) found that there was no significant difference in the calculated calcium concentration in the tests run from 400 rpm to 1500 rpm agitation speed.

2.8 Effect of temperature on $Ca(OH)_2$ dissolution

Temperature critically influences the kinetics of a reaction. Ideally, the change in dissolution rate as a function of temperature gives an idea whether a reaction is chemically controlled, or mass transfer controlled. Ritchie and Xu (1990) reported 13.6±1.2 KJ mol^{-1}, Giles et al. (1993) reported 15.0±2.0 KJ mol^{-1}. The activation energies in this range indicate mass transfer limited dissolution. This shows that the studies by Ritchie and Xu (1990) and Giles et al. (1993) were done under mass transfer limited system of RD, other than a preferably chemical reaction-control system. The advantage of a chemically reaction-control system is that it gives true kinetics of the system regardless of the type of reactor used. On the other hand, mass transfer-controlled kinetics are system specific and hence vary from one system to the other. Furthermore, the kinetics (shrinking sphere) models proposed by Ritchie and Xu (1990) and Giles et al. (1993) are based on the temperature differences (see Equation 2.11).

$$1 - \left(1 - \frac{\Delta T_t}{\Delta T_f}\right)^{1/3} = k_0 t / r_0 \qquad \text{...: 2.11}$$

Where,

- ΔT_t = is the temperature rise from the start of the reaction to time t;
- ΔT_f = is the temperature change from the start of the reaction to time t_f;
- r_0 = is the initial radius;
- k_0 = is the rate constant;
- t = is the dissolution time or time it takes for particles to dissolve;

The shrinking sphere model assumes that particles are mono-sized and spherical. Even though this model works perfectly for mono-sized spherical particles, it has been shown in the literature that spherical particles within a narrow size range can still work. Using different dissolution times, Bernard et al. (2000) found that even though $Ca(OH)_2$ has reverse solubility, its dissolution rate increases with the increase in temperature. In Equation 2.11, For simplification, put $\frac{\Delta T_t}{\Delta T_f} = X$; where X is the extent of reaction and equal to the temperature rise (or change) at time t divided by final temperature change. The changes in temperature were determined calorimetrically; then Equation 2.11 becomes Equation 2.12:

$$1 - (1 - X)^{1/3} = k_0 t / r_0 \qquad \text{...: 2.12}$$

2.9 Effect of pH on $Ca(OH)_2$ dissolution

In AMD treament, neutralisation is followed by precipitation of dissolved metals. Thus, the hydroxides from $Ca(OH)_2$ are constantly consumed, with the overall pH rising slowly. There were no studies found which perfectly demonstrats the role of pH in the kinetics of lime neutralisation of AMD; Wang *et al.* (1998) studied the effect of pH on the dissolution of $Ca(OH)_2$ rotating disc in aqueous solution using HCl. Also Bernard *et al.* (2000) considered the pH, however it was not incorporated on the final kinetic model.

In principle, pH needs to be controlled in order to avoid formation of undesired products (Bernard, et al., 2000). This means that the type of an acid to be used to control pH must not inhibit the dissolution reaction. The type of acid is dependent on the application or the end goal for that particular $Ca(OH)_2$ dissolution system. Bernard *et al.* (2000) studied the precipitation of hydroxyapatites, where $Ca(OH)_2$ suspension was neutralized with orthophosphoric acid (H_3PO_4). The addition of H_3PO_4 is such that the pH is controlled below 6, to prevent the formation of other calcium phosphates. The formation of hydroxyapatite and other calcium phospates occurs simultaneously with the dissolution of $Ca(OH)_2$. Even though pH is important, the dissolution model by Bernard *et al.* (2000) is not in terms of pH but rather the pH was varied by monitoring the flowrate of an acid. This is probably because it is difficult to

control the pH of a $Ca(OH)_2$ suspension system in a semi-batch reactor (Wang, et al., 1998). Wang *et al.* (1998) used a similar semi-batch set-up as the one used by Bernard *et al.* (2000), except that Wang *et al.* (1998) used a rotating disc (RD) method instead of a $Ca(OH)_2$ suspension.

Equation 2.13 shows the Bernard *et al.* (2000) dissolution model:

$$\frac{\mathrm{d[Ca]}}{\mathrm{d}t} = \frac{3{m_C}^0}{V_L \rho_C r_0}\left(1 + \frac{M_C V_L([\mathrm{Ca}]_0 - [\mathrm{Ca}])}{{m_C}^0}\right)^{2/3} \times k_d \Delta[\mathrm{Ca}] \quad \text{...: 2.13}$$

Where $[\mathrm{Ca}]_0$ and $[\mathrm{Ca}]$ represent the concentration of the bulk solution at time $t = 0$ and t respectively. V_L is the volume of the liquid phase which is assumed to be constant, ρ_C is the density of CaO and r_0 is the initial mean size at $t = 0$. M_C is the molar mass and ${m_C}^0$ is the mass of the CaO. $\Delta[\mathrm{Ca}]$ is determined by Equation 2.14.

$$\Delta[\mathrm{Ca}] = [\mathrm{Ca}]_{\mathrm{sat}} - [\mathrm{Ca}] \quad \text{...: 2.14}$$

Where $[\mathrm{Ca}]_{\mathrm{sat}}$, is the concentration of calcium at saturation, determined using Debye-Huckel law, k_d is mass transfer coefficient determined by Boon-Long, Laguerie and Couderc (1977) as cited in Bernard *et al.* (2000). In contrast, Wang *et al.* (1998) used the Arrhenius Equation to develop a pH-based dissolution model. The Equation 2.15 shows Wang *et al.* (1998) correlation.

$$\ln(N_s) = -17.68 - 280(1/\mathrm{T}) + 0.105(\mathrm{pH}) + 0.458\ln(\omega) \quad \text{...: 2.15}$$

Where N_s is the dissolution rate of calcium (in mg/g.min), T is the solution temperature from 298 to 323 K, pH is the solution pH in the range 4 to 7; ω is the stirring rate in the reactor (rpm) for the disc Reynolds' number greater or equal to 10000. Using this correlation, Wang *et al.* (1998) found that the rate of dissolution of $Ca(OH)_2$ increases with the decrease in pH (or increase in hydrogen ion concentration) in the pH range 4 to 7. These findings are inconsistent

with findings reported by Lewis and Boynton (1999), who claimed that unlike soda ash and limestone; $Ca(OH)_2$ and caustic soda react rapidly with acids when the acid is added slowly such that the pH at the end of acid addition remain above 7. This is because of the accessible hydroxyl group in NaOH and $Ca(OH)_2$. It is not explained how the hydroxyl ion enhances the reaction rate, however a possible explanation is through the hydrolysis of water. Intuitively hydrogen ions from self-ionization will react with hydroxyl ions around $Ca(OH)_2$ particle surface and hence favouring dissolution of $Ca(OH)_2$ particles. The lack of hydrogen ions in the solution inhibits the reaction rate of non-hydroxyl bases (Lewis & Boynton, 1999).

2.10 Effect of the anions and cations in $Ca(OH)_2$ dissolution

In lime neutralisation processes, cations or impurities in the dissolution of $Ca(OH)_2$ comes from the origin of the $Ca(OH)_2$, the most common cation is magnesium which is viewed as the companion of calcium. In the lime industry, the incorporation of magnesium on the lime ores results in dolomite or dolomitic lime. Other cations are dependent on the liquor that is being treated, for example municipality wastewater cations differ from mine water effluents or borehole water.

2.10.1 The effect of hydroxides and calcium ions

In $Ca(OH)_2$ - H_2O system, the system comprises three ions OH^-, H^+ and Ca^{2+}; as the dissolution of $Ca(OH)_2$ particles proceeds, OH^- and Ca^{2+} ions are expected to increase in bulk solution especially in a batch system. From the Equation 2.2, H^+ cations from self-ionization of water are expected to react with OH^- from the dissolution of $Ca(OH)_2$ (and those generated by self-ionization of water). Ritchie and Xu (1990) used NaOH-$Ca(OH)_2$-H_2O system to investigate the effect OH^- of on the dissolution of $Ca(OH)_2$; it was found that the increase in OH^- concentration suppresses the rate of $Ca(OH)_2$ dissolution. Whittington (1996) reported these findings, including the test done by the other authors such as Boynton (1980). This means that the $Ca(OH)_2$ dissolution decreases with time. In order to distinguish the effect of OH^- from that of Ca^{2+}, Giles *et al.* (1993) and Ritchie and Xu (1990) used calcium nitrate solution. Using the rate constant of a zero-order reaction rate, it was found that above 0.01 M of either OH^- or Ca^{2+};

the rate of dissolution decreases more rapidly in the presence of OH^- than in the presence of Ca^{2+}.

$$H_2O\,(aq) \leftrightarrow H^+\,(aq) + OH^-(aq) \quad \text{...: 2.16}$$

$$Ca^{2+}\,(aq) + OH^-\,(aq) \leftrightarrow Ca(OH)_2\,(s) \quad \text{...: 2.17}$$

2.10.2 The effect of carbonates on the $Ca(OH)_2$ dissolution

It is established that $Ca(OH)_2$ has a high affinity for CO_2 (Oates, 1998; Perry, 2011). According to Oates (1998) powdered $Ca(OH)_2$ reacts readily with acidic gases such as CO_2 and other oxides such as sulphur oxides and nitrogen oxides. The reaction of $Ca(OH)_2$ and CO_2 is dependent of the particle size and the degree of dispersion of hydrates (Oates, 1998). Equation 2.18 shows how this reaction occur;

$$Ca(OH)_2\,(s) + CO_2\,(g) \rightarrow CaCO_3(s) + H_2O\,(g) \quad \text{...: 2.18}$$

The reaction in Equation 2.18, occurs at ambient conditions. This means that powdered $Ca(OH)_2$ can pick up CO_2 from the atmosphere partially or completely, forming calcium carbonate and water vapour. This is one of the possible ways in which carbonates are introduced in dissolution of lime system. It is therefore expected that the dissolution of $Ca(OH)_2$ that was exposed to the atmosphere would be affected significantly due to the presence of carbonate ions. Papers by Boynton (1980) and Whittington (1996) show that the presence of carbonates supress the reactivity significantly, compared to the impurities in a free water system.

The other possible ways of introducing carbonates in the system are during milk of lime preparation or storage. As noted above, a high proportion of $Ca(OH)_2$ is used in the form of a slurry or 'milk of lime' or putty (Oates, 1998). However, one of the disadvantages of using milk-of-lime is the formation of calcium carbonate scaling on the walls of the vessels, especially at the gas-liquid interface where slurry is exposed to air. As reported by Oates (1998), the scaling or crystallisation is caused by the combination of the pH, temperature and the degree of super-saturation. It was observed during the preparation of the lime water and the

milk of lime that the flow of CO_2 is also a major contributing factor. During the lime water preparation, a network or cake of colourless crystals forming a layer on top the lime water and milk of lime was observed. This agrees with the argument reported by Oates (1998) that crystallisation can also occur on the surface of the $Ca(OH)_2$ particles forming scalenohedral crystals. Oates (1998) further argued that the crystallisation can also occur in the aqueous phase forming rhombohedral crystals.

The crystals or scales have the tendency to peel off the walls and fall in the milk-of-lime or lime suspension forming insoluble calcium carbonate grits which then sink to the bottom of the vessel. The grit dissolves (to some extent) in the dilute systems or acidic environment depending on the quality of a diluting water and the concentration of the acidic environment. This therefore introduces carbonate ions in the system. In industrial application, calcium carbonate scales are noticeable in milk-of-lime transfer lines, valves and pumps (Oates, 1998). This was shown during the preliminary experiment of this study, by conducting CO_2 tests on the layer that was formed on the $Ca(OH)_2$ suspension tank.

Chapter 3: Context and Motivation

This section covers the gap analysis, hypothesis, key research questions and research objectives. The gap analysis points out the partially addressed or undressed aspects of kinetics of $Ca(OH)_2$ dissolution in water and acidic solution that this study aims to investigate. The hypothesis proposes the research approach used in investigating the kinetics of $Ca(OH)_2$, furthermore, this approach is justified using the established theories or concepts. The key questions are formulated to address the gaps that exists, then eventually the objectives provide a step by step procedure to meet the deliverables of the study.

3.1 Gap analysis

Physical Chemistry (kinetics, crystallisation and agglomeration)

The chemical reactions that are involved in the conversion of quicklime to $Ca(OH)_2$ are well researched and documented (Boynton, 1980; Oates, 1998). However, the physical chemistry, especially the kinetics, are reported to be a complex subject with some contradicting information in the literature (Oates, 1998). Lime experts in Boynton (1980) and Oates (1998) report that these contradictions are presumably due to unquantified variations in process conditions and the quality of pre-cursor limestone calcined to produce quicklime and $Ca(OH)_2$. Furthermore, these variations in $Ca(OH)_2$ samples force researchers to spend the time they could be spending in studying dissolution kinetics on characterization (Johannsen & Rademacher, 1999).

It is therefore expected that the kinetics of $Ca(OH)_2$ are dependent on the type and source of parent quicklime used in its production. This is consistently shown by the two experimental studies conducted by Johannsen & Rademacher (1999) and Robinson & Burnham (2001). Johannsen & Rademacher (1999) studied the dissolution rates of eight different types of $Ca(OH)_2$s including two reagent grade $Ca(OH)_2$ samples. Robinson & Burnham (2001) studied the dissolution of seven different types of $Ca(OH)_2$s in de-ionized water. Both studies confirm that each sample reacts differently, however methods used in determining the particle size distribution (PSD) in these studies were limited.

Is it slaking or dissolution reaction:

Quicklime neutralisation is arguably the same as $Ca(OH)_2$ neutralisation because when quicklime is added into an aqueous solution, it will first be converted to $Ca(OH)_2$ through the slaking reaction (Whittington, 1996). Ideally this statement is expected to hold in AMD treatment, since it is true for pure quicklime and water system (Boynton, 1980; Oates, 1998). If quicklime is added in water as a powder, it is expected that slaking would proceed simultaneously with the dissolution of $Ca(OH)_2$ (Irabien, et al., 1989). It is further established that quicklime is more reactive than $Ca(OH)_2$ (Boynton, 1980; Oates, 1998). Most authors acknowledge that slaking of quicklime and dissolution of the formed $Ca(OH)_2$ is a complicated process with contradicting findings (Boynton, 1980; Irabien, et al., 1989; Oates, 1998; Johannsen & Rademacher, 1999). Therefore, studying both processes (slaking of lime and dissolution of $Ca(OH)_2$) simultaneously could be contributing to the reported complications.

Temperature rise argument (effect of temperature).

The kinetic models by Ritchie and Xu (1990) and Giles *et al.* (1993) are based on the measured rise in temperature during the reaction. This does not apply in the $Ca(OH)_2$ dissolution model because these studies used quicklime as a starting point, and they studied a combined slaking and dissolution system. Slaking is a highly exothermic reaction (with liberated heat of about 1.15 MJ/kg high-calcium quicklime reacted), and hence temperature sensitive; however, the dissolution reaction, though exothermic in nature is it not as sensitive to temperature changes.

These models are all mass transfer based (except Johansen & Rademacher)

In principle, dissolution in most cases is mass transfer controlled (Robinson & Burnham, 2001). However, it cannot be simply assumed that diffusion is a controlling factor in this case. This is because, the diffusion layer around $Ca(OH)_2$ particles can be significantly reduced by increasing the agitation speed. This therefore means at a higher agitation speed; the dissolution rate can be solely chemical reaction controlled.

The study by Johannsen and Rademacher (1999) is the only one that presented a dissolution rate model that is independently based on the chemical reactions. All the other $Ca(OH)_2$ dissolution studies consulted seemed to be done under mass transfer controlling conditions.

Mass transfer limitation:

A lot of studies have adequately covered the slaking reaction perfomance and parameters affecting it. Therefore, for a better understading of dissolution of $Ca(OH)_2$ in AMD neutralisation, it must be studied independently of slaking as highlighted above. Attempts to independently study dissolution of $Ca(OH)_2$ were made by Giles *et al.* (1993), Wang *et al.* (1998), Johannsen & Rademacher (1999) and Robinson & Burnham (2001). Even though these studies succesfully decoupled the slaking reaction from dissolution, almost all the consulted empirical studies explored the reaction in the mass transfer limited region (Ritchie & Xu, 1990; Giles, et al., 1993; Wang, et al., 1998; Johannsen & Rademacher, 1999; Bernard, et al., 2000; Robinson & Burnham, 2001). The challenge with mass transfer limited dissolution models is that they are system specific (see Chapter 2). They are likely to be affected by a change in hydrodynamics, type of reactor, size of a reactor, agitation rate and impellor type.

Rotating disk limitation:

Surface area is one of the most important parameters in dissolution studies or solid-liquid reaction or surface disintergration reactions (Oates, 1998). The rotating disk method allows the fixing of a surface area while exploiting other parameters such as the diffussion of calcium ions from the exposed surface to the bulk solution. Therefore, the rotating disk approach model is intrinsically a mass trasfer based model unless operated at high speeds. The limited surface area of the plane disk also limits the extend of the measurable dissolution as compared to a fine particulate system.

Shrinking core/sphere limitation:

The shrinking sphere model was adopted by most of the studies (Ritchie & Xu, 1990; Giles, et al., 1993; Bernard, et al., 2000), regardless of the fact that it strictly holds only for single particle size. It thus works effectively only when the particles are of the same size or a very narrow PSD; apart from that, the methods used in determining PSD presented in the literature have limitations when working with $Ca(OH)_2$ because of the its physical properties.

Calcium assay limitation:

In literature, calcium assays are critical; since the dissolution is confirmed by the increase in dissolved calcium concentration in bulk solution. The proposed models in Giles *et al.* (1993) and Bernard *et al.* (2000) are all based on the concentration of calcium in bulk solution. Johannsen & Rademacher (1999) on the other hand argued that to develop a model based on calcium concentration is impossible. This statement makes sense only if the reaction configuration is semi-batch or batch; in this configurations calcium assays are bound to change rapidly, depending on the sampling proceedure. Furthermore, the classic calcium assays are of limited accuracy especially when there are other cations or metals present in the system.

The gap in pH range

From Chapter 2, lime neutralisation is the first step of acidic effluent or AMD treatment, during this process, pH is increased slightly as hydroxides from lime react with diverse metals (including heavy metals) from AMD. Metals are then recovered or removed as metal hydroxide precipitates. The effective removal or recovery of each specific metal is a strong function of pH; therefore, it is very important to understand the dissolution rate as the function of pH.

The pH of the system is one of the significant parameters in $Ca(OH)_2$ dissolution. Apart from being controlled to prevent the formation of undesired product, it has been found that the rate of dissolution increases with the increase in hydrogen ion concentration (which in principle is the decrease in pH of the system) (Wang, et al., 1998; Bernard, et al., 2000). As explained in Chapter 3, both studies had difficulties in controlling pH at steady or desired levels because of the nature their experimental set-up or reactor configuration.

Reactor configuration limitation:

Neutralisation reactions are very fast in nature; they proceed in the order of tens of seconds to several minutes. All consulted studies were conducted in either a batch reactor or semi-batch reactor. This means that these studies were either done in a dynamic system (only for studies with in-situ mesurements) or measurement were done once the system was stabilised (Bernard, et al., 2000). In Bernard *et al.* (2000), the system took about four minutes to stabilise. It is therefore likely that by then the chemical based dissolution was already completed. The

advantages of the batch and semi-batch systems are that they are easy to operate and can generate many data points in a single run. A continous flow system (such as a CSTR) on the other hand takes a long time to reach steady state and under one set of conditions to allow measurement of one data point. The advantages of a continous flow system is that it is easy to sample since at steady state (chemostasis), the conversion and hence concentration of the reactant or products in the exit stream is the same as inside the reactor. The disadvantage is that only one data point is generated per run.

3.2 Hypothesis

The $Ca(OH)_2$ dissolution kinetics in acidic solution are inversely proportional to solution pH (hydrogen ion concentration or $[H^+]$). At a rotation speed sufficiently high to eliminate mass transfer control, under conditions of chemical control and moderate residence time, the rate at which $Ca(OH)_2$ dissolves in acidic solution decreases with an increase in pH. This is because during neutralisation reaction, protons deplete as the amount of hydroxyl ions are increased. The reverse is expected when the number of protons is increased. At sufficiently high agitation rate the system is chemical reaction controlled, therefore dissolution of $Ca(OH)_2$ can be effectively studied in a flow system (CSTR) using chemical kinetics and reaction engineering without the contribution of mass transfer. The approach is to study this in a chemostat (CSTR) system to allow a steady-state $Ca(OH)_2$ dissolution kinetics and constant steady-state measurement of pH and Ca^{2+}.

3.3 Key questions

The following are key questions that guided the outcome of this study;

1. What is the chemically controlled reaction rate for the dissolution of $Ca(OH)_2$ reaction?
2. What is the nature of $Ca(OH)_2$ neutralisation reaction, is it an acid attack or conventional dissociation reaction?
3. Is there a relationship between the rate of change in particle size (diameter) and the rate of reaction?

4. What are possible reaction mechanisms for a $Ca(OH)_2$ -H_2O-CH_3COOH system; how do they differ from a simple $Ca(OH)_2$ -water system?
5. How does the pH of the system change with $Ca(OH)_2$ dissolution rate for pH values higher than 7?
6. What number of residence times does it take for the CSTR system to reach steady state?

3.4 Objectives

The objectives stated here are directly linked to the influence of the factors that are discussed in chapter 2, on the dissolution of $Ca(OH)_2$. The objectives are therefore:

1. To investigate the effect of sulphates, magnesium and iron on the calcium assays determined by different calcium determination methods.
2. To investigate the efficiency of different particle size distribution measurement methods on this study.
3. To investigate the effect of the stirrer speed on the rate of dissolution of $Ca(OH)_2$.
4. To investigate the effect of the pH on the rate of dissolution of $Ca(OH)_2$.
5. To develop an efficient reaction system for the study of lime dissolution kinetics.

Chapter 4: Methodology

The methodology outlined in this section was used to achieve the objectives of this study as described in Section 3.4. This is partitioned into two sections, which are the experimental design and experimental set-up. The experimental design deals with the nature of the conducted experiments followed by the experimental set-up which covers the equipment used, measurements and experimental procedure.

4.1 Experimental design

Preliminary experiments:

The preliminary experiments were conducted in a batch reactor; the aim of these experiments was to investigate the hydro-dynamics of the $Ca(OH)_2$-H_2O system. The parameters focused on were agitation speed, selection of an impellor type, $Ca(OH)_2$ (powder) addition and PSD of $Ca(OH)_2$ analysis. In these experiments, pH change with time was used to confirm the dissolution of $Ca(OH)_2$. As $Ca(OH)_2$ dissolves, its hydroxyl anions and counter calcium cations are released to the bulk solution, the increase of hydroxyl anions is indicated by the increase in pH of the bulk solution. The rate of increase in pH was correlated to the rate of dissolution of $Ca(OH)_2$. Furthermore, to complement the change of pH with time, it was desired to trace the progress of the dissolution of $Ca(OH)_2$ particles by monitoring their size reduction simultaneously with pH trends.

Calcium assays experiments:

AMD comprises myriad of different species depending on the geological background or origin. However, there are three main common species which are present in relatively high concentrations. These includes magnesium cations (Mg^{2+}), ferric cations (Fe^{3+}) and sulphate ions (SO_4^{2-}). Even though magnesium (Mg^{2+}) varies, depending on the source of AMD, it is selected in this case since both AMD and industrial ($Ca(OH)_2$) contain it in significant amounts. Lime usually comprises magnesium from its pre-cursor material such as calcium carbonate, especially dolomitic limes. It is worth noting that the presence of the species discussed above

may affect the integrity of the pH trend as a measure of the rate of dissolution. Therefore, dissolved calcium cations concentration had to be used as measure of dissolution rate. Due to the nature of the experiments and the number of samples to be processed, it would require an atomic absorption spectroscopy (AAS) or inductively coupled plasma optical emission spectroscopy (ICP-OES) unit to be situated in the same laboratory where experiments are conducted, which is often not practical. Therefore, dissolved calcium determination methods were introduced, however the suitability of an adopted method with the species provided needed to be tested.

The methods tested in this study include complexometric ethylene-di-amine-tetra-CH_3COOH (EDTA) Erio-chrome black T (EBT) reverse titrations (EBT-EDTA – Reverse Titrations), o-cresolphthalein complexion spectro-photometric method (o-Cresolphthalein Complexone or o-OCPC) and inductively coupled plasma optical emission spectroscopy (ICP - OES). Apart from the methods described above, the oxalate precipitation method was also attempted but it was not successful in preliminary experiments, it was too far off from the other methods. Furthermore, it involved heating of the solution which introduces an additional source of error because of mass losses through evaporation. These methods were to be used to detect changes in dissolved calcium cations in the bulk solution during the neutralization process. The increase in calcium cations in bulk solution implies the progress of dissolution of suspended $Ca(OH)_2$ particles.

As part of preliminary experiments, the efficiency of EBT-EDTA – Reverse Titrations and o-Cresolphthalein Complexone (OCPC) method were investigated but ICP – OES was used as a reference method. The aim of this investigation was to determine the concentrations ranges at which each method can detect dissolved calcium cations quantitatively. This was done in the presence of increasing concentrations of magnesium ions (Mg^{2+}), ferric cations (Fe^{3+}) and sulphate ions (SO_4^{2-}). DI water was used as the reference solution.

The in-situ pH measurement in the preliminary experiment was essential for tracing the progress in the rate of dissolution; as explained above, pH was directly linked to hydroxyl anions in solution. However, it is insufficient to trace the progress of dissolution of $Ca(OH)_2$

using pH only, especially when other species such as sulphates, ferric ions and magnesium are introduced in the system (as the major components in $Ca(OH)_2$-AMD neutralisation system). In AMD systems, calcium is expected to react with sulphates forming calcium sulphate (gypsum) while ferric and other metals are precipitated out as metal hydroxides (see Chapter 2). The validity of different calcium determination methods was tested specifically for the above simplified systems in order to minimise interferences from other trace species in AMD.

Flow-through reactor experiments:

There were three types of continuous stirred tank reactors used, that is the overflow slurry continuous flow stirred reactor (CSTR) system and two controlled outflow CSTRs (one was unjacketed and the other was jacketed and fitted with thermostat). In each set-up, the operating conditions were informed by the objectives for that experiment or investigation. Each reactor set-up leads to the design and improvement of the next rector. The flow system was selected due to its ability to operate at steady state, where the condition of the exiting stream is the same as the reactor content (chemostat). Under this reactor configuration system, pH of the bulk solution was kept at the desired constant level by giving a reactor enough time to reach steady state. This was done by calculating the number of residence times it would take for the pH to remain constant over a period.

The summary of the experimental approach in the overflow slurry CSTR, constant temperature controlled outflow CSTRs and thermostatic CSTR are detailed in Table 4-1, Table 4-2 and Table 4-3 respectively.

Material handling and feed characterization:

Batch system feed characterization

The initial particle size distribution (PSDi) of the reagent grade $Ca(OH)_2$ powder (from Merck) was measured using vibrating screens ranging from -30 micrometers +125 micrometers. For the experiments, the particle size range of 65-73 micrometers reagent grade $Ca(OH)_2$ powder was used.

The challenges with material handling in batch system are as follows; according to Christian (2004) and Boynton (1980), $Ca(OH)_2$ can react with CO_2 in the atmosphere forming a crust of calcium carbonate. As the screens were not proofed against the ingress of CO_2 or atmospheric gases, it is nearly impossible to screen the powdered $Ca(OH)_2$ without CO_2 interference.

Flow-through reactor system

After realising the challenges of $Ca(OH)_2$ powder handling, flow-through reactor systems were adopted, starting with the overflow CSTR, followed by the constant temperature, controlled-outflow CSTR and eventually the thermostat regulated controlled-outflow CSTR. The reactors comprised of two feed streams, the acid feed solution (CH_3COOH, $HClO_4$ and H_2O) and milk of lime or lime suspension. These streams were fed above the four-pitched-blades turbine impellor for effective mixing. Acid feed streams were prepared by diluting concentrated solutions of CH_3COOH to desired dilute concentration (0.5; 0.25; 0.125, 0.1; 0.05; 0.025 and 0.01 M CH_3COOH). It is worth noting that perchloric acid (0.5 M $HClO_4$) was used only once to investigate the effect solid density (See Table 4-1).

For the overflow CSTR and constant temperature, controlled-outflow CSTR, the lime suspension was prepared by diluting 20 % solid fraction industrial milk of lime ($Ca(OH)_2$ suspension from Lhoist Minerals and Lime producers) to 2%. The $Ca(OH)_2$ suspensions of 6 % and 0% were also prepared for comparison purposes. 0% (limewater or saturated lime solution) was prepared by filtering all solid particles. For thermostat regulated controlled-outflow CSTR, only 2% milk of lime was used, prepared by adding 40 g of reagent grade $Ca(OH)_2$ powdered $Ca(OH)_2$ (from Merck) in 1L of saturated lime solution. This was done with caution, considering that the solution used was close enough to saturation point, such that the rate of $Ca(OH)_2$ re-precipitation (in case of supersaturation) or $Ca(OH)_2$ dissolution (in case of under-saturation) was negligible.

Table 4-1: Overflow slurry CSTR operation matrix

Experiment Set	***Aim***	***Manipulated Variable***	***Constant Variable***	***Measured variable***
1.	To investigate the effect of the residence time (and the number of residence times)	Flow rates of acid or DI water stream and suspended $Ca(OH)_2$ τ(min)=2.4;2.7 and 4.3	Temperature (22 ˚C), Agitation speed (600 rpm) Volume (1.2L), $Ca(OH)_2$ solid concentration (φ = 2%)	pH, dissolved calcium, initial and final particle size distribution (PSD).
2.	To investigate the effect of the $Ca(OH)_2$ suspension dosage.	Flow rate of $Ca(OH)_2$ suspension varied at 0.1 ml/s; 0.24 ml/s; 0.49 ml/s; 0.73 ml/s and 1 ml/s.	0.5M CH_3COOH (fed at the flow rate of 4.24 ml/s). Temperature (22 ˚C), Agitation speed (600 rpm), Volume (1.2L), φ = 2%	pH, dissolved calcium, initial and final particle size distribution (PSD).
3.	To investigate the effect of $Ca(OH)_2$ solid concentration.	$Ca(OH)_2$ solid concentration in the suspension tank was varied from 0%, 2% and 6%	Temperature (22 ˚C), Agitation speed (600 rpm), Volume (1.2L), 0.5M $HClO_4$ flow rate (4.24 ml/s). and $Ca(OH)_2$ suspension (0.1 ml/s)	pH, dissolved calcium, initial and final particle size distribution (PSD).

Table 4-2: The constant temperature, controlled-outflow slurry CSTR operation condition matrix

Experiment Set	***Aim***	***Manipulated Variable***	***Constant Variable***	***Measured variable***

1.	To investigate the effect of acid concentration (at steady state pH) on the reaction rate.	CH_3COOH concentration varied at the following levels; 0 M, 0.01M, 0.02M, 0.025M, 0.05M, 0.25M and 0.5M.	Temperature (22 ˚C), Agitation speed (600 rpm), Volume (400 ml), Solid concentration (2%), CH_3COOH flow rate (4.24 ml/s). $Ca(OH)_2$ suspension (0.1 ml/s), Exit stream flow rate (5.02 ml?)	pH, dissolved calcium, initial and final particle size distribution (PSD).

Table 4-3: The thermostat regulated controlled-outflow slurry CSTR operation condition matrix

Experiment Set	***Aim***	***Manipulated Variable***	***Constant Variable***	***Measured variable***
1.	To investigate the effect of residence time, and number of residence times.	Residence time varied between two levels (short residence time at 50s and long residence time at 70s) by changing reactor volume.	Temperature (25 ˚C), Agitation speed (1106 rpm), Solid concentration (2%), CH_3COOH concentration kept at 0.01 M; 0.04 and 0.125M. CH_3COOH flow rate (4.24 ml/s). and $Ca(OH)_2$ suspension(0.23 ml/s)	pH, dissolved calcium, initial and final particle size distribution (PSD).
2.	To investigate the effect of acid concentration on the Ca(OH)2 reaction rate.	CH_3COOH concentration varied at 0M, 0.02 M 0.04 and 0.125M.	Temperature (25, 35 and 45 ˚C), Agitation speed (1106 rpm), Volume (400 ml), Solid concentration (2%), CH_3COOH flow rate (4.24 ml/s). $Ca(OH)_2$ suspension (0.23 ml/s),	pH, dissolved calcium, initial and final particle size distribution (PSD).

3.	To investigate the effect of temperature on the reaction rate.	Reactor Temperature varied at 25, 35 and 45 ˚C:	Agitation speed (1106 rpm), Volume (400 ml), Solid concentration (2%), CH_3COOH concentration kept at 0.01 M; 0.04 and 0.125M. CH_3COOH flow rate (4.24 ml/s) and $Ca(OH)_2$ suspension (0.1 ml/s)	pH, dissolved calcium, initial and final particle size distribution (PSD).

Particle size distribution (PSD) experiments:

It is intuitive that as the $Ca(OH)_2$ dissolution reaction progresses, the individual particles are expected to shrink. The aim of these experiments was therefore to trace the size reduction as a measure or indication of dissolution rate. From preliminary studies, it was noted that the method of using vibrating screens was inadequate for the nature of the experiments conducted, therefore other PSD analysis methods such as microscope and particle image analysis were adopted. Eventually, scanning electron micrographs (SEM) for nano-images were used to characterize particles before and after the reactor. The other particle size analysis method considered laser diffraction method (Mastersizer), however, the laser sizers were not suitable for measuring the PSD because of the chemical properties of $Ca(OH)_2$; lime products have the tendencies to scale or armour the tubes and optical devices screens in laser diffraction devices (see Chapter 3). This resulted in analysis failure due to optical alignment errors.

The PSD of both the industrial $Ca(OH)_2$ suspension and reagent grade $Ca(OH)_2$ suspension were determined by analysing nano-SEM images in ImageJ image analysis (open source software) and then compared. It was therefore assumed that the conditions found from batch system experiments (reagent grade $Ca(OH)_2$ powder) are still applicable for experiments conducted using industrial $Ca(OH)_2$ suspension.

4.1.1 Operating conditions

This section deals with the operating conditions for each reactor system, including the control measures taken for calcium assays experiments and PSD and image analysis experiments.

Batch system

The conditions reported in Ritchie & Xu (1990), Johannsen & Rademacher (1999) and Bernard *et al.* (2000) were investigated in the context of AMD neutralisation with lime (current study). These experiments served as preliminary studies to determine the agitation rate beyond which bulk mass transfer no longer controls the rate of reaction. This needed to be established in order to be exploited in the next steps. Three agitation levels were chosen, lower level (225 rpm); medium level (325 rpm) and higher level (425 rpm). The overhead stirrer (IKA RW 20 Digital Dual-Range Mixer) was used to set the stirring rate values. The powder was fed into a 1.5 L baffled glass reactor with a smooth paper conduit, the conduit was inserted in such a way that it feeds the powder few millimetres above the 40° pitch-bladed turbine (PBT) stirrer. It was desired that the temperature be kept constant but found to vary marginally between 21 and 22 °C over the duration of experiments.

Reagent grade $Ca(OH)_2$ powder was added to one litre (1L) of DI water. The extent of dissolution was measured in-situ by monitoring the change in pH using an online Metrohm Titrando system (Pt1000/B/2/3M KCl glass electrode). The Metrohm system showed delayed responses due to slow probe response; alternatively, the samples where extracted by a syringe sampler, the pH values were then measured and recorded every two minutes, using GLP 21 Crison pH meter and Mettler Toledo S210 Seven Compact pH/ion Benchtop meter.

Challenges and limitations in a batch system

The main difficulty with this system was powder addition; for effective mixing, it was desired to feed the powder instantaneously above the agitator. The best option was to feed the powder using a conical conduit, even though there were some minor losses with the added powder

sticking to the walls of the conduit. Furthermore, the first few tests were done in air and thus risked interference by CO_2. Even though the system was improved in the later tests, it was not completely CO_2 proofed. It was further noted that the syringe sampler was a limiting factor because the minimum time it took for taking the first sample was two minutes, a concern was the fact that neutralisation reaction may be faster than two minutes (Robinson & Burnham, 2001). The syringe sampling was the only possible way of sampling (in the batch reactor), which means that there was a high possibility that the reaction continued. Furthermore, quenching the reaction with base means that the pH as a measure of dissolution becomes obsolete. Also, tracing particle size reduction in each sample was difficult due to the nature of syringe filtration arrangement.

The Overflow slurry CSTR system

Due to problem with powder PSD characterization, powder addition and sampling limitations in the batch system, the overflow continuous flow-through stirred reactor system was adopted. The operation of this system was relatively more challenging than the batch system as it required the determination of effective flow rates of the feed streams that will yield incomplete reaction while avoiding particles accumulating in the vessel due to gravity effects. This in turn required careful pump calibration, priming and balancing. This system was used to determine the operating conditions of a CSTR such as the number of residence times required to achieve steady state. The residence time was controlled by changing the flowrates of the feed streams.

The Overflow slurry CSTR set-up

The overflow slurry CSTR system (as depicted in Figure 4.1) was used as above. This setup comprised a 1.2L glass reactor (R-101) with an overflow port for the output or exit stream. In this reactor there were two inlet feed streams ($Ca(OH)_2$ suspension or 'milk of lime' feed stream and acid feed stream). Both feed stream pipes were positioned above the stirrer for effective mixing as discussed by Liu (2016). The acid stream was connected to a 502S Masterflex Pump (P-101) to transfer acid from acid storage tank (TK-101) to the reactor (R-101). Similarly, industrial $Ca(OH)_2$ suspension was fed into the reactor using $Ca(OH)_2$ suspension pump (p-102). The suspension was prepared in a 25L cylindrical plastic $Ca(OH)_2$ suspension storage bucket (TK-102). R-101 and TK-101 were fitted by Masterflex overhead stirrers, M-101 and

M-102 respectively. The overflow port was fitted with a 40 mm internal diameter (ID) silicon tube; this was done for sampling the product or waste stream and was directed to the waste or product storage tank (TK-103). The overflow port was not only used for product removal but also to control the level at 1200 mL. Mettler Toledo Seven Compact S210 pH meter was used to measure the pH of the reactor content with time. The progress of the reaction was monitored by pH; steady state was reached once the pH remained constant or oscillated by no more than 0.2 units. Nitrogen was sparged into the reactor to displace CO_2 in order to prevent formation of calcium carbonate.

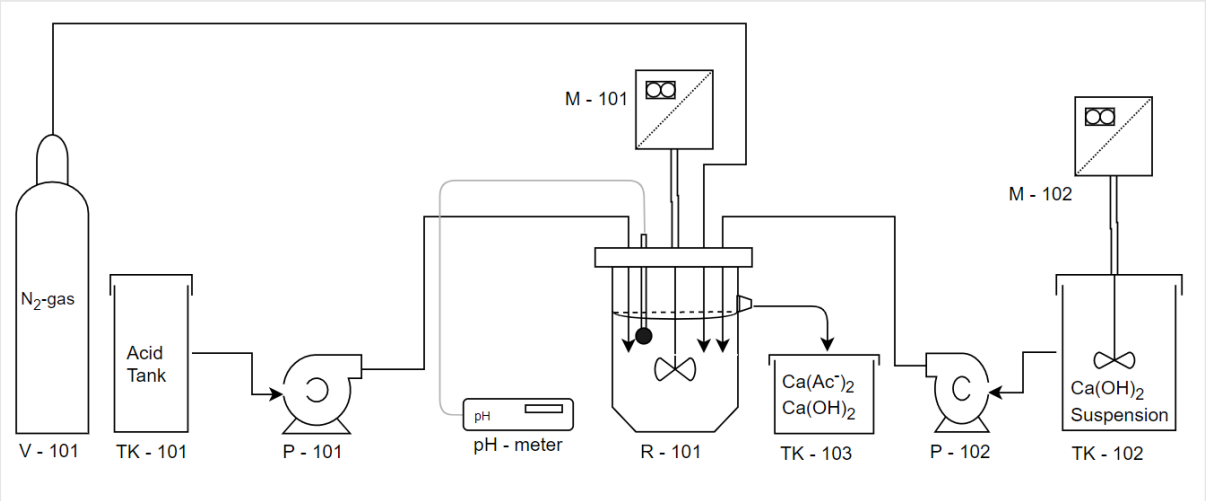

Figure 4.1: Experimental setup for overflow slurry CSTR

The advantages of the overflow CSTR system are as follows:

- Easy sampling procedure (it was sampled at the overflow port), the conversion in the reactor is the same as the conversion at the exit stream, assuming the volume of the exit pipe is negligible, and hence the further dissolution of $Ca(OH)_2$ particles while flowing through the exit pipe was negligible. It was also assumed that there were no concentration gradients.
- Easy to add $Ca(OH)_2$ as a suspension; the suspension was prepared by diluting the already existing milk of lime from industrial $Ca(OH)_2$ suspension.
- Easy addition of acid.
- Easy to control the volume by overflow.

The advantages listed above also apply to the jacketed CSTR and unjacketed CSTR set-ups except that these were used in experiments with a feed suspension prepared using reagent grade $Ca(OH)_2$ powder. Apart from these advantages, one major disadvantage of CSTRs is that one can obtain only one single data point from each steady state achieved under a given set of conditions.

Challenges and limitations in an overflow slurry CSTR system

The challenge that arose with the overflow slurry CSTR is as follows; the residence time was increased by decreasing the flow rate of acid streams (including DI water) while keeping the lime suspension constant. The reverse was done in order to decrease the residence time. Ideally the rate of acid (liquid) addition is expected to be the same as the rate of increase in the level of reactor content (or height of the liquid in the reactor) until the overflow is reached. In a homogeneous liquid system, the faster the rate of feed addition, the shorter the residence time. However, in a heterogeneous system, solid particles are likely to accumulate within the reactor vessels due to the difficulty of homogeneously suspending them in the vessel and effecting their overflow. Hence, to keep the reaction content at a specific residence time takes a significant amount of fine tuning of the feed flow rates and vessel agitation. In this set-up changing the residence time by changing the suspension flow rate was not effective due the accumulation of solids within the reactor vessel. This set-up could not allow the residence time below two minutes, the minimum residence time attainable was about 2 minutes, 20 seconds.

The constant temperature, controlled-outflow slurry CSTR

Residence time is a function of volume and through-put flow rate at steady state as shown in Appendix A (Equation A5). In the constant temperature, controlled-outflow slurry CSTR, it was desired to reduce the residence time in order to reduce the duration of experiments and also to reduce the amount of the acidic solution and $Ca(OH)_2$ used. This was achieved by reducing the volume of the reactor; 1.2L reactor was replaced by 400mL. The reactor did not have the overflow port therefore a rigid overhead silicon tube (connected to a peristaltic pump) was inserted as an exit stream. The silicon tube was adjusted up and down to increase and reduce the content volume of the reactor. The flow rate of the exit stream was controlled using a peristaltic pump. This allowed a more flexible operation with respect to the residence time

(content volume and exit flow rate). The hydrodynamics information from the batch reactor, feed conditions and feed stream ratios from the overflow slurry CSTR were applied. In this set-up, residence time was kept constant while investigating the effect of pH on the rate of the $Ca(OH)_2$ neutralisation. The pH was varied by using different concentrations of CH_3COOH at a constant residence time. Each acid concentration yielded a steady state pH which corresponded to a reaction rate at that point. At steady state, the conversion of the neutralisation reaction can be directly correlated to the rate of dissolution of $Ca(OH)_2$ particles via the extent of dissolution (see Section 5.11). This means that each run (experiment) yields only one data point. Even though this makes experimentation tedious, this approach provides a better control of residence time and thus determination of the steady state reaction rate.

The controlled-outflow slurry CSTR set-up

This was the improvement from the Overflow slurry CSTR system, 1.2L reactor was replaced by a marked or graduated 400 ml baffled glass reactor (R-101). The output silicon pipe was introduced as an exit stream; this was connected to 502S Masterflex Pump (P-103). The exit stream was used to remove the product and control the level to desired volume. Due to controlled volume and adjustable flow rate of exit stream, this setup controlled the residence time constant at 2 minutes.

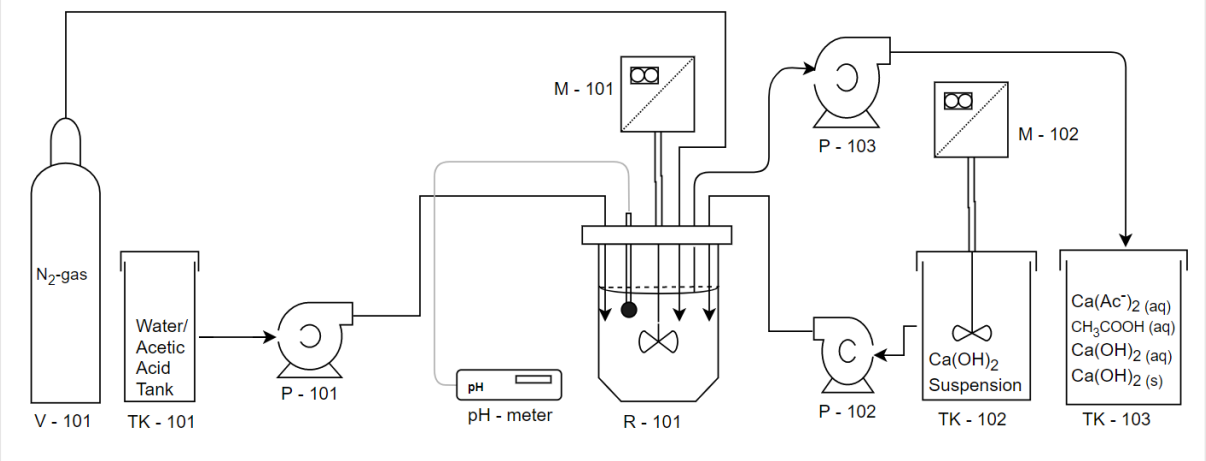

Figure 4.2: Baffled glass controlled-outflow slurry reactor

Challenges and limitations in an overflow slurry CSTR system

Relative to the overflow slurry CSTR, controlled-outflow slurry CSTR was efficient in terms of better control of residence time, the amount of the feed solutions and hence time to reach steady state. The only exception was that it had initial operational challenges, including the silicon tubing wearing out after as little as three runs, this was caused by pipe twisting and heating in the pump head mechanism. However, these technical difficulties were minimized by allowing the pump to cool off after few runs. The second challenge was the fact that the temperature was based on laboratory ambient condition (22 ˚C on average). Controlling the temperature was very essential as temperature was used to determine the Arrhenius activation energy from the change of reaction rate constants with temperature.

The thermostat regulated controlled-outflow CSTR

The challenges and limitations in the overflow slurry CSTR were rectified and improved in a slurry CSTR fitted with a heating jacket. Similarly, the limitations in unjacketed slurry CSTR were rectified and improved in this system. These improvements included the fitting of a more robust Master-flex tubes in the pump heads. A thermostat regulated bath and jacketed reactor were also used. Therefore, this is the relatively most advanced option when compared to other reactors.

The thermostat regulated controlled-outflow CSTR set-up

In this setup, 400 ml baffled glass reactor (R-101) was replaced with 400 ml jacketed glass reactor (R-101). The exit stream was kept at 300 ml mark for longer residence time (2 minutes), and it was lowered to 150 ml for shorter residence time (1 minutes). Nitrogen was sparged in TK-103 instead of R-101, this is because the effect of CO_2 is minimal in the reactor but more severe in the $Ca(OH)_2$ suspension tank.

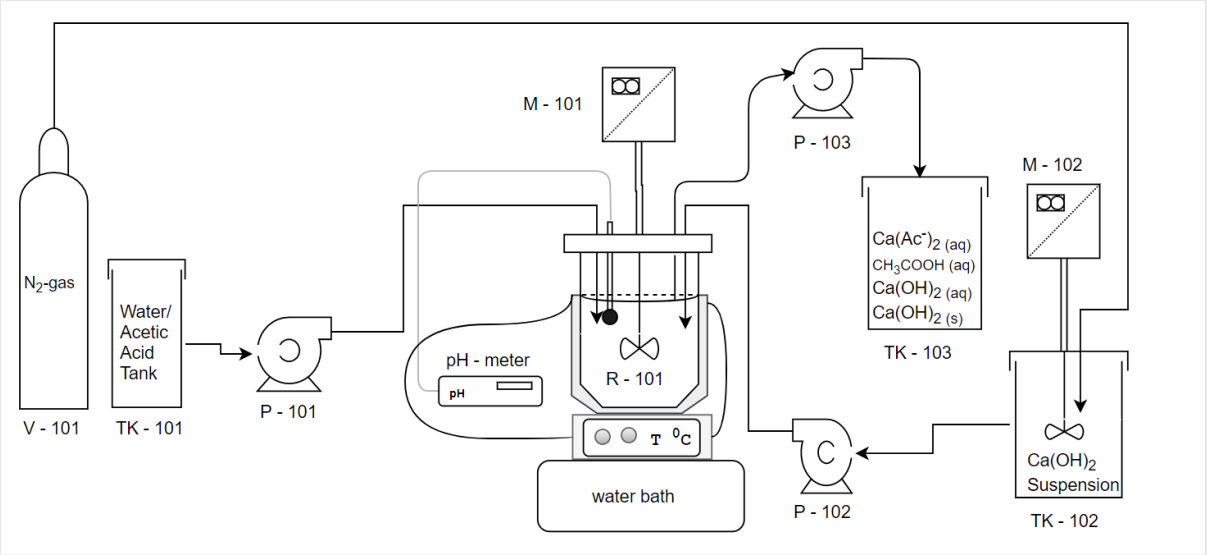

Figure 4.3: The thermostat regulated controlled-outflow slurry reactor

4.1.2 Measurements

Mixing

Effective mixing in the reactor (R-101) and in the $Ca(OH)_2$ suspension storage (TK-102) was done using IKA Digital RW20 overhead stirrer (M-101 and M-102). The rotation speed in R-101 was set to 600 rpm for the overflow CSTR, 1200 rpm for both the controlled-outflow slurry CSTR and the thermostat regulated controlled-outflow CSTR. To prevent settling of particles, TK-102 agitation rate was set to 750 rpm in all slurry CSTR set-ups.

Flowrates

Flowrates were determined by P-101, P-101 and P-102 (for 400 ml unjacketed slurry CSTR and 400 ml jacketed slurry CSTR). Pumps were calibrated for each concentration of acid and for each solid concentration.

pH measurement

The pH measurements were taken in TK-101 for every freshly prepared solution. This was done to confirm if the prepared solution reflected the expected pH as predicted by calculations

and OLI electrolyte modelling tool. The pH meter used for the batch system were a Metrohm 836 Titrando and GLP 21 Crison pH meter; fitted with Pt1000/B/2/3M KCl glass electrode for Metrohm 836 Titrando, and a specialized Pt 1000 for GLP 21 Crison pH meter. For slurry CSTRs, a Mettler Toledo Seven Compact S210 pH meter was used (including its electrodes). The pH meters were calibrated for each experiment due to the armouring nature of $Ca(OH)_2$ solution.

Temperature measurement

Temperature measurement for batch, the overflow slurry CSTR and 400 ml unjacketed glass reactor was not essential as these experiments were done at ambient temperature and pressure (25 ˚C and 1atm), however, a mercury thermometer was used to measure the temperature change consistently throughout each run. The temperature measurements were essential for a 400 ml jacketed slurry CSTR, therefore the IKA Digital RW20 thermostatic water bath was used to control temperature at 25, 35 and 45 ˚C.

4.2 Experimental procedure

4.2.1 Batch system

Before each run was conducted, the materials such as DI water and reagent grade $Ca(OH)_2$ powder were organised, weighed and measured. The electrodes were cleaned, and the pH meters were calibrated. Stainless steel baffles were placed into a clean glass reactor, and a 1.5L glass reactor was filled with the 1L DI water. The overhead stirrer was fitted and set to the desired stirring rate. 1.5g of reagent grade $Ca(OH)_2$ powder was added, then immediately the stirrer was switched on and simultaneously the stop watch. The samples were taken every five minutes (except for the first sample which was taken after two minutes after the experiment was started) using a syringe sampler fitted with 0.2-micrometers filter membrane. The sample was filtered and then the pH measured was taken before the sample was taken for dissolved calcium analysis. The first experiment was run for more than 24 hours to monitor the behaviour of the system with time, the samples were taken every five minutes for the first two hours, then taken every 30 minutes for 3 hours, then taken hourly for 12 hours then it was for overnight.

4.2.2 Overflow slurry CSTR system

The DI water, CH_3COOH solutions were prepared and stored in sealed glass bottles. The industrial $Ca(OH)_2$ suspension of desired solid concentration was prepared and stored in CO_2-free storage bucket (TK-102) achieved by bubbling nitrogen (See Figure 4.1). The industrial $Ca(OH)_2$ suspension storage bucket was sealed and stirred at 750 rpm to prevent particle settling. Silicon tubes on both acid and lime feed sides were connected from the storage tanks (TK-101 and 102) to the pumps (P-101 and 102) and then to the reactor (R-101). The acid solution pump (P-101) was then calibrated with a solution to be used (this was done before each run) then the desired flowrates were set. The pH electrodes were cleaned with dilute hydrochloric acid solution (0.1M HCl) and the pH meters were then calibrated. The nitrogen gas regulator was switched on (following safety procedure). The feed stream (acid and $Ca(OH)_2$ suspension) were filled with respective solutions, when all cautions were considered, the feed pumps were started simultaneously with the timer and pH meter. The time it took for the rector content to reach the overflow mark or the time it took for the first drop of the reactor content to be discharged was recorded, this was to be later confirmed by calculated residence time. The stirrer was started as soon as the impellor was submerged into the reactor content, it was then continuously increased (in order to prevent splashes) until 600 rpm was reached. All the experiments in this set-up were run at least 60 minutes. The pH was recorded as soon as the pH electrode got in contact with reactor content, this was then done every minute until the experiment was finished. The sample was taken every 15 minutes from the overflow or exit stream using Millipore disposable filter unit with 0.1-micrometre nylon membrane. The filtrate was analysed further for dissolved calcium. The membrane filter with the solid was dried under vacuum in a desiccator then captured particles were analysed for PSD analysis using nanoSEM.

4.2.3 The controlled-outflow slurry CSTR

The procedure in Section 4.2.2 was followed with the following exceptions: per-chloric acid replaced with CH_3COOH. For $Ca(OH)_2$ suspension, only 2% solid content was used. The outlet pump was calibrated and then balanced with other pumps to suit the desired rector content level (See Figure 4.2).

4.2.4 The thermostat regulated controlled-outflow slurry CSTR

The difference between the procedure in this section and 4.2.3 is usage of the thermo-regulated reactor. The temperature was set using a thermostatic water bath. The run time for experiments were shortened to 15 minutes since the residence times were also shortened. Nitrogen was sparged in TK-102 as opposed to being sparged in the R-101 (See Figure 4.3).

4.2.5 Dissolved calcium analysis methods

The aim of this subset of experiments was to determine a suitable dissolved calcium analysis method, and to determine the effect of AMD dominant species such as magnesium ions (Mg^{2+}), ferric cations (Fe^{3+}) and sulphate ions (SO_4^{2-}) on the selected method. In order to achieve this aim, varying concentrations of calcium standard solutions were prepared with increasing concentrations of magnesium ions (Mg^{2+}), ferric cations (Fe^{3+}) and sulphate ions (SO_4^{2-}). There were different methods that were attempted; however due to the time factor only two methods seemed promising, those are the complexometric ethylene-di-amine-tetra-CH_3COOH (EDTA) Erio-chrome black T (EBT) reverse titration and the OCPC colorimetric or spectro-photometric method.

The same experimental plan was followed for each method, the first test determined the integrity of the method without impurities, the second test was looking at the magnesium effect, the third test was looking at the sulphate and then last one was investigating the ferric cation effect. For the standard EDTA-EBT titration method, the procedures described in the Middle Tennessee State University Chemistry Department (2015) and University of Canterbury College of Science (2008) were modified to suit these experiments. For the o-cresolphthalein complexone colorimetric method, the procedures described in Pollard and Martin (1956) was followed with minor improvements or modification.

Experimental procedure for EDTA-EBT titration method:

The first step was to prepare a standard EDTA solution (0.01 M); this was done by weighing approximately 3.65 grams of disodium EDTA dehydrate and 0.1 grams of $MgCl_2$ (a small

amount of magnesium helps in making the endpoint of the titration very sharp) into a 1 L plastic bottle (because EDTA will leach out metal ions from soft glass containers). The bottle was filled to the mark with a 1 L DI water and then stirred vigorously with a magnetic stirrer until all the solids were dissolved.

A standard 100 ppm calcium solution was prepared by weighing 0.277 gram of calcium chloride ($CaCl_2$) on an analytical balance and then it was transferred to a 1 L beaker. Then a 25 mL of standard Ca^{2+} solution pipetted into a 250 mL Erlenmeyer flask. After that the pH was measured using a pH meter and then adjusted to 7 where necessary (using dilute sodium hydroxide solution for acidic samples and dilute HCl for basic samples). When the pH was approximately 7, 10 mL of 8.5M NH_3-NH_4Cl buffer was added (The buffer was prepared by dissolving NH_4Cl salt in ammonia solution). A 20 mL of DI water and 2-3 drops of the EBT indicator were added. The Ca^{2+} standard solution was then titrated with the EDTA solution until the colour changed from wine red, through purple, to a pure rich blue colour (the endpoint). The endpoint of the titration was compared to a reference sample made from 50 mL of DI water, 10 mL of 8.5M NH_3-NH_4Cl buffer, and 2– 3 drops of EBT indicator solution. The titration was performed in triplicate; the three titrations were within 0.08 mL EDTA volume difference. From the known mass of $CaCl_2$, and a 1:1 stoichiometry between the Ca^{2+} and the EDTA solution, the molarity of the EDTA solution was calculated. This was used in determining the molarity of the EDTA, based on the initial concentration of calcium used.

Similarly, as in the above procedure, the effect of magnesium ions (Mg^{2+}), ferric cations (Fe^{3+}) and the sulphate ions (SO_4^{2-}) were determined as follows; 5 mL of the calcium and species of interest standard solution was pipetted into a 250 mL volumetric flask and it was filled to the mark with DI water. Then a 50 mL aliquot of the Ca^{2+} solution (from the volumetric flask) was pipetted into a 250 mL Erlenmeyer flask. The pH was adjusted to 7 (where necessary). A 10 mL of 8.5M NH_3-NH_4Cl buffer, and 2-3 drops of the EBT indicator were added to the Erlenmeyer flask, following the same procedure as previous cases. Apart from the calcium chloride and the $Ca(OH)_2$, other chemicals that were used to prepare the samples include magnesium chloride, calcium sulphate and ferric chloride. The chlorides were selected because of their high solubility; calcium sulphate was used because of the common cation effect.

Experimental procedure for o-cresolphthalein complexone colorimetric method:

This method was developed in order to be used as the dissolved Merck calcium test kits for the Merck Nova 60 Spectroquant, however, the readings were not successful with the used test cells (results found were inconsistent). This method was then adopted and redeveloped for the JENWAY Model 6405 Spectrophotometer.

The first step was to prepare the reagents; the following is the list of the reagents used:

Standard calcium solution: An analytical-reagent grade calcium chloride in approximately 0.005 N hydrochloric acid, containing 100mg of calcium per litre. This was prepared by dissolving a 0.277g of $CaCl_2$ into a 0.005 M HCl solution (prepared by diluting a concentrated HCl {12.4 N}; then a 0.403 mL drop of a 12.4 N HCl into a 1 L Volumetric Flask, then filled to the 1000 mark with DI water).

Dilute ammonia solution: A mixture of 5% w/v of ammonia solution, specific gravity of 0.880, and 95 % v/v of water. This was prepared by adding 200 mL of concentrated ammonia solution (25%) into 1 L volumetric flask then filled by DI water to the mark.

Ammoniac buffer solution: A 0.75 % w/v solution of analytical-reagent grade ammonium chloride in dilute ammonia solution. This was prepared by adding 7.4g of NH_4Cl into the dilute ammonia solution (5%) prepared above.

o-Cresolphthalein complexone indicator solution: A 0.03 % w/v solution of o-cresolphthalein complexone (OCPC) in a mixture of 28 % v/v of buffer solution A and 72 % v/v of water. This was prepared by adding 0.075 g of OCPC in 250 mL volumetric flask, then 180 mL of water, and lastly 70 mL of ammoniac buffer solution prepared above to make it to the 250 mL mark (this solution was freshly prepared each day of experiment).

Procedure:

The first step was to generate a calibration curve using calcium only standard solutions (1, 2, 3 ppm etc.). This was done by increasing calcium concentration by 1 ppm until the concentration where the absorbance remained constant with the increase in calcium concentration. The influence of magnesium ions (Mg^{2+}), ferric cations (Fe^{3+}) and sulphate ions (SO_4^{2-}) was determined by generating calibration curves with standard solutions of varying

concentrations of magnesium, sulphates and ferric cations. This was done by investigating the ratio of each species to calcium cation.

A 5 ml portion of the sample was poured into the 100 mL volumetric flask. 25ml of ammonia buffer solution was added. The walls of the volumetric flask were washed with de-ionized water to about 90 mL (graduation mark) then the flask was carefully shaken to mix. Then eventually, 10mL of OCPC indicator solution was added to make up to 100 mL graduation mark, this resulted to the purple colour and pH of about 10.15. The correct amount was then poured into a cuvette and then the absorbance was measured at the wavelength of 575 nm (which was the optimum wavelength).

4.2.6 PSD analysis

As explained in section 4.1, PSD analysis plays a significant role in the kinetics of dissolution of $Ca(OH)_2$. It also is important for $Ca(OH)_2$ feed characterization as both powder and suspension. Therefore, samples for PSD analysis were taken before $Ca(OH)_2$ suspension was fed in the reactor (powder in case of the batch reactor), inside the reactor and after the reactor. However, for a CSTR at steady state, the reactor content conditions (including the PSD, assuming no dissolution un the exit stream) are the same as in the exit stream. As an additional step, the reactor product was quenched with 1-propanol to stop the $Ca(OH)_2$ dissolution however this did not work. The particles were therefore filtered immediately from the exit stream, assuming the PSD in the reactor is the same as the PSD in the exit stream. The samples for PSD analysis were taken for both the commercially prepared industrial $Ca(OH)_2$ suspension and freshly prepared reagent grade $Ca(OH)_2$ suspension. This was done for two reasons, mainly to check how reagent grade and industrial $Ca(OH)_2$ suspension particle characterization compared and also to characterize if a change in the concentration of the solids in the suspension (as the industrial $Ca(OH)_2$ suspension was diluted from 40% to 6% and 2%) would affect the PSD.

Sampling and sample preparation procedure for powder PSD analysis:

The samples were first analysed by Olympus Microscopy's analySIS software. In the Olympus optical microscopy, the powder sample specimens were placed on the rectangular glass sample

holder, then inserted in the measuring area. The PSD was then measured from the captured images using built-in Olympus Microscopy's image analysis software known as analySIS. The Olympus optical microscopy had limited resolutions hence SEM image analysis was adopted. The SEM analysis was preceded by the sample preparation, which is a mini-process and required careful consideration. The sample preparation for powder was done as follows: the SEM specimen stubs were covered with an adhesive gel then the dry powder specimens were stuck onto the stub and coated with conductive carbon paint. After that, the images were produced using SEM, due to the high degree of agglomeration noted on the images from the initial optical microscope and SEM analysis. Instead of using an adhesive gel, the powder particles were directly placed onto the double-sided sticky carbon tape however the resulting images were not clear due to charging. For PSD, the images were then analysed using a third party, Image J image analysis software which worked relatively better. Due to the irregularity of the particles, the shorter and longer distance measurements were used to come up with an effective PSD.

Sampling and sample preparation procedure for suspension PSD analysis:

The suspension samples were dewatered using small filtration unit, mounted with 0.1-micrometers nylon membrane. This was done in the presence of nitrogen to displace CO_2 ingress in the filtration unit funnel. The filtration unit funnel which was directly connected to the CSTR exit stream to immediately filter the solid before they could dissolve further. The filtered solids samples were then dried under vacuum in the desiccator at ambient temperature 22ºC to prevent the interference of CO_2. The dried solids samples were prepared and analysed using the same procedure as the one applied for powder analysis.

4.3 The $Ca(OH)_2$ dissolution rate expression derivation.

The aim of the rate expression development is to show the steps taken in establishing an expression that will suitably represent the dissolution of $Ca(OH)_2$ in acidic environment (or the link between $Ca(OH)_2$ surface disintegration and neutralisation of reaction between hydroxide ions and hydrogen release from CH_3COOH). Even though most of the lime dissolution kinetics have been conducted in batch and semi-batch systems, the rate expression proposed for this

study is from a CSTR system. Therefore, the rate expression explored incorporates CSTR system and established fundamental understanding of the CSTR mass balance were explored to derive an expression for the dissolution rate and extent of dissolution.

In principle, the rate of reaction is dependent on the concentration and temperature of the system, therefore as the starting point, the development of the proposed kinetic expression was based on the established relationship of the rate of reaction and reactants (or products) concentration and temperature. However other factors, such as specific surface area were explored. Three options were followed in determining the rate expression or correlation in terms of reactants or product concentration, temperature and specific surface area. The resulting rate expressions were solved using multiple linear regression.

4.3.1 The reaction rate in CSTR.

The general mole balance (for a species A) around a reactor is given as:

$$F_{A,in} - F_{A,out} + \int_0^V r_A \, dV = \frac{dN_A}{dt} \qquad \text{...: 4.1}$$

From the above general mole balance (Equation 5.3); for a perfectly mixed continuous stirred tank reactor (CSTR) at steady state, the rate of reaction in terms of concentration becomes:

$$r_A = \frac{v_{in}C_{A,in} - v_{out}C_{A,out}}{-V} \qquad \text{...: 4.2}$$

Where; v is the volumetric flowrate, $C_{A,in/out}$ is the concentration of specie A in and out of the CSTR, V is the reactor volume, r_A is the rate of reaction in terms of specie A, N_A is the number of moles of specie A, t is time and F_A is the molar flowrate of specie A.

The reaction rate (r_A) in the above Equation represents $Ca(OH)_2$ dissolution rate in mol/L.s. The values of $V(\text{in L}), v_{in}\ (\text{in } {}^{\text{L}}/_{\text{s}}), v_{out}\ (\text{in } {}^{\text{L}}/_{\text{s}})$ and $C_{A,in}$; $(\text{in } {}^{\text{mol}}/_{\text{L}})$ were determined from experimental data. $C_{A,out}$; $(\text{in } {}^{\text{mol}}/_{\text{L}})$; is the concentration of species A coming out of a reactor (which is at the same as concentration of A in the reactor at steady state). This concentration was determined using ICP-OES, then the Equation above was used to calculate the rate of $Ca(OH)_2$ dissolution. The calculated rate was used together with kinetic theory to develop the kinetic expression in terms of pH, temperature and the extent of reaction (surface area). The extent of dissolution is the fraction of the $Ca(OH)_2$ that is dissolved from the amount fed into the reactor as the Equation 5.5 below shows:

$$\chi = \frac{C_{A,in}v_{in} - C_{A,out}v_{out}}{C_{A,in}v_{in}} \quad \text{...: 4.3}$$

4.3.2 Basic kinetic theory.

There are several kinetic theories reported in literature, including Arrhenius Theory, Collision Theory and Transition State Theory (Connors, 1990). This section focuses on Arrhenius Theory. In general, the reaction rate is a strong function of reactant or product concentration and temperature; based on the Equation below:

$$r_A = k[A]^{\alpha}[B]^{\beta} \quad \text{...: 4.4}$$

In above equation, the reaction rate (r_A) is a function of the rate constant (k), and concentration of reactants A and B; letters (α) and (β) are reaction orders. If both (α) and (β) are unity then rate is first order with respect to reactant A and also first order with respect to reactant B. In principle, the overall reaction rate order is the sum of individual orders ($\alpha + \beta$); the rate is negative if expressed in terms of reactants and positive if it in terms of products. The rate constant (k) is a function of temperature and it is given by the Arrhenius Equation as shown below.

$$k = Ae^{-E/RT} \quad \text{...: 4.5}$$

The linearized version of the above Equation becomes:

$$\log k = \log A - \frac{E}{3.2RT} \quad \text{...: 4.6}$$

The temperature (T) of the reactor system is in Kelvin and (R) is the gas constant. The activation energy (E) is in J/mol., the empirical values of (E) can be determined from a straight-line plot of $\log k$ versus $^1/_T$. The magnitude of the activation energy determines the sensitivity of (k) to temperature; (A) is the frequency factor or pre-exponential factor with same units as (k) depending on the order of reaction. Similarly, as (E), the value of (A) can be estimated as the intercept of a straight-line plot of $\log k$ versus $^1/_T$. Fogler (2006) reported that there is no typical value, however it can be approximated to 10^{13} per second for most first order reactions. The Equation above implies that both (A) and (E) are temperature independent (Connors, 1990). However (k) is a strong function of temperature as shown in the Equation 5.7 below.

$$k(T_2) = k(T_1)\exp[^E/_R \left(\frac{1}{T_2} - \frac{1}{T_1}\right)] \quad \text{...: 4.7}$$

Similarly, as in equation 5.5 and 5.6; below is the linearized version of the Equation 5.7:

$$\log k(T_2) = \log k(T_1) + ^E/_R\left(\frac{1}{T_2} - \frac{1}{T_1}\right) \quad \text{...: 4.8}$$

The above Equation allows the determination of other rate constants choosing T_1 as a reference temperature. From above equations, the reaction rate is directly proportional to the rate constant, and the rate constant increases with the increase in temperature of the system. This means that the molecules in the system will have a higher kinetic energy which will allow them to overcome repulsion forces more easily, resulting in an increase in the reaction rate.

The value of activation energy is indicative of whether the reaction is diffusion or chemical reaction controlled. In principle, instantaneous or ultra-fast reactions have extremely low

activation energy. It is therefore intuitive that for a diffusion-controlled reaction, the activation energy is relatively small, according to Connors (1990) the typical range is 8.37 - 25.1 kJ/mol. of reactant. Above 25.1 kJ/mol., the rate can be influenced by both diffusion and reaction until about 40 kJ/mol. (which is a ball-park value). Beyond 40 kJ/mol., the rate said to be strictly reaction controlled. This is because for a bimolecular reaction between A and B to occur in a dilute solution, molecule A and B must contact or interact, the second requirement is that A and B must overcome the required minimum energy (activation energy) necessary to break steric and repulsion forces that exist between them in order to react. The rate of contact or interaction between A and B is dependent on the diffusion of A through the solution to B or vice versa. It has been established that the mixing time can be reduced to about 10 seconds using conventional mixing techniques (Connors, 1990). This can be achieved by increasing the stirrer speed or agitation rate to beyond diffusion-controlled region. Using the same approach, as detailed in chapter 4; it is possible to study if the reaction rate is chemical controlled.

Proposed rate expression derivation

From chapter 2, the equilibrium version of $Ca(OH)_2$ dissolution Equation is as follows:

$$Ca(OH)_2 \leftrightarrow Ca^{2+} + 2OH^- \quad \text{...: 4.9}$$

Therefore, the rate expression or rate law for the dissolution of $Ca(OH)_2$ is as follows:

$$r = k[Ca(OH)_2]^{\alpha} \quad \text{...: 4.10}$$

Using the equilibrium constant Equation; $K_{HA} = [Ca^{2+}][OH^-]^2/[Ca(OH)_2]$;

Such that $[Ca(OH)_2] = [Ca^{2+}][OH^-]^2/K_{HA}$

$$r = k\left\{\frac{[Ca^{2+}][OH^-]^2}{K_{HA}}\right\}^{\alpha} = k'[OH^-]^{2\alpha}[Ca^{2+}]^{\alpha} \quad ; \quad k' = \frac{k}{K_{HA}{}^{\alpha}}$$

In Equation 5.11 $\beta = 2\alpha$

$$r = k'[OH^-]^{\beta}[Ca^{2+}]^{\alpha} \quad \text{...: 4.11}$$

The rate, r, represents the rate of dissolution of $Ca(OH)_2$ ($-\frac{d_{Ca(OH)_2}}{dt}$) in mol/s. As discussed above, the rate is mostly a function concentration of reactants and temperature; however other factors such as total pressure in cases of gaseous phase reactions. In a liquid phase reaction, ionic strength and dielectric constant may also influence the rate of reaction. In the case of $Ca(OH)_2$ dissolution, there are additional factors such as particles surface area and or diameter (Carr, 2007). Therefore, the rate expression can be expanded as follows;

$$r = f\{T, [Ca(OH)_2], \dots, \text{other quantities}\} \quad \dots: 4.12$$

Dissolution of solid particles is a strong function of a dissolving particle surface area or size. Ideally, the rate of dissolution is directly proportional to the specific surface area and indirectly proportional to the particle's diameter (Carr, 2007). It has been established by studies such as Furrer & Stumm (1986) and Zinder *et al.* (1986) that the dissolution kinetics of sparingly soluble oxides is controlled by chemical reactions at the surface of the dissolving particle. Apart from the rate equation in terms of the concentrations of the reactants or product (and by proxy temperature due to the relationship of temperature with the rate constant). According to Carr (2007) and Coker (2001), the rate law can be expressed in terms of specific surface area and temperature as independent terms (see the derivation below).

$$r \propto [Ca(OH)_2]^{\alpha} \quad \dots: 4.13$$

Similarly, as in above cases, rate Equation can be also expressed in terms of products as follows;

$$r \propto [Ca^{2+}]^{\alpha}[OH^{-}]^{\beta} \quad \dots: 4.14$$

Furthermore, the rate of dissolution is proportional to the specific surface area and temperature. Therefore, the general rates can be as follows;

$$r \propto [Ca^{2+}]^{\alpha}[OH^{-}]^{\beta}A_s{}^{\gamma}$$ ...: 4.15

The exponents α and β are orders with respect to calcium and hydroxide ion concentration but γ is an empirical exponent that relates to the change of the $Ca(OH)_2$ particles specific surface area A_s (which is by proxy related to the shape of the particles and their size distribution).

$$r = k_r[Ca^{2+}]^{\alpha}[OH^{-}]^{\beta}A_s{}^{\gamma}$$ ...: 4.16

Equation 4.16 is a general rate expression for the dissolution of $Ca(OH)_2$ in DI-water. In this study pH-dependent Ca(OH)2 dissolution tests were investigated in acetic acid solutions. Therefore an overall reaction for the dissolution of $Ca(OH)_2$ in acetic acid is as follows (See Equation 4.17).

$$\mathrm{Ca(OH)_2 + 2HAc \leftrightarrow Ca(Ac)_2 + 2H_2O}$$ ...: 4.17

The liquid phase reaction can be broken down into the following steps;

$$\mathrm{Ca(OH)_2\ (aq) + H^+\ (aq) \leftrightarrow CaOH^+\ (aq) + H_2O\ (aq)}$$ ...: 4.18

$$\mathrm{CaOH^+\ (aq) \leftrightarrow Ca^{2+}(aq) + OH^-\ (aq)}$$ ...: 4.19

$$\mathrm{HAc\ (aq) \leftrightarrow Ac^-\ (aq) + H^+\ (aq)}$$ ...: 4.20

$$\mathrm{Ca^{2+}(aq) + Ac^-\ (aq) \leftrightarrow CaAc^+\ (aq)}$$ ...: 4.21

$$\mathrm{CaAc^+\ (aq) + Ac^-\ (aq) \leftrightarrow Ca(Ac)_2\ (aq)}$$ ...: 4.22

$$\mathrm{OH^-\ (aq) + H^+\ (aq) \leftrightarrow H_2O\ (aq)}$$ ...: 4.23

The dissolution of $Ca(OH)_2$ can be characterized by the release of calcium and hydroxide ions from the solid $Ca(OH)_2$ particles to the bulk solution. On the other hand, the pH of the system is determined by the concentration of acetic acid fed into the reactor. Therefore, the pH is represented by concentration of protons and or hydroxide ions in the bulk solution. This means that the proposed $Ca(OH)_2$ dissolution rate expression can be expressed as a function of calcium concentration and the pH (proton concentration).

$$r = k_r(T_1) = k_r(T_0)\exp\left\{E/_R\left(\frac{1}{T_1} - \frac{1}{T_0}\right)\right\}[Ca^{2+}]^{\alpha}[H^{+}]^{\beta} \quad \text{...: 4.24}$$

The calcium concentration and the pH were measured variables from the experiments while the parameters k_r , α and β were determined empirically from the experimental data, using goal-seek function in Microsoft Excel.

Chapter 5: Results and discussion

This chapter is divided into four sections; the first two sections (Section 5.1 and 5.2) deal with PSD analysis and dissolved calcium assays. The final two sections (Section 5.3 and 5.4) comprises the preliminary experiments results and rate determination experiments results. The preliminary results comprise hydrodynamics studies in the batch system, overflow slurry CSTR and ambient-temperature controlled-outflow CSTR. The main dissolution rate section consists of results for the thermostatic controlled-outflow CSTR.

Section 5.1 and 5.2 report results on the critical analysis (such as PSD analysis and dissolved calcium assays) that will be suitable for the $Ca(OH)_2$ dissolution rate in an acidic environment and synthetic AMD. The PSD analysis of the reactor content (as the reaction time lapses) is important as it can be used as a measure of $Ca(OH)_2$ particle size reduction with time (which is complimentary in tracing kinetics). Dissolved calcium assays were necessary for reliable rate calculations as they are indicative of the increase or decrease of calcium cations in the bulk solution with time.

Section 5.3 (the preliminary results) included results of the effect of the stirring rate experiments which were done in the batch system. Section 5.3 also covers the discussion of the results for the overflow slurry CSTR and ambient-temperature controlled-outflow CSTR. The results for the steady-state pH determination, the effect of changing the residence time, the effect of the dosage or solid density, the effect of a strong acid, and the number of residence times it took both the H_2O-$Ca(OH)_2$ and $HClO_4$-$Ca(OH)_2$ system to reach the steady-state were all generated in the overflow slurry CSTR. The results for investigating the effect of using a weak acid (CH_3COOH-$Ca(OH)_2$ system) were generated using ambient-temperature controlled-outflow CSTR.

The ambient-temperature controlled-outflow CSTR yielded better results than all previous set-ups, furthermore weak acid, CH_3COOH-$Ca(OH)_2$ system allowed a moderate kinetic study-friendly dissolution when compared to the rapid dissolution observed in a relatively strong acid, $HClO_4$-$Ca(OH)_2$ system. However, this was only limited to ambient conditions (22°C),

and therefore temperature-dependent rate parameters such as activation energy and rate constant could not be calculated using this set-up. Due to the limitations of the ambient-temperature controlled-outflow CSTR, the jacketed thermostatic controlled-outflow slurry CSTR was introduced.

The jacketed thermostatic controlled-outflow slurry CSTR allowed the investigation of the effect of temperature (at 25°C, 35°C and 45°C) and the calculation of activation energy and rate constants. Section 5.4 therefore covers the dissolution of $Ca(OH)_2$ in DI-water and CH_3COOH in details. DI-water was used as a reference solution for comparison purposes, while CH_3COOH solutions (0.02 M, 0.04M and 0.125M) were used for the main dissolution reaction study. This is achieved by looking at the relationship between the pH, temperature and the concentration of calcium cations in bulk solution. Eventually, the rate of reaction was calculated and studied as a function of pH and temperature at the constant residence time.

5.1 The PSD analysis

5.1.1 Reagent grade $Ca(OH)_2$ powder PSD analysis

After realising that vibrating screens and optical microscopy (to some degree) were not suitable for the PSD analysis of the reagent grade $Ca(OH)_2$ powder, SEM images were analysed using third party ImageJ image analysis tool. The additional advantages of using SEM Image analysis for PSD is that it also gives information on the shape and morphology of the particles. Figure 5.1 and Figure 5.2 show two different snapshots of the same specimen of the reagent $Ca(OH)_2$ powder sample.

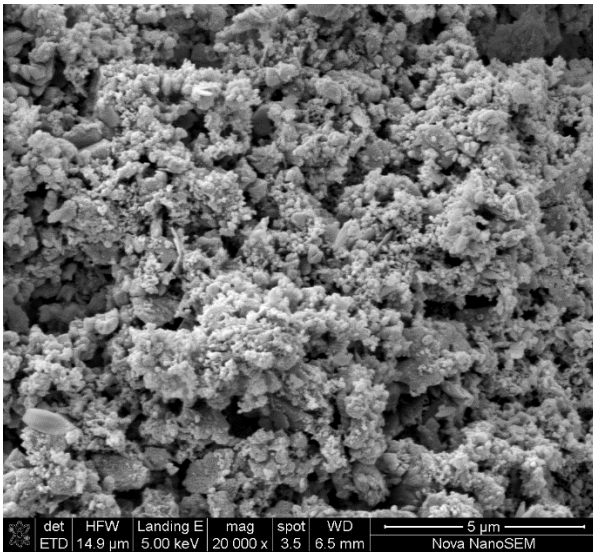

Figure 5.1: Reagent grade $Ca(OH)_2$ powder SEM image specimen 1

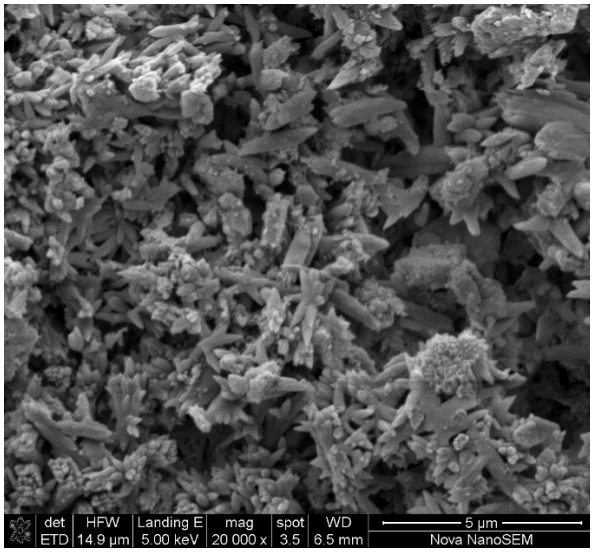

Figure 5.2: Reagent grade $Ca(OH)_2$ powder SEM image specimen 2

Figure 5.1 consists of small and big particles; the small particles are fluffy and big particles are irregular in shape. In contrast, Figure 5.2 comprises mostly big, columnar and acicular (needle-like) particles; in the same figure, the small fluffy particles resemble those in Figure 5.1. The small fluffy particles in both figures match the description of $Ca(OH)_2$ particles as described by Oates (1998) and Boynton (1980). Boynton (1980) claims that most authors confuse the fluffiness of the particles with being amorphous, which is not the case. Similar to Boynton, Oates (1998) agrees that the fluffiness is due to the micro-crystallinity of the colloidal sized or submicron particles. To confirm this, submicron particles in both Figure 5.1 and Figure 5.2 would need further magnification for effective PSD, shape or morphology analysis; it has been shown in studies such as that by Tadros et al. (1976) that the shape of submicron $Ca(OH)_2$ particles is in fact that of a hexagonal prism (see Figure 5.3 and Figure 5.4). Figure 5.3 shows SEM micrographs of primary particles of $Ca(OH)_2$; Figure 5.4 shows the same particles after growing for 90 minutes. The similarities between particles in Figure 5.1 and Figure 5.2 and those in Figure 5.3 are not obvious because images in Figure 5.1 and Figure 5.2 are at lower resolution; furthermore, particles in these figures are finer because the powder has been pulverised from larger crystals during manufacture. In Figure 5.4, some crystals are not perfectly hexagonal prismatic but pseudo-hexagonal prismatic as explored by Galan et al. (2015).

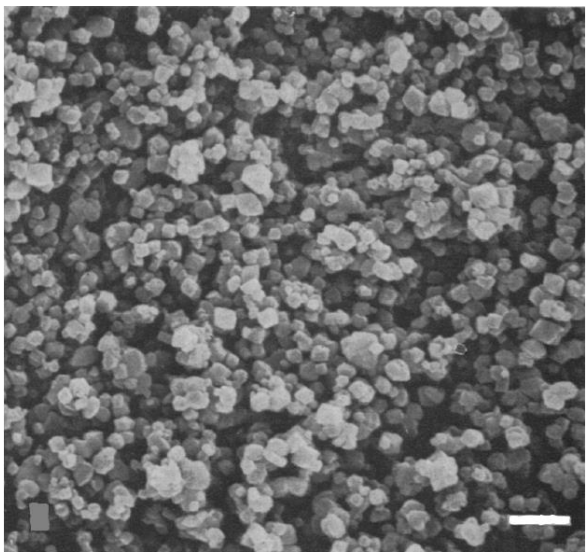

Figure 5.3: SEM micrograph of $Ca(OH)_2$ primary seed crystals from ; white bar is 2µm. Image from Tadros et al. (1976)

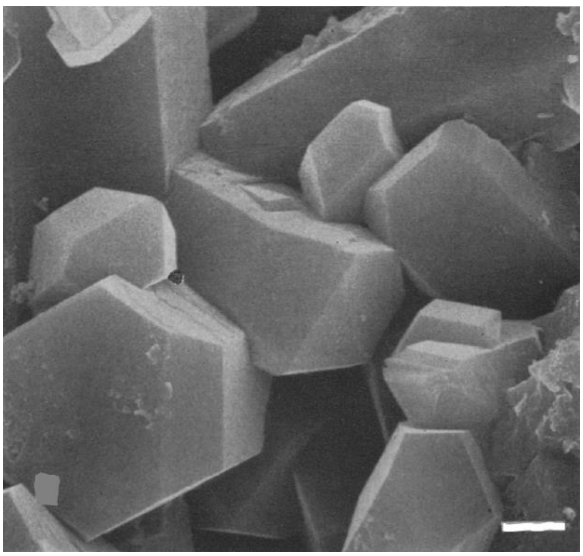

Figure 5.4: SEM micrograph $Ca(OH)_2$ crystals after 90 minutes of growth; white bar is 2µm. Image from Tadros *et al.* (1976)

The individually columnar and acicular shaped (but collectively dendritic or branched) particles in Figure 5.2 resemble calcium carbonate crystals, especially those of aragonite form or shape (Ridgley, 2016). Due to $Ca(OH)_2$ hygroscopicity in powder form, it absorbs CO_2 from the atmosphere, forming calcium carbonate (aragonite). Ideally, the more stable form of calcium carbonate is calcite. Also, it has been shown and reported by authors such as Ikornikova (1973) and Burival (2016) that calcite has differing shapes, depending on the factors such as pressure, temperature and impurities. However, the observed crystallographic structure in Figure 5.2 is that of aragonite. According to Ridgley (2016), aragonite is a structurally non-identical twin of calcite; it crystallises to an elongated three-sided orthorhombic prism contrary to trigonal rhombohedral crystal form for calcite. It is not clear if it was formed during the SEM specimen preparation or powder sampling. However, according to Galan et al. (2015) shapes like those displayed in Figure 5.2 were formed under 100% CO_2 atmospheric conditions. As reported by Galan et al. (2015), exposing $Ca(OH)_2$ particles to a100% CO_2 atmosphere results in the formation of both calcite and aragonite particles of which aragonite's columnar and acicular structures are found to be dominant. This, therefore, suggest that the interference with CO_2 most likely occurred during powder sampling. Figure 5.5 shows the pictorial formation of aragonite crystals as published by Ridgley (2016).

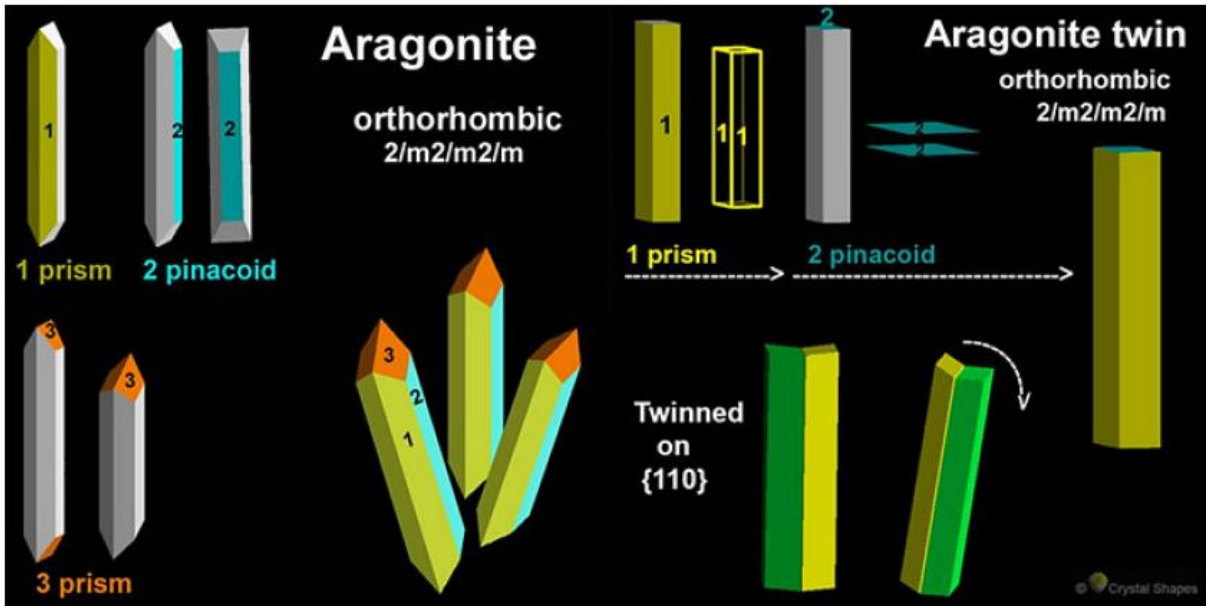

Figure 5.5: The twinning growth of three individual crystals of aragonite; drawing by Crystal Shapes as published in (Ridgley, 2016)

5.1.2 Laboratory prepared vs commercial prepared suspension

There were two main reasons the PSD of laboratory prepared suspension and industrially prepared suspension were thoroughly analyzed. Firstly, was to characterize the size and shape of particles fed into a reactor to monitor the progress of dissolution through size reduction. The second reason was to determine which $Ca(OH)_2$ suspension was suitable for the main kinetics of dissolution of $Ca(OH)_2$ studies. It was desired that the particles be of the regular shape, uniform size or at least of narrow PSD. Due to the limitations of the other techniques in determining the PSD of the $Ca(OH)_2$ suspension, PSD was determined using image analysis of SEM images. After filtration and drying of filtered particles, images were taken by SEM and then analyzed as shown in Figure 5.6 and Figure 5.7.

Based on the arguments made in Section 5.1.1, SEM images in Figure 5.6, showed that the suspension prepared by reagent grade $Ca(OH)_2$ powder comprises hexagonal prismatic submicron crystals. Submicron crystals co-exist with what seems like colloids or re-precipitated smaller particles. The initial PSD is expected to be even wider than it is in Figure

5.1 and Figure 5.2. As expected, the submicron particles resemble those in Figure 5.3, this is because during the preparation of the suspension CO_2 was prevented by bubbling nitrogen gas.

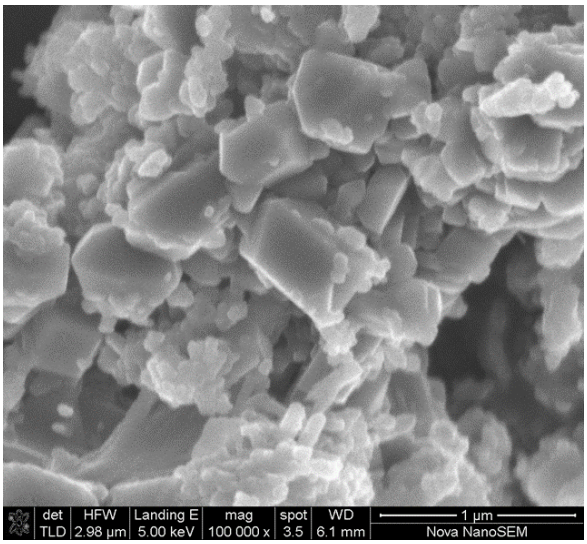

Figure 5.6: 2% solid content reagent grade (Merck) $Ca(OH)_2$ suspension SEM image

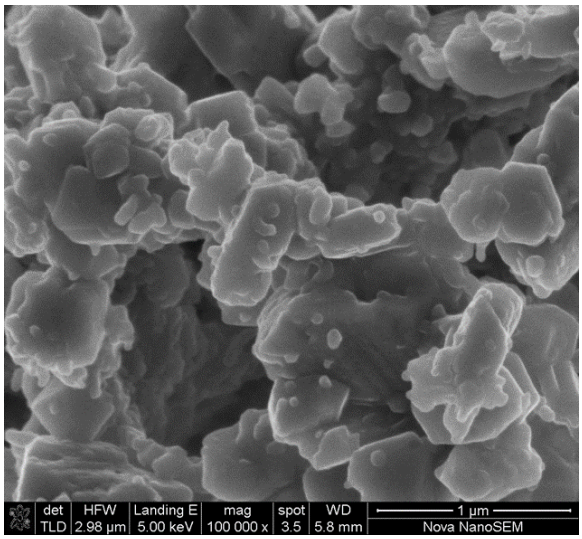

Figure 5.7: 2% solid content industrial (Lhoist) $Ca(OH)_2$ suspension SEM image

Both Figure 5.6 and Figure 5.7 show that the materials are comprised of relatively bigger particles and relatively smaller particles (submicron). This is consistent with particle properties published by Boynton (1980) and Oates (1998). The smaller particles are likely primary particles and bigger particles are agglomerates formed by micro-crystalline primary particles. According to Boynton (1980) and Oates (1998), the shape of the micro-crystalline particles is a hexagonal prism, however, this claim cannot be supported using the images in Figure 5.6 and Figure 5.7. Bigger particles in Figure 5.6 resemble the hexagonal prism; the edges (corners) are sharper. The bigger particles in Figure 5.7 have no definable shape, this may be due to the abrasion and friction between particles and water molecules and between particles themselves. This is likely because the 20% industrial $Ca(OH)_2$ suspension from which the 2% solution was prepared had been stored as a suspension for a long time, whereas the reagent grade $Ca(OH)_2$ suspension was freshly prepared from powder. Figure 5.6 and Figure 5.7 show that there are mostly larger particle co-existing with small particles, this means that the smaller particles are likely to dissolve first.

5.1.3 The results for reagent grade $Ca(OH)_2$ powder PSD analysis

The PSD of the reagent grade $Ca(OH)_2$ powder from Figure 5.1, Figure 5.2 and Figure 5.6 is expected to be very wide because of the co-existence of the relatively small and relatively big particles. Figure 5.8 shows the SEM micrograph of the reagent grade $Ca(OH)_2$ powder, representing the powder fed to the batch system as well as the powder used to make the reagent grade $Ca(OH)_2$ suspension fed to the thermostatic slurry CSTR.

As shown in this figure, the particles have varying sizes and different shapes which makes it difficult to analyze the PSD using the ImageJ image analysis tool. Similarly, as in Figure 5.1, Figure 5.2 and Figure 5.6, the co-existence of the relatively small and relatively big particles is noticeable. Therefore, the small particles were analyzed separately from the big ones. Also, because of the irregular shape of the bigger particles, the PSD was analyzed in terms of both the width and length of particles. The width represents the shorter diameter and the length for the longer. As shown in Figure 5.9, the mean size for smaller particles was found to be 0.15 micrometers. From the cumulative plot, we can deduce that 71% of the particles are less or equal to 0.15 micrometers. These particles are in the submicron or colloidal range. These are therefore expected to dissolve very rapidly because of the higher specific surface area, which means that there is more interaction between the solid surface and the solvent or solution.

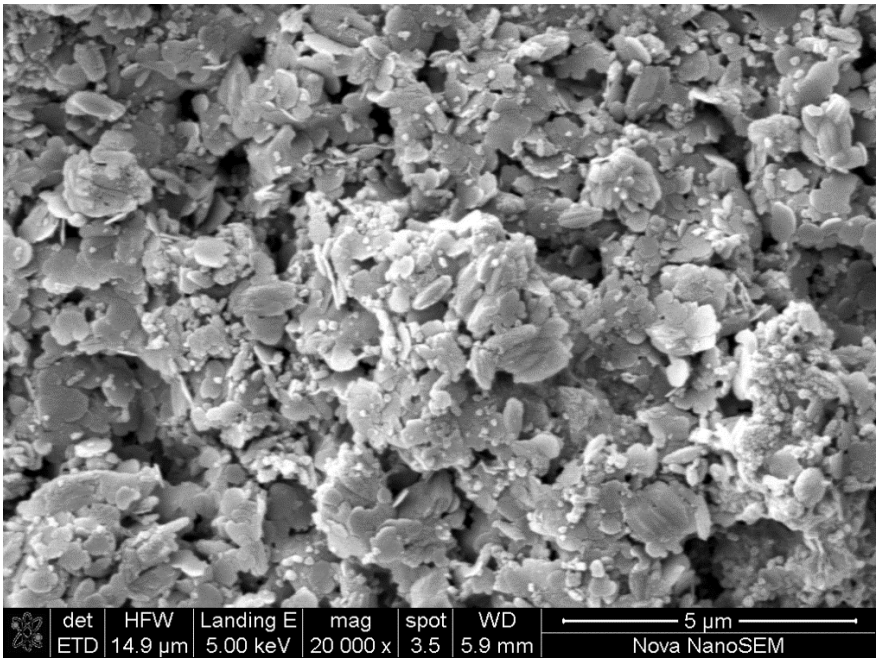

Figure 5.8 SEM micrograph showing the reagent grade $Ca(OH)_2$ powder used for PSD analysis, the measuring bar is 5 µm.

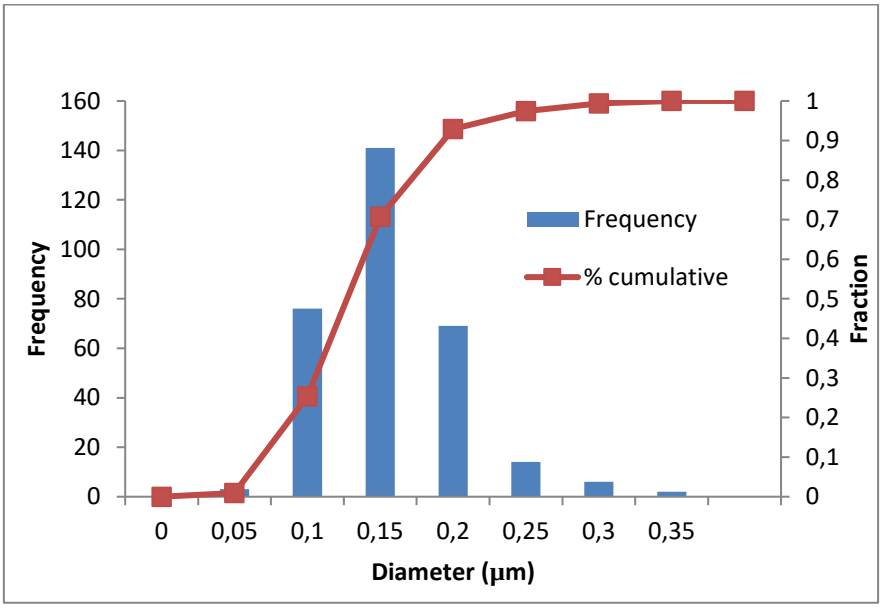

Figure 5.9: The PSD analysis for smaller particles in Figure 5.8

In Figure 5.10 and 5.11, the mean size for the bigger particles is 0.3 micrometers in terms of the width (Figure 5.10) and 1.75 micrometers in term of the length (See Figure 5.11). Even though this analysis provides information on the initial PSD, it was not useful for tracing the

dissolution of $Ca(OH)_2$ particles in the context of this study. This was because of the wider PSD, which means that all the smaller particles dissolved completely. For this technique to work, the particle size must be uniform or of a narrow size range. However, the same technique is applicable for $Ca(OH)_2$ suspensions or reactor content (Figure 5.6 and Figure 5.7) and could be very useful for future studies with a controlled narrow or uniform size range.

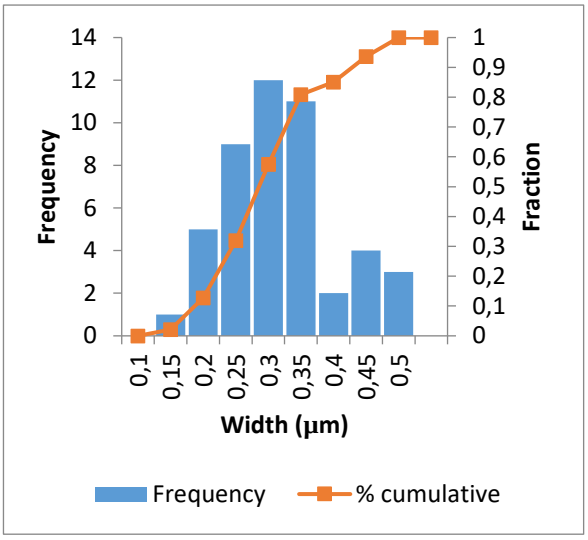

Figure 5.10: The PSD analysis in terms of the width of the bigger particles in Figure 5.8.

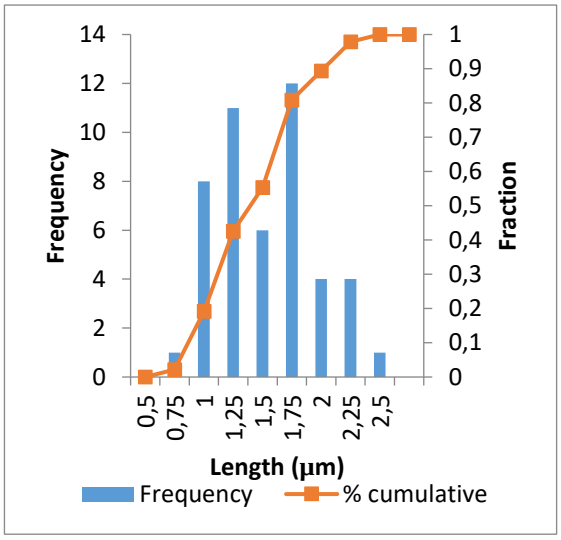

Figure 5.11: The PSD analysis in terms of the length of the bigger particles in Figure 5.8.

5.1.4 The PSD analysis results for CSTR content or exit stream

DI-water-reagent grade $Ca(OH)_2$ suspension system:

The PSD analysis of the feed ($Ca(OH)_2$ powder for batch or suspension for CSTR) was easily obtained because of accessible sampling, however, the sampling for reactor content at the exit stream was difficult. Figure 5.12 shows the SEM image of indistinguishable $Ca(OH)_2$ particles, in this figure colloidal $Ca(OH)_2$ particles clog the nylon membrane pores. Figure 5.13 shows the SEM image of the nylon membrane without particles. Comparing Figure 5.12 and Figure 5.13, it can be deduced that what seems like bigger particles is, in fact, an agglomeration of smaller particles. The agglomeration process was likely enhanced by filtration, as smaller particles were pressed against one another and against the filter membrane because of the

suction pressure. This becomes clear in the zoomed SEM images, see Figure 5.14, Figure 5.15 and Figure 5.16.

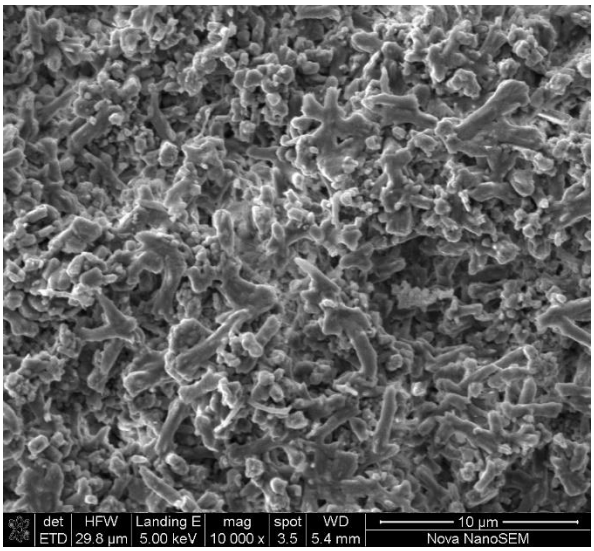

Figure 5.12: SEM image showing indistinguishable $Ca(OH)_2$ particles covering the surface of a nylon filter membrane. Scale bar = 10 microns.

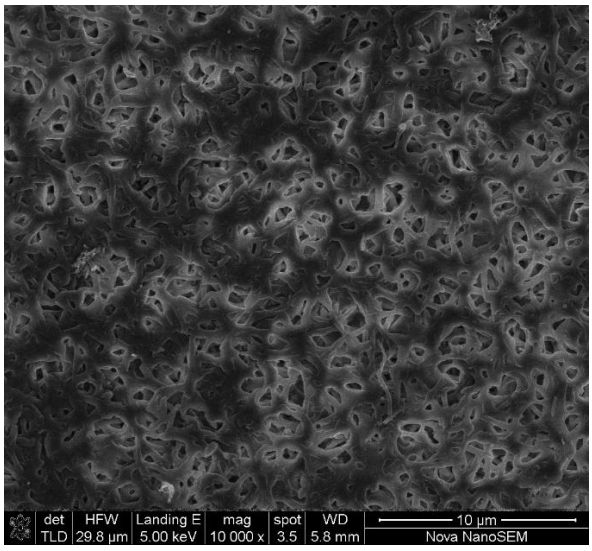

Figure 5.13: SEM image of a nylon filter membrane without $Ca(OH)_2$ particles at the same magnification as Figure 5.12. Scale bar = 10 microns.

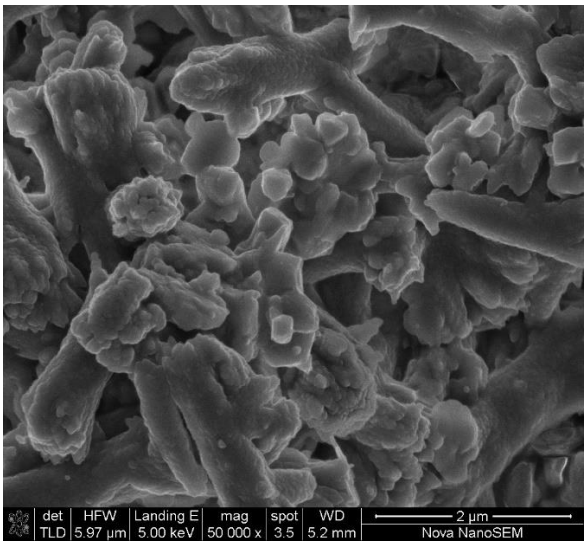

Figure 5.14: SEM micrograph for a DI-water-$Ca(OH)_2$ system at 25 °C , taken at the slurry CSTR exit stream. The scale bar is 2 microns.

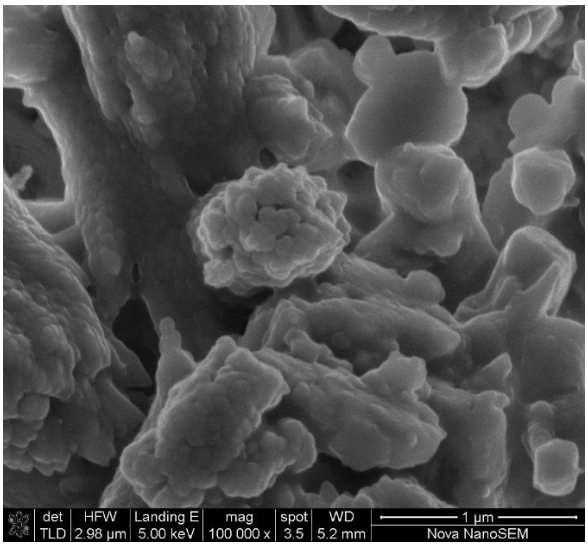

Figure 5.15: Zoomed image of Figure 5.15 taken at 2x Figure 5.14 magnification. The scale bar is 1 micron.

Figure 5.14 and Figure 5.15 show the SEM images for a DI-water-reagent grade $Ca(OH)_2$ suspension system specimen of a sample taken at the slurry CSTR exit stream. Figure 5.14

consists of a few smaller particles that look like dissolved hexagonal prismatic submicron crystals (see Figure 5.15). In Figure 5.15, the surfaces of the nylon filter membrane seem like agglomerates because of the colloidal particle's attachment. When compared to the feed suspension or inlet particles (in Figure 5.6 and Figure 5.7), it is noticeable that most of the finer particles would have been dissolved in Figure 5.14.

In summary, these images were hard to use for PSD analysis, because at lower magnification (less than 50 000x), the particles were indistinguishable (Figure 5.12). At higher magnification (more than 50 000x) only a few particles were scanned per SEM image. While this is possible, it would be very costly and cumbersome as it would require the analysis of more than 50 SEM images sampled and scanned under the same conditions.

Acetic acid-reagent grade $Ca(OH)_2$ suspension system:

Figure 5.14 shows the SEM micrographs for two samples taken at the slurry CSTR exit stream, the image with a scale bar of 5 microns was for a 0.1 M CH_3COOH-H_2O system at 25 °C, at the residence time of 1.85 minutes. The image with a scale bar of 2 microns was for a 0.125 M CH_3COOH-H_2O system at 25 °C, at the residence time of 1.85 minutes. The filtration media was 0.22 micrometer nylon membrane. In Figure 5.16, the images of the CSTR exit stream particles (Figure 5.16). Figure 5.17 and Figure 5.18 show that the particles captured were further apart for effective PSD analysis, especially at the desired magnification. As mentioned in the case of the DI-water- $Ca(OH)_2$ system, the scanned particles in the SEM image are far less than the required number of 500 particles for effective analysis (Vigneau, et al., 2000).

According to Vigneau *et al.* (2000), the Kolmogorov–Smirnov statistically determined minimum number of particles for effective PSD analysis is 500; this was further validated by Souza and Menegalli (2011) using three different statistical methods. Therefore, the effective analysis for the CSTR exit stream would require at least 6 quality SEM images per each 100 particles sample specimen (Souza & Menegalli, 2011). This had to be sampled under the same conditions as described in Chapter 4 (Section 4.2.6). The quenching of the reactor content (with alcohol) to stop dissolution reaction did not work; however, the reactor content was filtered immediately as it left the reactor because in a CSTR the content of the exit stream is same as the reactor content.

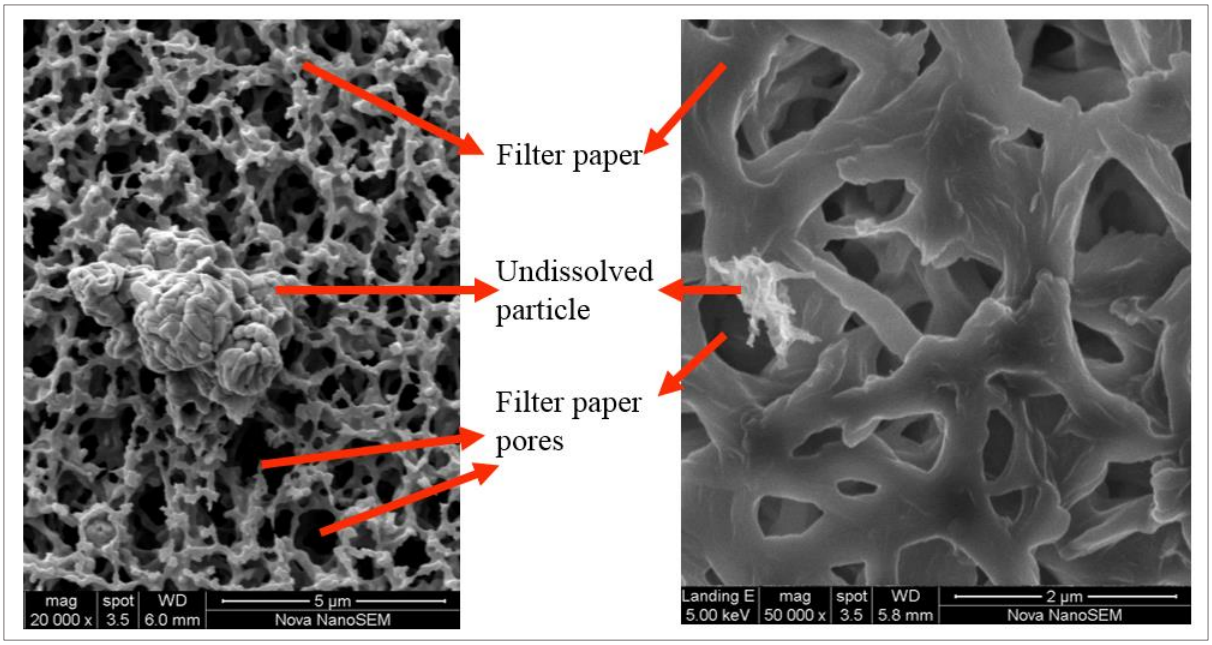

Figure 5.16: SEM micrographs for two samples taken at the slurry CSTR exit stream, the image with a scale bar of 5 microns was for a 0.1 M CH_3COOH-H_2O system at 22 °C, at the residence time of 1.85 minutes. The image with a scale bar of 2 microns was for a 0.125 M CH_3COOH-H_2O system at 25 °C, at the residence time of 1.85 minutes. The filtration media is 0.22 microns nylon membrane.

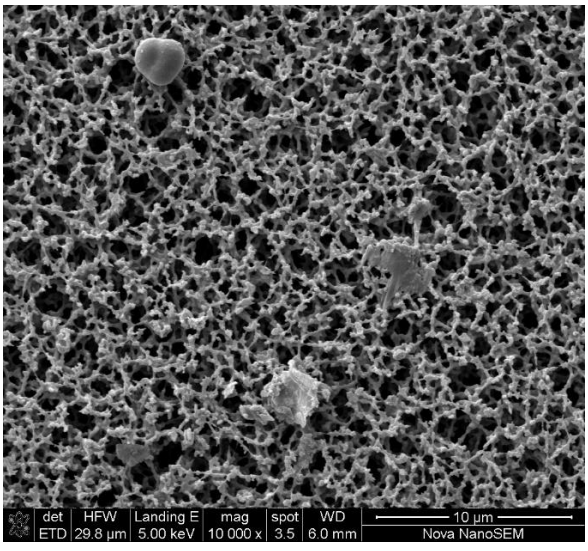

Figure 5.17: SEM image for a 0.1 M HAc-H_2O system at 25 °C, the scale bar of 10 microns.

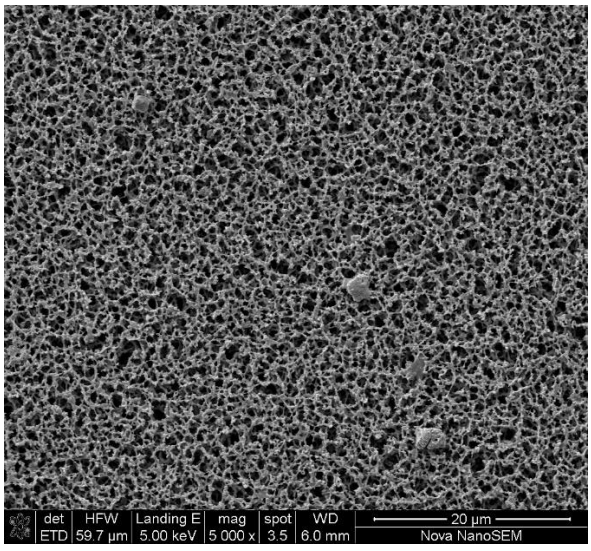

Figure 5.18: Zoomed out SEM image for a 0.1 M HAc-H_2O system at 25 °C, the scale bar of 10 microns.

5.2 The dissolved calcium analysis

After exploring the limitations of the other dissolved calcium analysis wet methods, the OCPC method was compared to the standard EBT-EDTA – Reverse Titration (complexometric titration) method. Both methods were tested under the same conditions, however the calcium concentration ranges were different because each method worked at different levels of concentration. Four systems (liquid mixtures) were tested using for both methods (OCPC method and EBT-EDTA – Reverse Titration (complexometric titration) method), that is $CaCl_2$-H_2O system ('Pure' calcium system), $MgCl_2$ - $CaCl_2$ - H_2O system (Mg^{2+} effect), $CaSO_4 \cdot 2H_2O$-$CaCl_2$ - H_2O system (SO_4^{2-} effect) and $FeCl_3$ - $CaCl_2$ - H_2O system (Fe^{3+} effect).

o-Cresolphthalein Complexone method

$CaCl_2$-H_2O system ('Pure' calcium system):

Figure 5.19 shows the OCPC Method Calibration Curve for $CaCl_2$-H_2O system. In this figure, the absorbance of light at the optimal wavelength of 575 nm is plotted as a function of dissolved calcium concentration in $CaCl_2$ standard solutions. There are two plots in this figure, that is the relative calibration plot and the absolute calibration plot. The relative calibration curve shows the absorbance values, subtracting the absorbance of the blank solution. The Absolute calibration curve shows the original values as they were read directly from the spectrophotometer.

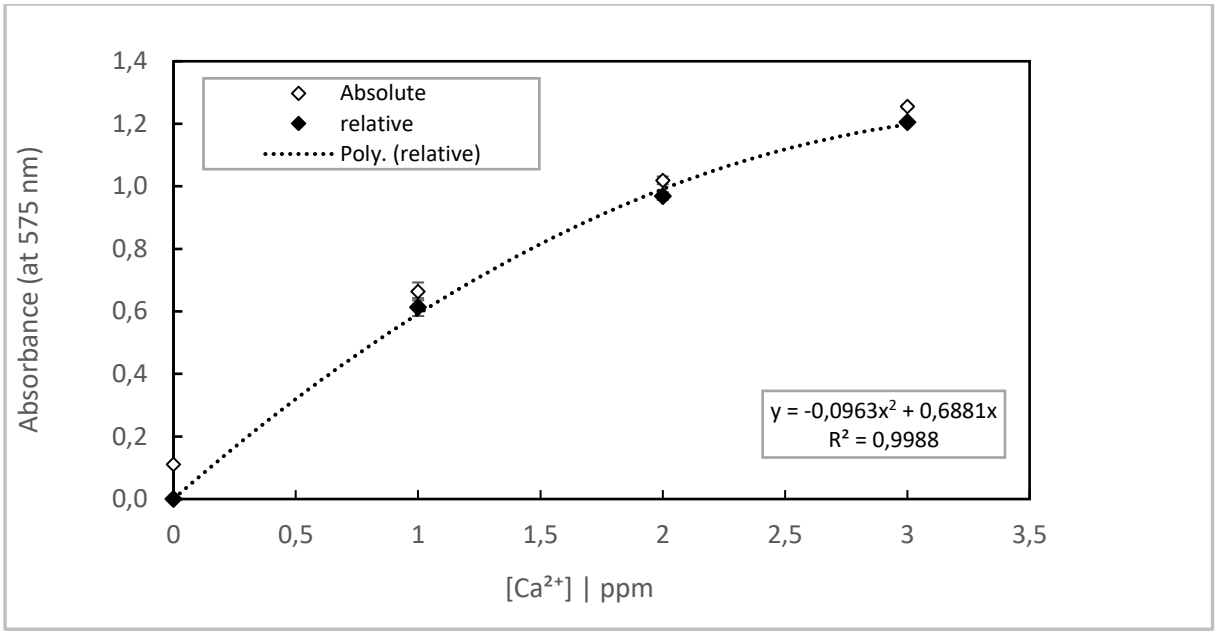

Figure 5.19: The o-Cresolphthalein Complexone Method Calibration Curve for $CaCl_2$-H_2O system. The absorbance at optimal wavelength of 575 nm as a function of dissolved calcium concentration in $CaCl_2$ standard solutions.

The optimal calcium concentration ranged from 0 – 3 ppm and the corresponding values for absorbance were between 0 – 1.2. The initial tests showed that the absorbance increases non-linearly with the increase in concentration until 3 ppm; above (or beyond) this value, the absorbance remained constant as the concentration of calcium cations was increased (See Figure 5.20, Figure 5.21 and Figure 5.22). As shown in Figure 5.19, R^2 was 0.999, this value is close to 1 which means that the absorbance as the function of calcium concentration (from 0 – 3 ppm) is defined by a quadratic equation as depicted. This means that OCPC Method calibration curve for the $CaCl_2$-H_2O system cannot be interpreted by the Beer-Lambert Law (from 0 – 3 ppm), according to which the absorbance or calibration curve is expected to be linear with the increase in absorbing species concentration.

$MgCl_2$ - $CaCl_2$ - H_2O system (Mg^{2+} effect):

Figure 5.20 compares four OCPC Method calibration curves for determining calcium, generated by keeping the concentration of calcium constant while varying magnesium concentration to desired ratios. The calibration curves in Figure 5.20 are for the magnesium-

only, calcium-only and the calibration curves generated with both calcium and magnesium at the ratio of 0.08 and 5 respectively.

The absorbance for the magnesium-only calibration curve increases with the increase in magnesium concentration from 0 ppm to 2 ppm, then, the absorbance remained constant with the increase in concentration from 2 ppm to 3 ppm. The same trend noticed for the calibration curve generated with both calcium and magnesium at the ratio of 0.08. However, in this curve, the absorbance remained constant as the concentration increased from 1 to 3 ppm. On the other hand, the absorbance for the calibration curve generated with both calcium and magnesium at the ratio of 5, increased linearly with the calcium concentration from 0 to 2 ppm and it flattened linearly from 2ppm to 3 ppm. This curve respects the Beer-Lambert law from 0 to 2 ppm, even though this seems to be a narrow range, it is validated by the calibration curves in Figure 5.21. Similarly, as in Figure 5.20, Figure 5.21 compares four OCPC Method calibration curves for determining calcium, however, the calibration curves in Figure 5.21 were generated with both calcium and magnesium concentration for the ratios 1, 1.25, 1.67 and 2.5. The calibration curves approach linearity (in concentration range of 0 to 2 ppm) as the ratio of calcium to magnesium concentration increases from 1 to 2.5. The explanation is that, as discussed in Chapter 4, a amount of magnesium is necessary to complex with OCPC to make a stable coloured-solution (Harvey, 2019). This argument is consistent with the study by Puall *et al*. (1997) who state that OCPC is a sensitive metallochromic ligand which complexes with most alkaline earth ions.

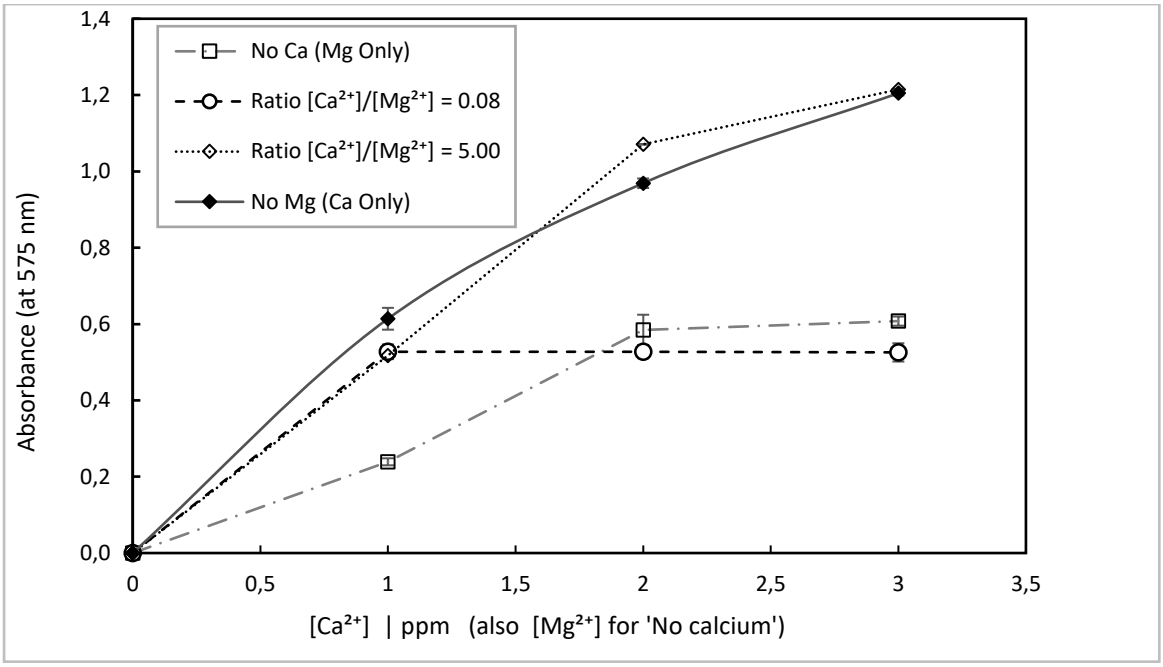

Figure 5.20: The OCPC Method Calibration Curve for $MgCl_2$-$CaCl_2$-H_2O system. The absorbance at optimal wavelength of 575 nm as a function of dissolved calcium concentration in $MgCl_2$-$CaCl_2$ standard solutions.

According to the Beer-Lambert law, the absorbance is linear with the increase in the absorbing species concentration, however, the deviations are common at higher concentrations of the absorbing species (Harvey, 2000). The deviations observed in Figure 5.20 are known as negative deviations. According to Harvey (2000), if the concentration remains constant as the absorbance increases, the deviations are positive.

As explained in Harvey (2000), the deviations are likely to be caused by three reasons, the first one can be explained in term of Beer Lambert's law (see Equation B.1 in Appendix B). In equation B.1, the absorbance is directly proportional to the absorptivity (ε) of the absorbing species, which is dependent on the refractive index. At lower concentrations, the change in ε is almost negligible, however as the concentration is increased, ε also increases and hence the refractive index of the sample. The second reason is likely to be due to the participating acid-base reaction; water forms a large part in these analyses, intuitively water act as a conjugate base which results in equilibrium acid-base reaction. From Harvey (2000), it is mechanistically shown that the absorptivity of the weak acid is given by a non-linear equation (which includes both the fraction of unreacted weak acid and participating ligands or complexes as the conjugate base). The third reason is due to the instrumental limitation: Beer's law is strictly

valid only for purely monochromatic radiation; that is, for radiation consisting of only one wavelength. Using polychromatic radiation always gives a negative deviation from Beer's law (Harvey, 2000). The same argument holds for Figure 5.20 and Figure 5.21 which show that higher concentrations of magnesium contribute significantly to the deviation from the pure Ca^{2+} curve.

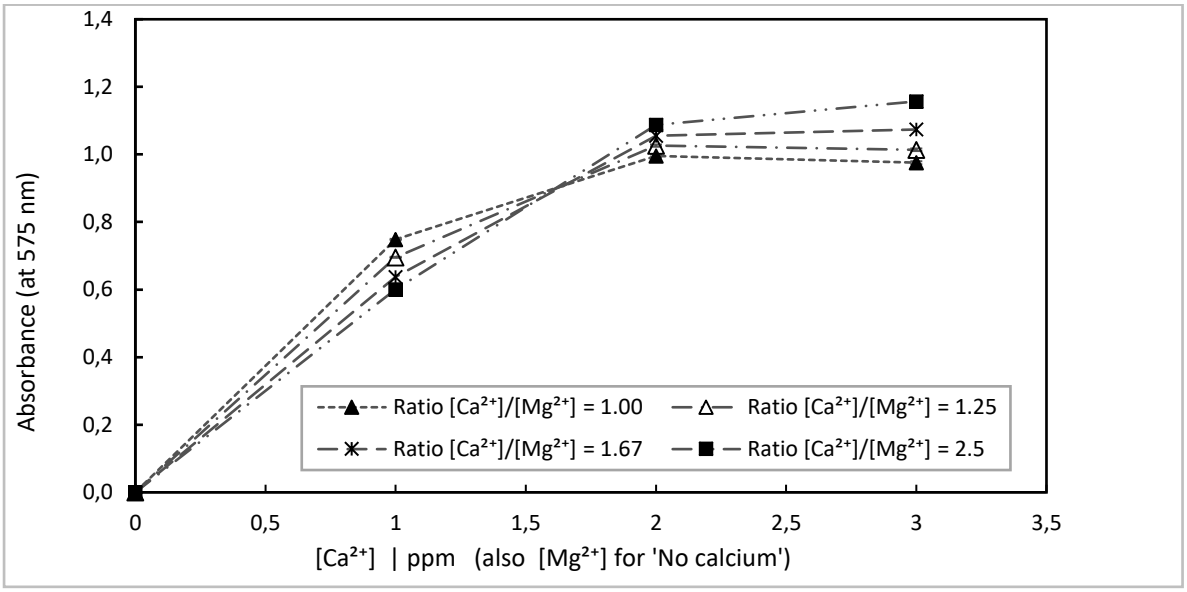

Figure 5.21: The OCPC Method Calibration Curve for $MgCl_2$-$CaCl_2$-H_2O system. The absorbance at optimal wavelength of 575 nm as a function of dissolved calcium concentration in $MgCl_2$-$CaCl_2$ standard solutions.

$CaSO_4 \cdot 2H_2O$-$CaCl_2$ - H_2O system (SO_4^{2-} effect):

Similarly, as in Figure 5.21, Figure 5.22 compares four OCPC Method calibration curves for determining calcium, generated by varying the concentration of calcium to sulphate ratio at 0.42, 1, 20 and 100.

The negative deviations observed in Figure 5.22 may not be due to the reasons discussed in Figure 5.20 and Figure 5.21 because there is no data point between 0 and 1 ppm. Apart from the arguments presented for the effect of Mg discussed above, it is noticeable that the

absorbance values (especially for cases where the ratio of calcium to sulphate is greater than 1) at 1 ppm calcium concentration is relatively higher than observed in Figure 5.20 and Figure 5.21. This is plausible because the solubility of calcium sulphate compounds is significantly lower than calcium chloride and magnesium chloride. Furthermore, the presence of chloride ions maintains calcium in solution. Because of the lower solubility of calcium sulphate, the light absorptivity is more than that in a chloride environment.

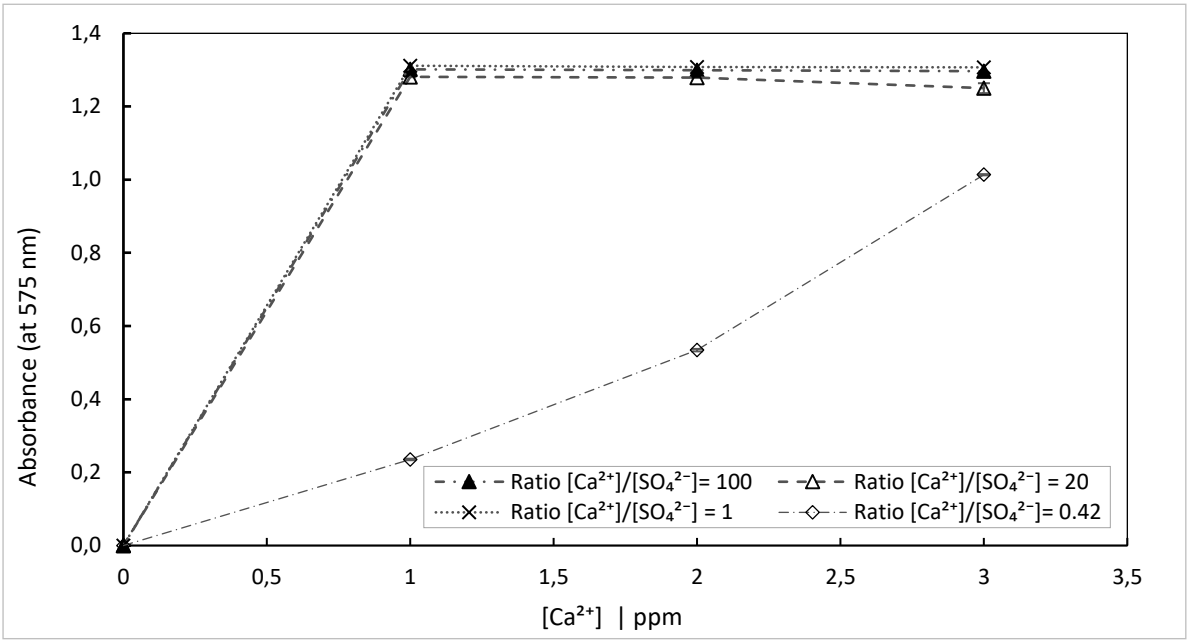

Figure 5.22: The OCPC Method Calibration Curve for $CaSO_4 \cdot 2H_2O$-$CaCl_2$-H_2O system. The absorbance at optimal wavelength of 575 nm as a function of dissolved calcium concentration in $CaSO_4 \cdot 2H_2O$-$CaCl_2$ standard solutions

For the ratio of 0.42, the calibration curve was non-linear with calcium concentration from 1-3ppm. However, the absorbance values were found to be less than the absorbance values found in the calcium only calibration curve. At this stage, we cannot conclude on the minimum allowable sulphate concentration, however it is safe not to use this method for cases where there are sulphates present.

EBT-EDTA – Reverse Titration (complexometric titration) method:

$CaCl_2$ - H_2O system ('Pure' calcium system):

EBT-EDTA – Reverse Titration is a standard method of determining calcium and the other divalent metals such as magnesium, zinc and others. Table 5-1 below shows the results for the calcium content in the 100ppm standard solution using EBT-EDTA – Reverse Titration. The 100ppm calcium solution was split into three aliquots, then tested for dissolved calcium concentration using the procedure highlighted in Chapter 4. From the titration results, the volume of EDTA used to reach the endpoint in samples 1 and 2 is 2.52 ml. This value is 0.3 ml higher than the value found for sample 3. Therefore, the volume of EDTA used in each case is comparable. The calcium content was found to be 100.43 ppm with a standard error of 0.3% this value is very close to the anticipated 100 ppm. This, therefore, shows that EBT-EDTA – Reverse Titration method works well for $CaCl_2$-H_2O system (It can be noted that chloride ions do not affect the system).

Table 5-1: EBT-EDTA – Titration Test for 100 ppm calcium standard solution

$CaCl_2$ - H_2O system	***Sample 1***	***Sample 2***	***Sample 3***
Volume Ca^{2+}; mL	25	25	25
Molarity Ca^{2+}	0.0025	0.0025	0.0025
Volume EDTA; mL	6.61	6.59	6.53
Ca^{2+}; mg, aliquot	2.52	2.52	2.49
Ca^{2+}; ppm, unknown	100.9	100.6	99.7
Mean unknown Ca^{2+} (ppm)	**100.43**		
StdDv (ppm)	**0.52**		
StdEr (ppm)	**0.3**		

The results in Table 5-1 served as a control or reference experiment. The error shown in Table 5-1 is relatively small. This is possibly due to the nature of the titration experiments which are always dependent on human error. The apparatus (burette) used in this method experiment requires careful monitoring, especially near the endpoint, because of a small excess drop or leak that could result in a deviation from the endpoint (Rancke-Madsen, 1972).

$MgCl_2$ - $CaCl_2$ - H_2O system (Mg^{2+} effect):

In Table 5-2, the same procedure used in Table 5-1 was used except the addition of 20 ppm magnesium (the system, in this case, is $MgCl_2$-$CaCl_2$-H_2O system). Using EBT-EDTA – Titration method, a solution comprising 100 ppm Ca^{2+} and 20 ppm Mg^{2+} was titrated. Table

5-2 show the results of this system, the endpoint for this system was not accurate, the concentration of calcium read in sample 1 is 163.4 ppm which is 19.7 and 18.6 ppm higher compared to samples 1 and 2, respectively. The average concentration was found to be 150.63 ppm with the standard error of 5 ppm (3.32%).

Comparing the results of Table 5-2 to those of Table 5-1, the anticipated calcium detection was 100 ppm if only calcium is detected. However, from the result is it clear that the presence of magnesium increases the volume of EDTA required to reach the endpoint. According to the data given in Bishop (1972) and Harvey (2000), the complexation of calcium in the presence of magnesium cannot be isolated. The complexation factor ($\log \beta_{11}$) of EBT to calcium is 5.4, which is 1.6 less than magnesium's factor of 7. (See appendix B, Figure C 1). This agrees with the method from (Harvey, 2000) which states that EBT determines the total hardness of water due to both calcium and magnesium ions. Similarly, to the results obtained, the same results were observed with calcium to magnesium ratio of 100 ppm to 130 ppm and 100 ppm to 0.85 ppm (see Table B1 and Table B2 in Appendix B).

Table 5-2: EBT-EDTA – Titration Test showing the effect of Mg^{2+} on calcium

Ca^{2+} = 100 ppm; Mg^{2+} = 20 ppm	***Sample 1***	***Sample 2***	***Sample 3***
Vol. Ca^{2+}; mL	25.26	25.31	25.30
Volume EDTA; mL	10.7	9.71	9.79
Ca^{2+}; mg, aliquot	4.08	3.59	3.62
Ca^{2+}; ppm, unknown	163.40	143.66	144.84
Mean Ca^{2+}; ppm, unknown	**150.63**		
StdDv	**9**		
StdEr	**5**		

<u>$CaSO_4 \cdot 2H_2O$- $CaCl_2$ - H_2O system (SO_4^{2-} effect):</u>

Similarly, as in Table 5-1 and Table 5-2, Table 5-3 was generated by keeping the calcium concentration constant at 100 ppm, the sulphates concentration was 0.85 ppm. The volume of EDTA titrated in each sample determines the concentration of calcium in each sample. Following the same procedure as in Table 5-1 and Table 5-2, the concentration of calcium in Sample 1 was 140.34 ppm, which is 8.52 ppm higher than Samples 1 and Sample 2 calcium

concentration of 131.82 ppm. These results suggest that Sample 1 is the outlier. The average concentration was 135 ppm with 1.48% standard error of 4 ppm.

Table 5-3: EBT-EDTA – Titration Test showing the effect of SO_4^{2-} on calcium

Ca^{2+} = 100 ppm; SO_4^{2-} = 0.85 ppm	*Sample 1*	*Sample 2*	*Sample 3*
Vol. Ca^{2+}; mL	25.30	25.27	25.32
Volume EDTA; mL	9.19	8.91	8.91
Ca^{2+}; mg, aliquot	3.51	3.30	3.30
Ca^{2+}; mg, unknown	140.34	131.82	131.82
Mean Ca^{2+}; mg, unknown	**135**		
StdDv	**4**		
StdEr	**2**		

<u>$FeCl_3$ - $CaCl_2$ - H_2O system (Fe^{3+} effect) in both analysis methods:</u>

The test for the effect of Fe^{3+} was unsuccessful for both methods (OCPC UV/VIS spectrophotometer method and EBT-EDTA – Reverse Titration method). This was due to the formation of $Fe(OH)_3$ precipitates (see Figure C2 and Figure C3 in Appendix B). As discussed above, the standard solutions required for the analysis (of the samples) are mostly dilute, which means that there was an appreciable amount of free water molecules or hydroxide ions which then react with ferric ions via hydrolysis (See Equation 5.1).

$$Fe^{3+}_{(aq)} + 3H_2O_{(l)} \leftrightarrow Fe(OH)_{3\,(s)} + 3H^{+}_{(aq)} \quad \text{...: 5.1}$$

It is evident in sources such as Cornell & Schwertmann (2003) and Lottermoser (2010) that the formation of ferric hydroxide is inevitable, because ferric cations have a high affinity for hydroxide anions, as it can be seen from Equation 5.1. The precipitation of $Fe(OH)_3$ increases with the concentration of ferric cations, because each ferric cation reacts with three hydroxide ions, which increases the supersaturation of the system as the hydroxides are depleted (Cornell & Schwertmann, 2003; (Lottermoser, 2010). The equilibrium of Equation 5.1 is therefore expected to lie towards the right. In the OCPC Method, the $Fe(OH)_3$ precipitates interfered with the final colour of the solution and therefore compromised the absorbance of the solution, hence

generating inaccurate results. In the EBT-EDTA – Reverse Titration method, the $Fe(OH)_3$ precipitates interfered with the titration end-point hence producing inconsistent results (see Appendix B).

Overall summary for the dissolved calcium analysis.

In summary, the OCPC method yielded a non-linear calibration curve within the selected calcium concentration range (1-3ppm) for $CaCl_2$ - H_2O system. Similarly, to the EBT-EDTA – Reverse Titration method, OCPC method required a small amount of magnesium to yield a stable colour for solutions, which worked for the calcium concentration range of 1-2ppm. At higher concentrations of magnesium and sulphates, negative deviations were observed. However, this method yielded non-linear calibration curves in the presence of low sulphates and failed in the presence of ferric ions. Similarly, the EBT-EDTA – Reverse Titration method worked relatively well for the $CaCl_2$ - H_2O system, and failed in the presence of magnesium, sulphates and ferric ions.

Except for the ferric ions, the OCPC method shows promising results in the presence of magnesium and sulphates. Further tests need to be conducted to define the exact limits for sulphates and magnesium. Due to these limitations, both methods were not used in this study and they were replaced by ICP-OES.

5.3 Preliminary experiments results

5.3.1 Effect of the stirring rate

The stirring rate is essential for predicting whether the rate of dissolution of $Ca(OH)_2$ is chemical reaction-controlled or mass transfer-controlled. Figure 5.23 shows the effect of stirring rate on the dissolution of $Ca(OH)_2$ powder in a batch of de-ionized water, by measuring and monitoring the pH of the bulk solution as a function of time. As shown in Figure 5.23,

three levels of stirrer speed were chosen, the lowest at 225 rpm, the medium rate was 325 rpm and the higher rate was 425 rpm. At all levels of stirring, the system pH reached a constant or saturation value in about 2 minutes. Due to the difficulties in feeding the powder into the reactor, 2 minutes was the fastest sampling time possible for this set-up. The saturation pH for the system when the stirring rate was kept at 425 rpm, is 12.1± 0.03 which is slightly higher than the saturation pH at 325 and 225 rpm which is 11.8±0.1 and 11.7±0.04, respectively. Using the OLI^{TM} model stream analyser for a batch system under the given conditions, the saturation pH at 25°C was calculated to be 12.4. Even though OLI^{TM} is a thermodynamics-based model, all the measured steady-state pH values fell below 12.4; this is likely to be due to the undersaturation of the system. Even though there is no data point between 0 and 2 minutes, these results show that the reaction rate of pure reagent-grade Merck $Ca(OH)_2$ powder and de-ionized water is fast and expected to be completed in less than 2 minutes. In conclusion, the results at the three stirring rates are statistically the same (error-bars overlap), therefore there is no significant difference between the three.

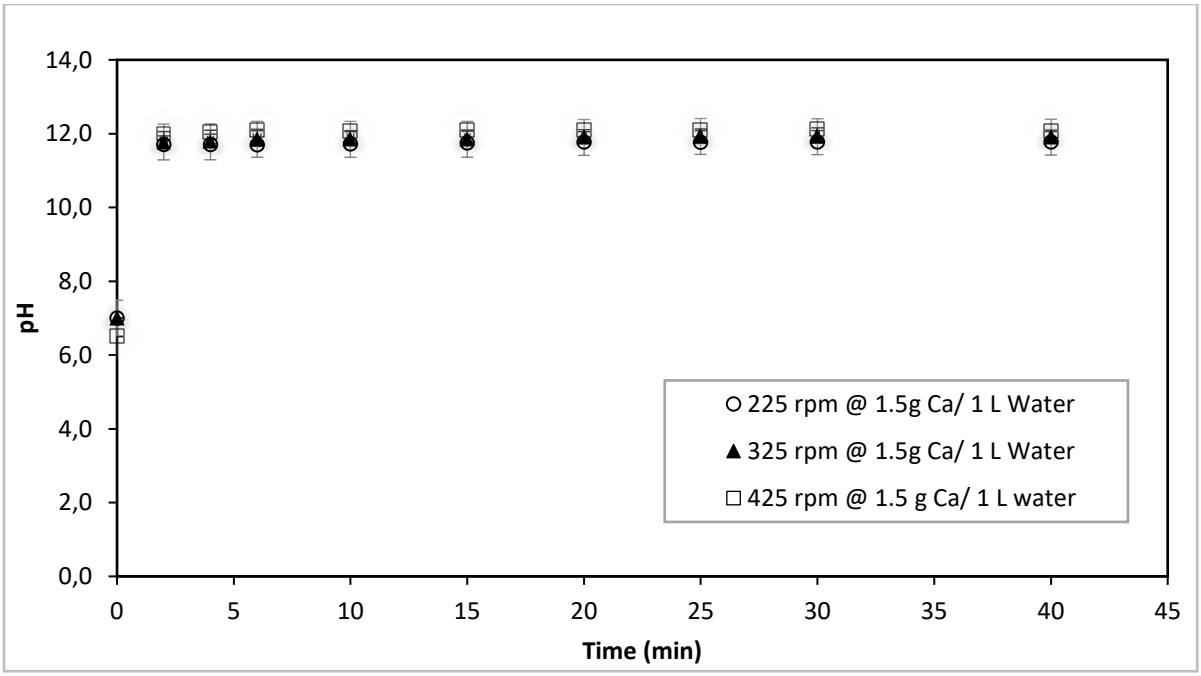

Figure 5.23: Effect of stirring rate on the dissolution of reagent grade $Ca(OH)_2$ powder in de-ionized water using a batch system set-up, at ambient conditions (22 °C and 1 atm).

5.3.2 Effect of the residence time on the steady-state pH

Figure 5.24 shows the effect of the mean residence time on the dissolution of $Ca(OH)_2$ in de-ionized water in a continuous system. In this figure, the temperature and the stirring rate were kept constant at 25°C and 600 rpm, respectively. Three different mean residence times were tested: 2.4, 2.7 and 4.3 minutes. The corresponding flow rates for de-ionized water feed stream were 4.57 ml/s, 5.22 ml/s and 6.55 ml/s, respectively, while keeping the flow rate of $Ca(OH)_2$ suspension feed stream constant at 0.1 ml/s.

When the mean residence time was 4.3 minutes, the initial pH value was 4.5, this value was lower than the expected value of neutral 7, because of the carbonation reaction between de-ionized water and atmospheric CO_2. For both the mean residence times of 2.4 and 2.7 minutes, the measured pH value was indeed approximately 7; in these experiments, the de-ionized water was added directly to the reactor from the de-ionized water dispenser. In all three experiments, the pH increased with time from 0 to 8 minutes. During this period, the system was unsteady because of the imbalance between hydroxide ions and hydrogen ion. After 8 minutes, the system reached the steady-state pH.

For the mean residence time of 4.3 minutes, the steady-state pH is 12.6, which is 0.3 units higher than 12.3 at the mean residence time of 2.7 minutes and 0.4 units higher than pH of 12.1 found at the mean residence time of 2.4 minutes. All these steady-state pH values are relatively comparable to the pH of a $Ca(OH)_2$ saturated solution (pH of 12.4, at 25 °C, as determined by OLI^{TM} , see Figure C5 in Appendix C). The steady-state pH was higher than 12.4 when the mean residence time was 4.3 minutes due to the inverse solubility of $Ca(OH)_2$ with temperature, considering that, the laboratory ambient temperature was measured to be 22 °C. The predicted pH at this temperature is 12.5 (See Figure C5 in Appendix C).

In conclusion, the longer the particles of $Ca(OH)_2$ stay in the reactor, the more they dissolve, releasing more alkalinity. Therefore, the shorter residence times yield lower pH values because not all $Ca(OH)_2$ has dissolved. Furthermore, a constant pH is attainable by fixing the mean residence time. Therefore, the overflow CSTR is an appropriate reactor system for controlling pH. However, its ability to control the mean residence time is limited.

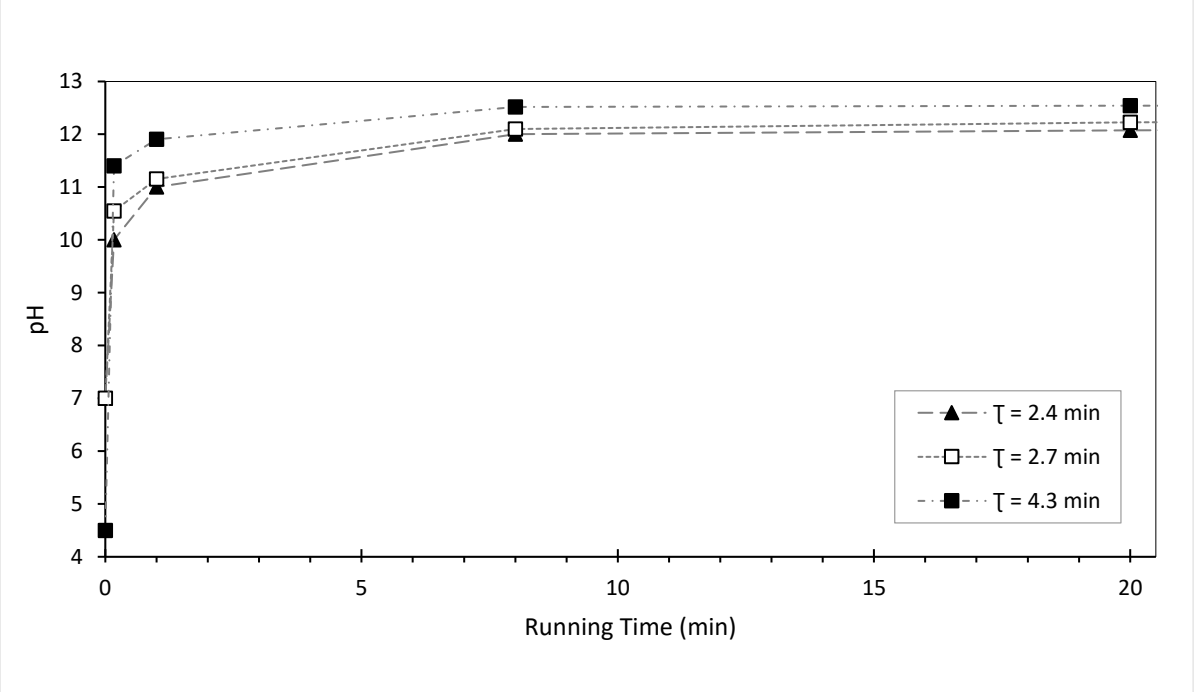

Figure 5.24: Effect of residence time on the dissolution of industrial $Ca(OH)_2$ in de-ionized water in the overflow slurry CSTR system; measured at (22 °C and 1 atm). This is a zoomed version of Figure C4 in Appendix C. Figure C4 has the running time of 120 minutes.

5.3.3 Effect of the $Ca(OH)_2$ dosage on the pH

Figure 5.25 depicts the effect of the $Ca(OH)_2$ suspension dosage on the steady-state pH. There were five different dosage levels tested, namely: 0.1 mL/s, 0.24 mL/s, 0.49 mL/s, 0.73 mL/s and 1 mL/s. The corresponding mean residence time for each dosage was 8.9 minutes, 9.4 minutes, 8.1 minutes, 7.5 minutes and 6.7 minutes. The temperature and the stirring rate were kept constant at 22°C and 600 rpm respectively. The suspension solid density and CH_3COOH concentration were also kept constant at 2% and 0.25 M, respectively.

In Figure 2.25, for the $Ca(OH)_2$ suspension dosage of 0.1 mL/s, the pH of the bulk solution increased slightly with time over the first 24 minutes because of the unsteady state. After 24 minutes, the pH remained constant at 3.92. In other words, it took 3 mean residence times to reach the steady-state pH. The same trend was noticed with 0.49 mL/s dosages except that the steady-state pH was 4.7. For the $Ca(OH)_2$ suspension dosage of 0.24 mL/s, the system

immediately reached the steady-state pH of 4.30 without any unsteady-state time lag. When the dosages rate was 0.73 mL/s, the pH increased slightly with time for the duration of the experiment. At this dosage the supply of $Ca(OH)_2$ begins to influence the amount of acid supply, however, the system is still acidic, which means the supply of $Ca(OH)_2$ is still lower than that of acid. A more pronounced over-supply of $Ca(OH)_2$ is noticed at 1 mL/s where $Ca(OH)_2$ is supplied beyond the equivalence point, beyond which it approaches saturation or equilibrium. It is clear that at this dosage there is complete depletion of acid because of the excess $Ca(OH)_2$.

In summary, Figure 5.25 gives a suitable range of $Ca(OH)_2$ suspension dosages necessary for keeping the $Ca(OH)_2$-CH_3COOH-H_2O system in the acidic region, provided all other parameters remain constant.

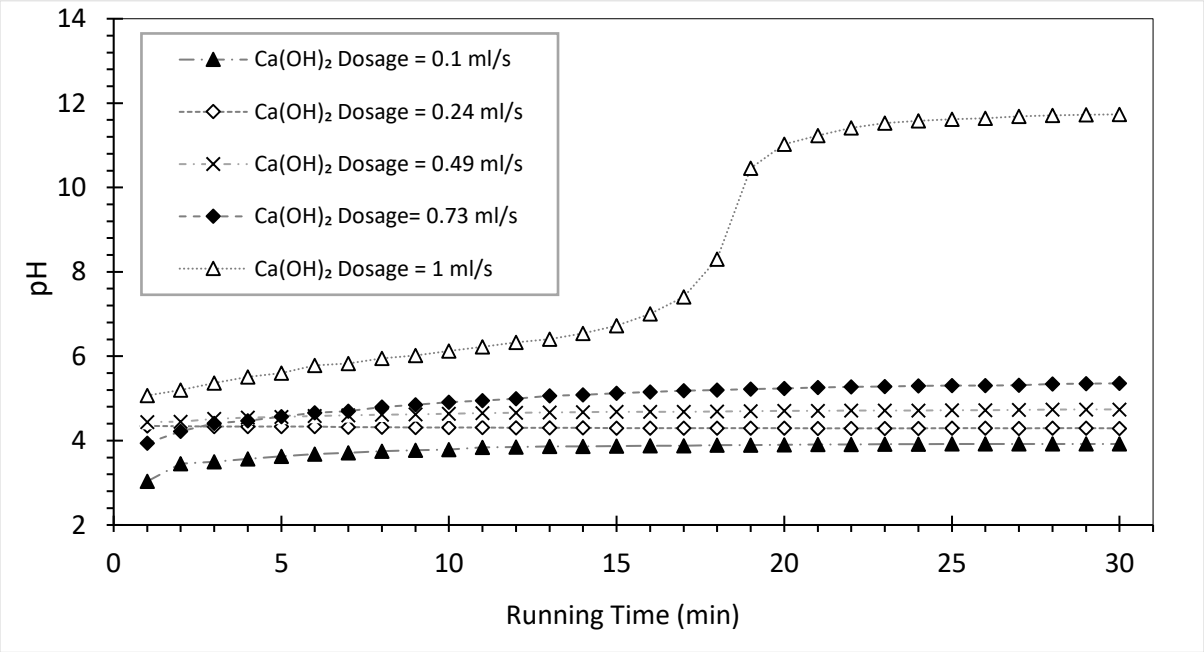

Figure 5.25: The effect of the $Ca(OH)_2$ suspension dosage on controlling the steady-state pH for the in 1.2 L overflow CSTR. The $Ca(OH)_2$ suspension dosage was varied from 0.1 ml/s to 1 ml/s while the flowrate of CH_3COOH was kept constant at 2.24 ml/s.

5.3.4 Effect of solid density in the $Ca(OH)_2$ suspension

Figure 5.26 shows the effect of the $Ca(OH)_2$ suspension density on the pH of the $HClO_4/Ca(OH)_2$ system, in the overflow slurry CSTR. There were three levels of the $Ca(OH)_2$ suspension density tested: 0%, 2% and 6%, at a constant flow rate of the feed streams, which was 2.42 mL/s for $HClO_4$ flow rate and 0.1 mL/s for $Ca(OH)_2$ suspension. The concentration of $HClO_4$ was constant at 0.05 M. However, the mean residence time varied from 8.3 minutes to 9.2 minutes for the $Ca(OH)_2$ suspension density of 0%, 2% and 6% respectively. The mean residence time increased with suspension density for two reasons. The first is that the suspended particles reduce the flowability of the $Ca(OH)_2$ suspension feed stream. The second reason is that particles inside the reactor tended to clog the overflow port and therefore reduce the exit stream flow rate.

For the $Ca(OH)_2$ suspension density of 0%, the pH of the system increased over 16 minutes from 1.93 to 2.08. It then stabilized at the steady-state pH of 2.08. Similarly, for the $Ca(OH)_2$ suspension density of 2%, the pH increased with time from 2.18 to 2.22 over 10 minutes. After 10 minutes, the pH fluctuated between the pH of 2.22 and 2.24, and therefore the steady-state pH was taken as 2.23. The difference between the steady-state pH for the $Ca(OH)_2$ suspension density of 0% and 2% was 0.15. Contrary, when the $Ca(OH)_2$ suspension density was 6%, the pH increased slightly with time from 2 to 4 over 9 minutes. After that it increased sharply to 11.5 for a minute before reaching a saturation point at 12.7. Similarly, as in Section 5.3.3, this graph resembles an acid-base titration curve because of the excess supply of $Ca(OH)_2$ particles.

In summary, the increase in $Ca(OH)_2$ suspension density increases the mean residence time of the system. The $Ca(OH)_2$ suspension density of 6% was too high for the feed conditions investigated resulting in the acid being completely consumed. However, there was no significant steady-state pH difference between the $Ca(OH)_2$ suspension density of 0% and 2%. Furthermore, at 0% there was no dissolution, whereas at 2% there was a small amount of dissolution at steady-state resulting to the marginally higher pH, whereas at 6% Ca(OH)2 was in large excess and hence all acid is consumed and the pH increased.

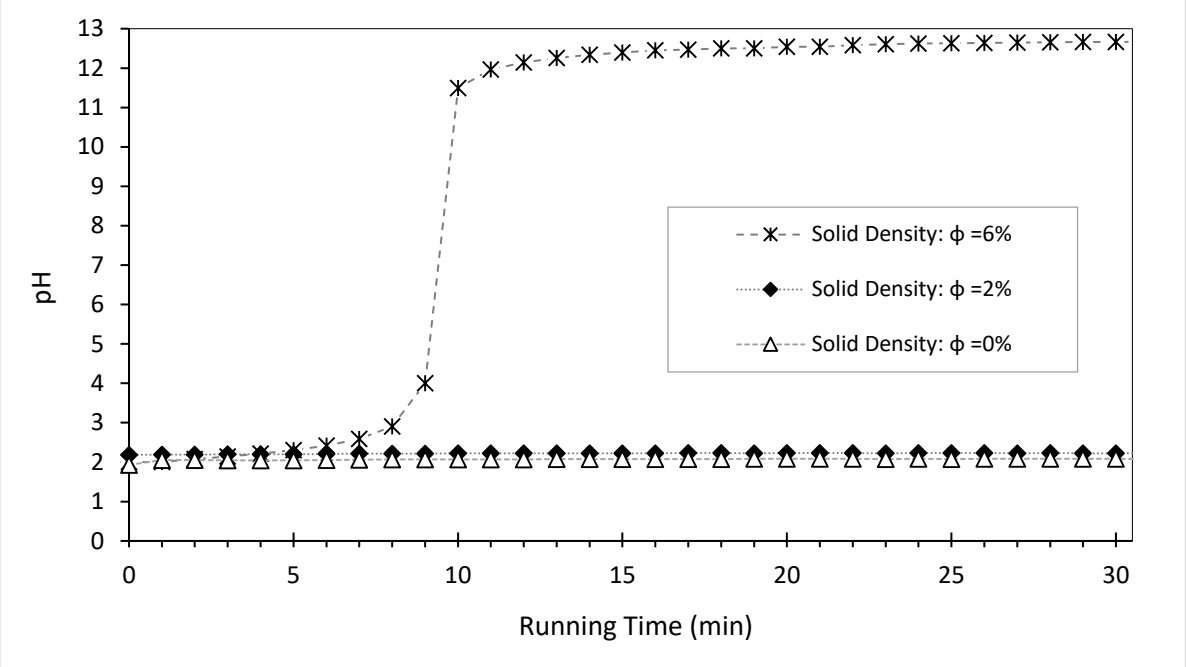

Figure 5.26: The effect of particle density on the pH response for the overflow slurry CSTR each experiment was generated at a constant temperature (22°C).

5.3.5 The effect of acetic acid strength on the pH

Figure 5.27 shows the relationship between the pH of the bulk solution and the inlet CH_3COOH concentration or strength, at a constant mean resident time (1.85 minutes), $Ca(OH)_2$ particle density (2%), temperature (22°C) and the stirring rate of 600 rpm. These constant conditions were found using the controlled-outflow slurry CSTR, which was an improvement from the overflow slurry CSTR.

The general trend for the experimental pH curve in Figure 5.27 is effectively a titration curve of CH_3COOH and $Ca(OH)_2$, with the equivalent point between 0.04M and 0.05M CH_3COOH concentration. For the CH_3COOH strength increment of 0.03M (from 0.01M to 0.04 M), the pH decreased from 12.1 to 10.8. The pH is high in this concentration range because the acid is very dilute. When the CH_3COOH strength increased from 0.04M to 0.05M, the pH decreased sharply from 10.8 to 5.14. As the strength of the acid increased beyond 0.05M, the pH decreased asymptotically to the pH curve of the pure CH_3COOH (generated by OLI^{TM} at the

same conditions). The stronger the acid, the more protons are available to react with hydroxide ions. This leaves excess protons to pull the pH to a lower value.

In summary, the controlled-outflow slurry CSTR generated a constant steady-state pH for each CH_3COOH concentration data point. Therefore, each CH_3COOH concentration has its corresponding dissolution rate. The mean residence time values achieved were reasonably similar and have been approximated by the average of 1.85 minutes for further calculations (See Table 5-4).

Table 5-4: The relationship between mean residence time and CH_3COOH strength

CH_3COOH Strength (M)	0.01	0.025	0.04	0.05	0.125	0.25	0.5
Residence time (min)	2.09	1.85	1.86	1.87	1.83	1.81	1.73

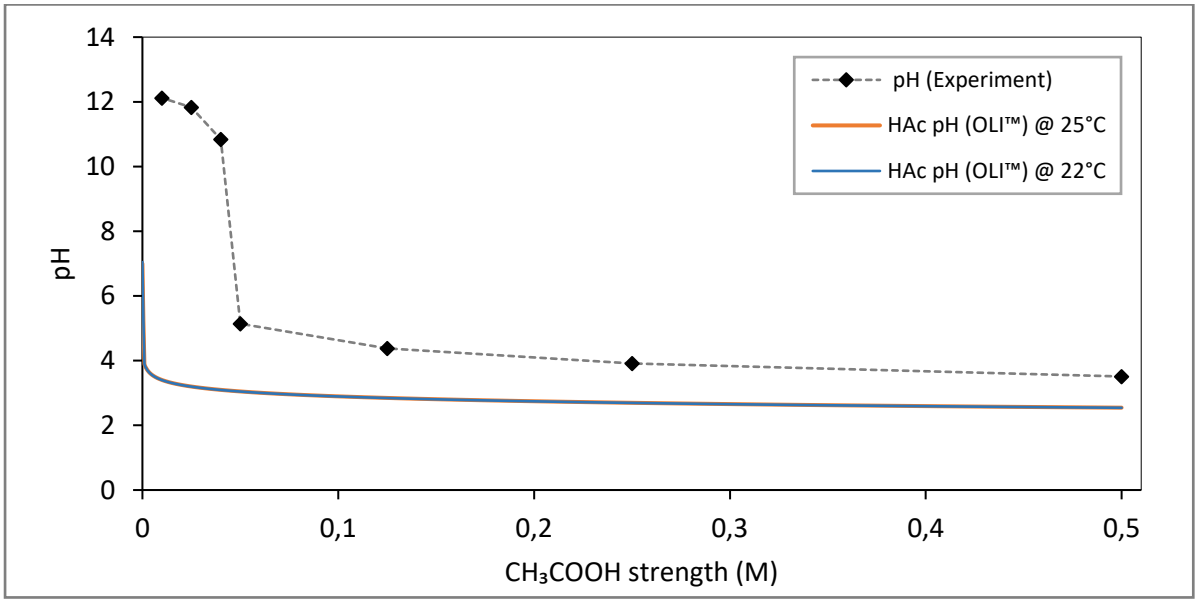

Figure 5.27: The effect of acid concentration on the steady state pH of the bulk solution for controlled-outflow slurry CSTR; each data point was generated at a constant temperature (22°C) and residence time of 1.85 minutes.

Summary from the preliminary experiments

The aim of the preliminary experiments was to investigate a suitable reactor system to effectively investigate the effect of the pH on the hydrated lime neutralization of acid. The

objective was to have a distinct constant pH for each experiment. Therefore, three reactor systems were tried, that is the 1L batch reactor, 1.2L and 400mL CSTR or chemostat systems. The 400mL CSTR emerged as a better reactor option compared to the others. The 1L batch reactor was necessary for the effect of the stirring rate experiments. The stirring rate of 600 rpm was a reasonable rate of agitation at which the system is likely to be reaction controlled. However, the batch reactor system was clearly limited in determining the true rate of dissolution because of the unsteady state conditions, which means that the effect of pH could not be determined.

On the other hand, the 1.2L overflow slurry CSTR yielded the desired constant pH levels for each experiment. It was also useful for investigating the effect of the mean residence time, $Ca(OH)_2$ suspension dosage and $Ca(OH)_2$ suspension concentration. The selected $Ca(OH)_2$ suspension dosage and $Ca(OH)_2$ concentration were 0.24 ml/s and 2%, respectively. The selected acid feed flowrate was 2.24mL/s. However, this system is more complicated to run as it takes at least 3 residence times to reach steady state, because larger reactors need to operate at longer residence time to achieve steady-state, which consumes more reagents.

Due to the limitations of the 1.2L overflow slurry CSTR, a 400 mL slurry CSTR with a pumped-out exit stream was selected for subsequent work, this system investigated the effect of acid strength in controlling the pH, resulting in a consistent mean residence time of about 1.85 minutes. Furthermore, as the preliminary experiments assumed the constant ambient temperature of 22°C, temperature-dependent rate constant calculations could not be done using the data generated by a rector running only at ambient temperatures. Therefore, a 400mL thermostatic CSTR was the preferred set-up and was used to vary the temperature control at three levels, that is 25°C, 35°C and 45°C.

5.4 Rate determination experiments results

Section 5.1 discussed the effect of PSD as a measure of size reduction during dissolution reaction using image analysis. The ICP-OES was found to be the better method for calcium assays (Section 5.2). Section 5.3 discusses the findings on the effect of the $Ca(OH)_2$ suspension

dosage, acid strength and other operational parameters such as pH of the reactor content with the change in time, residence time and agitation rate. Sections 5.1 to 5.3 serves as the exploratory work in ultimately defining a suitable system for investigating the kinetics of $Ca(OH)_2$ in an acidic environment.

In this section (Section 5.4), the jacketed, controlled outflow, thermostatic chemostat was used to investigate the rate of the $Ca(OH)_2$ dissolution reaction as a function of the pH, the residence time and temperature in DI water and CH_3COOH. DI-water was used as a reference solution for comparison purposes, while CH_3COOH was used for the main dissolution reaction study. Section 5.4.1 discusses the dissolution of $Ca(OH)_2$ in DI-water in details. This is achieved by looking at the relationship between the pH, temperature and the concentration of calcium cations in bulk solution. Eventually, the rate of reaction is calculated and studied as a function of pH and temperature at the constant residence time. In a similar approach, Section 5.4.2 explores the dissolution of $Ca(OH)_2$ in three standard solutions of CH_3COOH (0.02 M, 0.04M and 0.125M).

5.4.1 Steady state dissolution of $Ca(OH)_2$ in DI-water

Figure 5.28 depicts the relationship between both the pH and the concentration of the dissolved calcium in de-ionized water as a function of temperature. There were three temperature levels, 26°C, 34°C and 42 °C, investigated by monitoring the pH of the bulk solution as time proceeded, at a constant reactor volume of 400 mL, constant stirring rate of 1106 rpm and constant feed flowrates of 2.42 mL/s for DI-water and 0.23 mL/s for $Ca(OH)_2$ suspension. Similarly, to preliminary cases, the mean residence time was fixed to 76 seconds.

In the $Ca(OH)_2$ - H_2O system (as presented in Figure 5.28), there were five dominant species, namely OH^-, H^+, Ca^{2+}, $CaOH^+$ and undissolved $Ca(OH)_2$. Ions such as OH^- and H^+ are responsible for the change in pH. The assumption is that at the steady-state pH the concentration of calcium cations in the bulk solution is also constant and hence the $Ca(OH)_2$ dissolution rate. When the $Ca(OH)_2$ suspension dosage is too high; the solution inside the

reactor will be saturated. At saturation, the system will reach the maximum pH of 12.4 at 25°C; where calcium concentration is 675 ppm (from OLI^{TM}).

The effect of pH and temperature on $Ca(OH)_2$ dissolution in DI-water

As described above, the pH of the $Ca(OH)_2$-H_2O system was varied by changing the temperature of the circulating heating fluid, while keeping other factors constant. From the curve generated by OLI^{TM} (see Figure 5.28), it is expected that the pH of the $Ca(OH)_2$-deionized water system decreases with an increase in temperature of the system. As anticipated, the pH of the system decreases almost linearly with the increase in temperature (see experiment pH curve in Figure 5.28). In this figure, it is noticeable that the experimental pH line approaches the equilibrium pH line at higher temperatures, but the extent of equilibrium is lower.

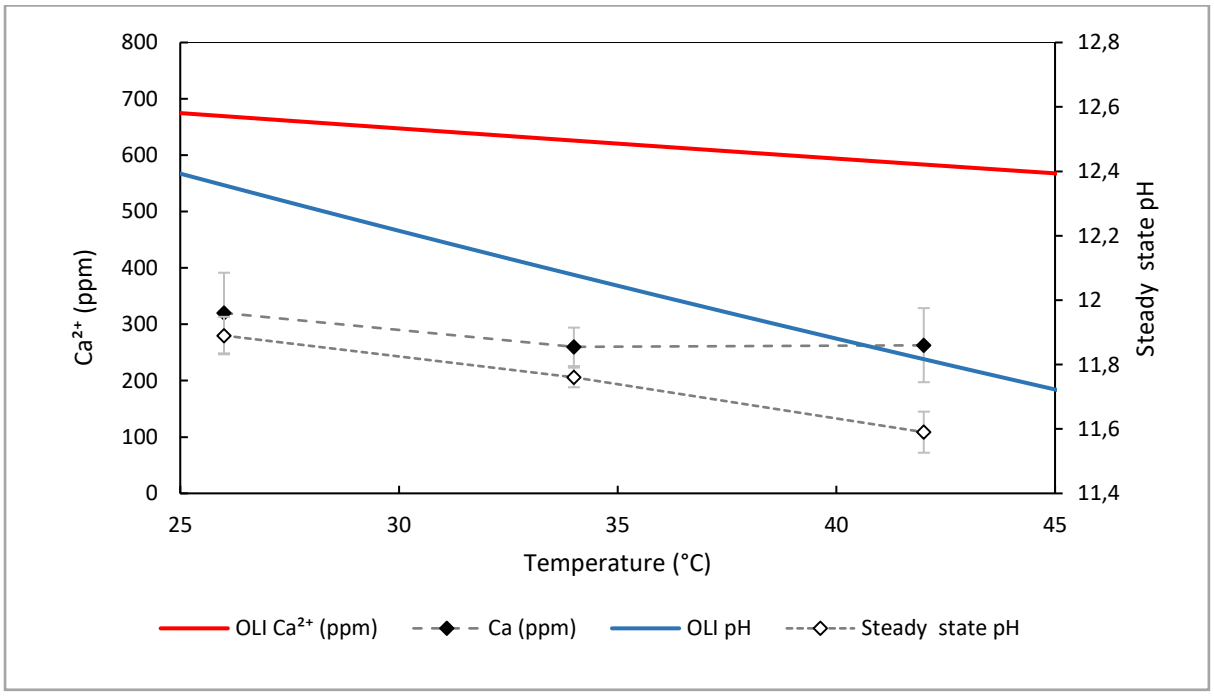

Figure 5.28: Effect of temperature on the dissolution of reagent grade $Ca(OH)_2$ in de-ionized water in a thermostat slurry CSTR; for 76 seconds mean residence time; experiment operated for about 12 residence times. The concentration of the dissolved calcium was measured at steady state.

The ANOVA analysis in Table 5-5 shows that the difference between the steady-state pH data for the temperatures used here is statistically significant. The *P-value* is $2{,}85\times10^{-31}$, which is

less than 0.05, furthermore, *F* is greater than *F critical* which means that the change in pH data as function of temperature is significant and likely to yield meaningful rates.

Table 5-5: ANOVA for steady-state data at 26ºC, 34ºC and 42ºC

Groups	*Count*	*Sum*	*Average*	*Variance*
Steady-state pH at 26ºC	15	178	11,87	0,000634
Steady-state pH at 34ºC	15	176	11,74	0,000366
Steady-state pH at 42ºC	15	173	11,56	0,000815

ANOVA

Source of Variation	*SS*	*df*	*MS*	*F*	*P-value*	*F crit*
Between Groups	0,6984	2	0,3492	577	2,85E-31	3,220
Within Groups	0,0254	42	0,0006			
Total	0,7238	44				

The pH data for the $Ca(OH)_2$ dissolution in deionized water is essential because it reflects the in-situ activities of the species in the system. However, this is only true for a $Ca(OH)_2$-deionized water system; in an acidic environment the pH is determined by the acid strength or acid concentration (excess hydrogen proton) which is not directly linked to the dissolved calcium concentration. This means that the pH data cannot be directly used to calculate $Ca(OH)_2$ dissolution rate in acidic environment as it represents only free acid. It is the dissolved calcium assays that are very essential for quantitative determination of the kinetics.

Similarly, as in the pH case, Figure 5.28 shows the equilibrium dissolved calcium data (OLI^{TM} Ca^{2+} line) and experimental or measured calcium in the bulk solution as a function of temperature at a constant residence time. The OLI^{TM} Ca^{2+} line decreases linearly with the increase in temperature. The measured calcium decreased with an increase in temperature from 26ºC to 34ºC, but then increased with temperature from 34ºC and 42ºC. There is no distinguishable trend; moreover, the measured calcium data is half of the OLI^{TM} Ca^{2+} data. Using statistics to quantify the error in measured Ca^{2+} data, where the error bars were determined from the standard deviation of the mean. The overlapping error bars in dissolved calcium assays means that the error in measured Ca^{2+} data is significant. However, this needed to be confirmed by an ANOVA statistical method (See Table 5-6).

Table 5-6: ANOVA for dissolved calcium data at 26ºC, 34ºC and 42ºC

Groups	*Count*	*Sum*	*Average*	*Variance*
Ca^{2+} (ppm) at 26ºC	6	1917	320	5115
Ca^{2+} (ppm) at 34ºC	6	1558	260	1166
Ca^{2+} (ppm) at 42ºC	6	1579	263	4319

ANOVA

Source of Variation	*SS*	*df*	*MS*	*F*	*P-value*	*F crit*
Between Groups	13531	2	6766	1,915	0,182	3,682
Within Groups	53002	15	3533			
Total	66533	17				

Table 5-6 shows the ANOVA statistical analysis for the dissolved calcium assays at 26ºC, 34ºC and 42ºC respectively. Using the ANOVA, *P-value* is 0.182, this value is greater than 0.05 which means that there is no statistical difference between the means of the dissolved calcium assays at 26ºC, 34ºC and 42ºC. Therefore, the measured calcium data is not statistically sound to be used for the rate calculations.

Therefore, the pH data was used to calculate the OH^- concentration and then calcium concentration assuming an acid to lime molar ratio of 2:1. The calculated calcium concentration was then used to calculate or estimate the rate of $Ca(OH)_2$ dissolution (see Figure 5.29 and Table 5-7). It is worth noting that the calculated rate based on the pH data is not a CSTR's steady-state dissolution rate, but it is a rate at which the system approaches equilibrium.

As shown in Figure 5.29, the calculated $Ca(OH)_2$ dissolution rate in deionized water decreased linearly with an increase in temperature, and the average calcium data and calculated dissolution rate were within reasonable error (See Table 5-7, *P-value* is 0.002). The results in Figure 5.29 is in contrast to the findings by Bernard *et al.* (2000), which stated that the $Ca(OH)_2$ dissolution rate increases with temperature. However, Bernard *et al.* (2000) used a semi-batch reaction system, furthermore, their study was conducted under mass transfer-controlled conditions.

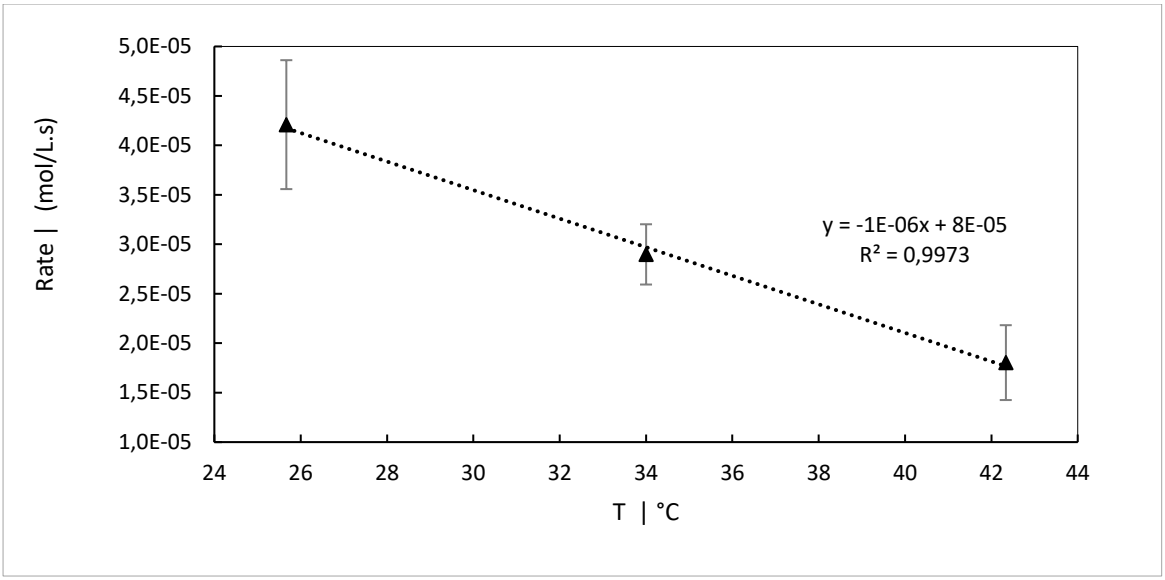

Figure 5.29: The Ca(OH)2 dissolution rate as function of Temperature, at a constant residence time (76 seconds) and feed conditions. The pH was varied by changing the temperature of the system

Table 5-7: ANOVA for the Ca(OH)2 dissolution rate at 26ºC, 34ºC and 42ºC

Groups	*Count*	*Sum*	*Average*	*Variance*
Temperature: 26ºC	3	1,19E-04	3,97E-05	4,10E-11
Temperature: 34ºC	3	8,03E-05	2,68E-05	9,28E-12
Temperature: 42ºC	3	4,82E-05	1,61E-05	1,40E-11

ANOVA

Source of Variation	*SS*	*df*	*MS*	*F*	*P-value*	*F crit*
Between Groups	8,41E-10	2	4,21E-10	19,64	0,00233	5,143
Within Groups	1,29E-10	6	2,14E-11			
Total	9,70E-10	8				

The findings by Bernard *et al.* (2000) are consistent with the Nernst-Brunner Equation, which states that the dissolution rate of a solid in liquid solution is directly proportional to the diffusivity of a solute or dissolving species, surface area of the particles, intrinsic dissolution rate constant and difference between the saturated and bulk concentration of the dissolving species (see Equation 5.2). In Equation 5.2, the rate of $Ca(OH)_2$ dissolution is inversely proportional to the volume and the thickness of the diffusion layer around the particles, and directly proportional to the diffusivity coefficient, specific area of the particles and the driving

force, which is the difference between the concentration of calcium at saturation and calcium concentration in the bulk solution.

$$\frac{dC_{Ca(OH)_2}}{dt} = \frac{D \cdot A \cdot K_{DC}}{\delta \cdot V}\left(C_{Ca^{2+};\,sat.} - C_{Ca^{2+};\,bulk}\right) \quad \ldots: 5.2$$

As the temperature increases, the dissolved species kinetic energy increases, which promotes a rapid diffusion of the species from the boundary layer to bulk solution and vice versa. Therefore, the slower rate determining (diffusion) step becomes faster with the increase in temperature. However, in this study, the mass transfer influence was eliminated by operating at a very high rotation speed (1106 rpm). The reasonable assumption is that; at a higher rotation speed, the system is under turbulent condition, and the diffusion layer around the particle is negligible.

Figure 5.30 depicts the $Ca(OH)_2$ dissolution rate as function of pH. In Figure 5.30, the $Ca(OH)_2$ dissolution rate increased with the pH, within the same margins of error, as presented in Table 5-7. From the chemical reaction rate equation, the dissolution rate is directly proportional to the concentration of calcium ions and hence hydroxide ions (which is by proxy pH). It is therefore expected that the $Ca(OH)_2$ dissolution rate increases with the increase in pH.

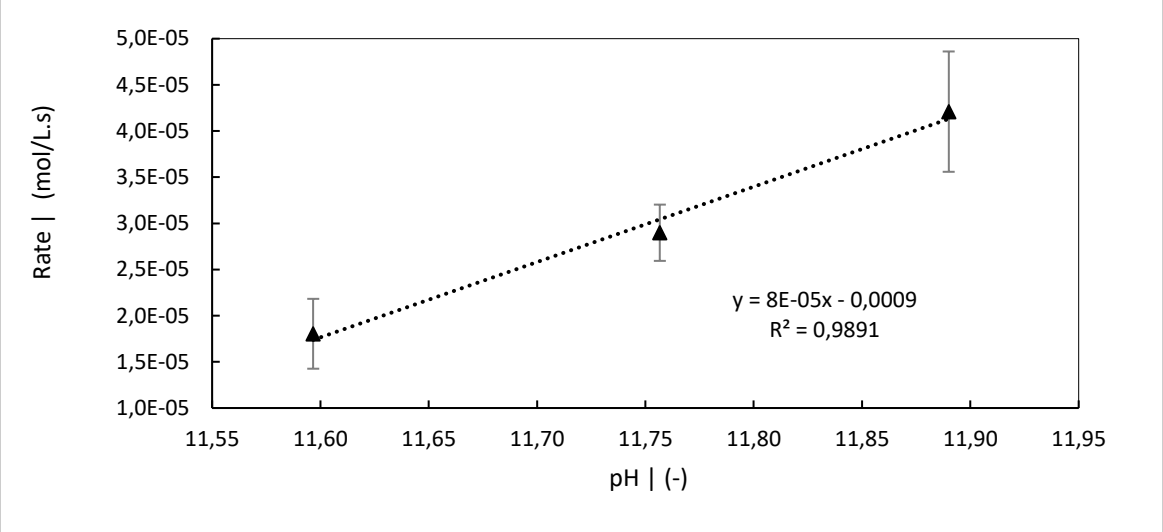

Figure 5.30: The $Ca(OH)_2$ dissolution rate as function of pH, at a constant residence time (76 seconds) and feed conditions. The pH was varied by changing the temperature of the system

Determination of the rate constant and the activation energy

$$-r_{Ca(OH)_2} = k[Ca(OH)_2]^{\sigma} = -k[Ca^{2+}]^{\alpha}[OH^{-}]^{\beta} \quad \text{...: 5.3}$$

$$r_{Ca(OH)_2} = k[Ca^{2+}]^{\alpha}[OH^{-}]^{\beta} \quad \text{...: 5.4}$$

In a $Ca(OH)_2$ -DI-H2O system, the increase in pH is as a results of the dissolution of $Ca(OH)_2$, specifically due to the increase in hydroxide ions. From the dissolution reaction, 1 molar increase in hydroxide ions means that calcium cations will also increase by half. Therefore, the rate of reaction becomes:

$$r_{Ca(OH)_2} = k[Ca^{2+}]^{\alpha}\left[\frac{1}{2}Ca^{2+}\right]^{\beta} \quad \text{...: 5.5}$$

Alternatively, in terms of hydroxide ion:

$$r_{Ca(OH)_2} = k(2[OH^-])^{\alpha}[OH^-]^{\beta} \quad \text{...: 5.6}$$

$$r_{Ca(OH)_2} = 2^{\alpha}k([OH^-])^{\alpha}[OH^-]^{\beta} \quad \text{...: 5.7}$$

$r_{Ca(OH)_2} = k_d([OH^-])^{\alpha}[OH^-]^{\beta} = k_d\,[OH^-]^{(\alpha+\beta)} = k_d\,[OH^-]^{\theta}$ for $k_d = 2^{\alpha}k$ and $\theta = \alpha + \beta$ (where theta is the overall order of reaction).

$$\log_{10}[r_{Ca(OH)_2}] = \log_{10} k_d + \theta \log_{10}[OH^-] \quad \text{...: 5.8}$$

$$-\log_{10}[OH^-] = pOH = 14 - pH \quad \text{...: 5.10}$$

$$\log_{10}[r_{Ca(OH)_2}] = \log_{10} k_d + \theta \log_{10}[OH^-] = \log_{10} k_d - \theta\,(14 - pH) \quad \text{...: 5.11}$$

Therefore;

$$\log [r_{Ca(OH)_2}] = \log k_d - \theta\,(14 - pH) \quad \text{...: 5.12}$$

Table 5-8: Dissolution of hydrated lime in deionized water data for rate determination (average data)

Exp. Set	T | °C	Exp. pH	Ca^{2+}_{in} | (ppm)	$[OH^-]_{out}$ | (mol/L)	Ca^{2+}_{in} | (mol/L)	Ca^{2+}_{out} | (mol/L)	r_a | (mol/L. s)	Log (r_a)
1	26	11.89	671	0.00780	0.0167	0.00390	0.0000365	-4.401
2	34	11.76	626	0.00572	0.0156	0.00286	0.0000251	-4.572
3	42	11.60	584	0.00398	0.0146	0.00199	0.0000156	-4.794

Using data in Table 5-8 to plot $\log [r_{Ca(OH)_2}]$ as a function of $(14 - \text{pH})$; where $\log k_d$ is a constant and θ is the slope (See Figure 5.31). The plot in Figure 5.31 yield a straight line (see Equation 5.13):

$$y = -1.3405x - 1.5699 \quad \text{...: 5.13}$$

$$\log\left[r_{Ca(OH)_2}\right] = -\theta\,(14 - \mathrm{pH}) + \log \mathrm{k_d} \qquad \text{...: 5.14}$$

Therefore, the overall order of reaction is 1.34, since the overall order is a combined order with respect to both calcium and hydroxide ions, definite values with respect to each ion are unknown. The value of 1.34 can be approximated to 1 when accounting the error associated with rate, therefore the overall order of $Ca(OH)_2$ dissolution rate is 1. The dissolution rate constant is $1\times10^{-1.57}$ s^{-1}, this value can be approximated to 1×10^{-2} s^{-1}. This is consistent with studies such as Dokoumetzidis & Macheras (2006) and Dokoumetzidis *et al.* (2008) which state that most of the dissolution rate are first order, which is evident also in correlations such as Nernst-Brunner Equation. Equation 5.15 is the modified Nernst-Brunner Equation used to calculate the rate constant values presented in Table 5-9. The rate constant values in Table 5-9 are relatively smaller than 1×10^{-2} s^{-1} but relatively comparable to 0.00442 s^{-1} found by Giles *et al.* (1993) using a shrinking core model at 25°C.

$$\frac{\mathrm{dC_{Ca(OH)_2}}}{\mathrm{dt}} = k_d\left(\mathrm{C_{Ca^{2+};\,sat.}} - \mathrm{C_{Ca^{2+};\,bulk}}\right) \qquad \text{...: 5.15}$$

In order to determine if the rate of $Ca(OH)_2$ dissolution in DI-water is chemical reaction controlled, activation energy of 6kJ mol^{-1} was determined by the Arrhenius plot, however when the values of the rate constant determined by Nernst-Brunner Equation were used, 18.1 kJ mol^{-1} was found. This value is comparable to range of 13.7-15 kJ mol^{-1} reported by Giles *et al.* (1993). Based on the calculated values of activation energy and rate constants, the dissolution of $Ca(OH)_2$ in DI-water is mass-transfer controlled and it can be expressed in terms of Nernst-Brunner Equation.

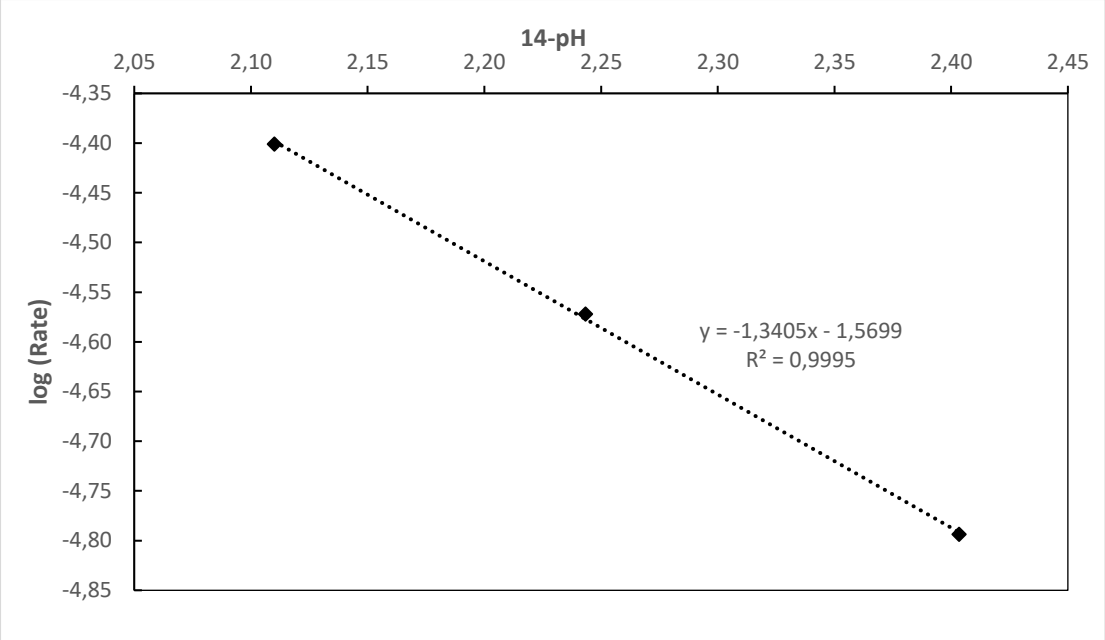

Figure 5.31: The log (rate) as a function of (14-pH).

Table 5-9: Dissolution of hydrated lime in deionized water data with rate constant values calculated using Nernst -Brunner Equation.

Exp. Set	T | °C	Exp. pH	Ca^{2+}_{in} | (ppm)	$[OH^-]_{out}$ | (mol/L)	Ca^{2+}_{in} | (mol/L)	Ca^{2+}_{out} | (mol/L)	r_a | (mol/L. s)	k_r | (1/s)
1	26	11.89	671	0.00780	0.0167	0.00390	0.0000365	0.00285
2	34	11.76	626	0.00572	0.0156	0.00286	0.0000251	0.00197
3	42	11.60	584	0.00398	0.0146	0.00199	0.0000156	0.00124

5.4.2 Steady state dissolution of $Ca(OH)_2$ in CH_3COOH

The dissolution rate (in terms of dissolved calcium) in deionized water served as a reference point (0 M CH_3COOH) to test the comparability of the rate of reaction in de-ionized water or aqueous environment to that of the acidic environment. Similarly, as in Section 5.4.1, experiments were conducted under the same conditions (average constant mean residence time of 75 seconds and temperatures of 25°C, 35°C and 45°C) except that instead of deionized water, different solutions of CH_3COOH (0.02M, 0.04M and 0.125M) were used. Figure 5.32 and Figure 5.33 show the steady-state pH in each case as a function of temperature and acetic

acid strength. Similarly to Figure 5.27, Figure 5.32 presents the steady-state pH as a function of acid strength while Figure 5.33 shows the steady-state pH as a function of temperature.

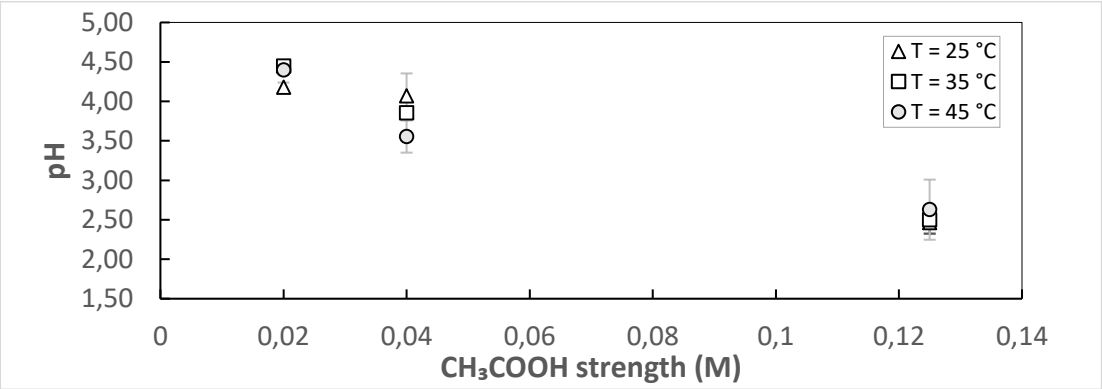

Figure 5.32: The effect of acid strength and temperature on the $Ca(OH)_2$ dissolution in CH_3COOH in terms of steady state pH in a thermostat slurry CSTR; for 75 seconds mean residence time; experiment operated for about 12 residence times. Version 1

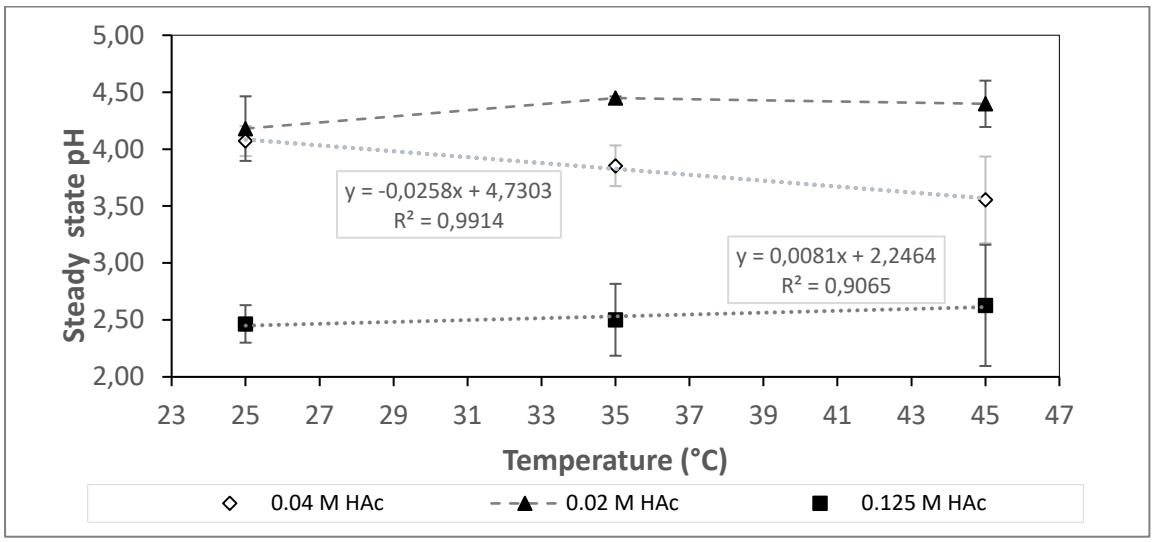

Figure 5.33: The effect of acid strength and temperature on the $Ca(OH)_2$ dissolution in CH_3COOH in terms of steady state pH in a thermostat slurry CSTR; for 75 seconds mean residence time; experiment operated for about 12 residence times. Version 2.

In Figure 5.32 at 0.02 M CH_3COOH, the pH of the system increased with the increase in temperature from 25 °C to 35 °C and slightly decreased from 35 °C to 45 °C. Similarly, at 0.04

M CH_3COOH, the pH of the system decreased linearly with the increase in temperature from 25 °C to 45 °C. In contrast to these two, the pH of the system at 0.125 M CH_3COOH increased linearly with the increase in temperature from 25 °C to 45 °C (See Figure 5.33).

As discussed in the preliminary experimental results (see Section 5.3.1, Figure 5.27), in all the trends in Figure 5.32 and Figure 5.33, the steady-state pH decreases with the increase in CH_3COOH strength. As shown in Figure 5.27, the decrease is expected to be asymptotical to the pure CH_3COOH pH curve (see Section 5.3.1). This was confirmed for the data generated at 35°C and 45°C but not for 25°C. At 25°C, the steady-state pH for 0.04 M CH_3COOH (acid strength) is 4.07 which is 0.11 unit lower than 4.18 found in 0.02 M CH_3COOH, but these values are close to one another. However, the error bars at pH 4.07 shows that this value is likely to be an outlier. Similarly, as in the de-ionized water experiment (0 M CH_3COOH), statistically, there is no significant difference between the mean of the steady-state pH as a function of temperature, and this is clear in Figure 5.32.

Figure 5.27 and Figure 5.32 or Figure 5.33 show the relationship between steady state pH, temperature and acid strength or concentration. Similarly, as in Figure 5.27 (preliminary experiments), at lower concentrations of CH_3COOH (below 0.02 M CH_3COOH), a small change in CH_3COOH feed concentration results in a larger change in pH. It is clear from Figure 5.27 that the shape of the curve for the system resembles that of a titration curve; this is expected since the rate of acid addition (acid flowrate) is kept constant while increasing the concentration of the acid. Therefore, in this case, CH_3COOH is treated as a titrant and the $Ca(OH)_2$ suspension acts as a titrate. However, the analogy of the titration curve is not perfectly applicable in Figure 5.32 because only three acid concentration data were used as opposed to 7 used for Figure 5.27.

Therefore, for Figure 5.32, above 0.02 M CH_3COOH, the larger the increment of CH_3COOH concentration is, in the feed, the smaller the change in steady state pH. Apart from the outlier (at 25 °C), the shape of the pH curve trends in Figure 5.32 resembles the points after the titration equivalent point when compared to Figure 5.27. The point of equivalence in Figure 5.27 is between 0.025 M CH_3COOH and 0.05 M CH_3COOH; this is because of the different feed ratio between $Ca(OH)_2$ suspension and CH_3COOH. In Figure 5.27, the $Ca(OH)_2$ suspension flowrate was kept constant at 0.10 ml/s, however in Figure 5.32 the $Ca(OH)_2$ suspension flowrate was

increased to 0.22 ml/s. The additional possible reason for lower pH values is in Figure 5.32 is lower mean residence times (75 seconds) while in Figure 5.27, the average mean residence time was 111 seconds. Therefore, $Ca(OH)_2$ solids had plenty of time to dissolve and hence raise the pH in Figure 5.27.

5.4.3 The effect of the number of residence times on the steady state pH.

The residence time is a critical variable in the kinetics of a reaction in a CSTR. In a homogeneous reactor content, residence time is the average time a fluid element spends in the reactor. It was therefore assumed that in this system (liquid solid heterogeneous system), residence time is average amount of time at which the particle will spend in a volume element of a reactor. Due to reactor design and fluid dynamics (hydrodynamics) in a flow system, it could take several number of residence times for a system to reach a steady state. This can be seen in Figure 5.24, Figure 5.25 and Figure 5.35 (discussed below). Figure 5.35 shows the relationship between the number of residence times and steady state pH for 0.02 M CH_3COOH-$Ca(OH)_2$ system, at a constant mean residence time of 76 seconds and constant temperature of 25 °C. Similar results were obtained for 0.04M and 0.125M (see Appendix C.1.2).

The residence times investigated in Figure 5.35 were 57 seconds and 75 seconds. For the shorter residence time (57 seconds), the steady state pH is 4.83 after one residence time, this 0.185 unit lower than the steady state pH of 5.01 which is the pH value which is reached after two residence times. These results agree with the preliminary results (see Figure 5.24, which shows that after about two residence times the pH reaches steady state). The calculated standard deviation of the mean for longer residence time trend was approximately 0.08 unit. The pH of 5.01 is the lowest steady state pH value for the shorter residence time (57 seconds) trend, the highest steady state pH was 5.1 which was found after 8.3 residence time. The average steady state pH for the shorter residence time is 5.07.

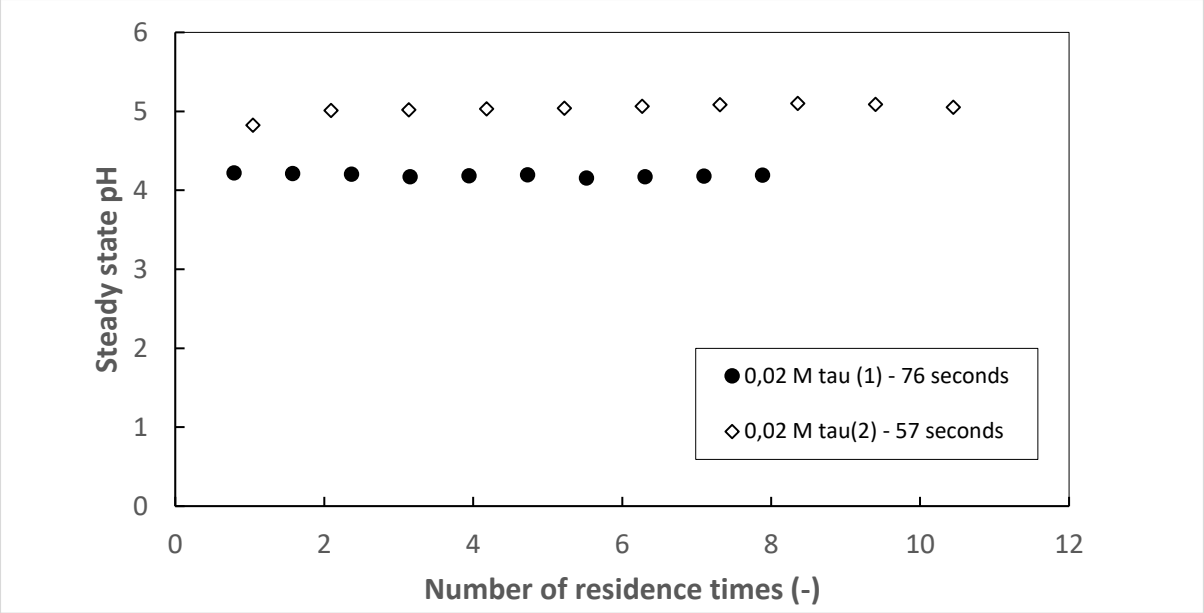

Figure 5.34: Effect of residence time in $Ca(OH)_2$ dissolution in 0.02 M CH_3COOH solution at 25 °C

For the longer residence time (76 seconds), after one residence time a pH value of 4.22. Beyond one residence time, the pH fluctuated between 4.22 and 4.16 and settled at this value when the number of residence time was 5.5. The calculated standard deviation of the mean for longer residence time is 0.02 (see error bars in Figure 5.32) and the average steady state pH for the longer residence time is 4.18.

In the case of the longer residence time, the system is given more time to reach equilibrium; considering the fact that there are 3 reactions: Neutralisation, $Ca(OH)_2$ dissolution and the CH_3COOH buffer (formation of calcium acetate or dissociation of CH_3COOH). All these reactions proceed simultaneously towards equilibrium. The fact that the solution pH is higher at the shorter residence time is an indication that the reactions providing alkalinity (neutralisation, and $Ca(OH)_2$ dissociation) proceed more rapidly than that providing acidity (which is the reverse reaction of the CH_3COOH buffer). The $Ca(OH)_2$ dissolution reaction releases calcium cations to the bulk solution but also provide OH^- (alkalinity). Therefore, calcium assay in this case would give the indication of the contribution of the dissolution reaction on the pH. However, calcium assays for shorter residence time were not determined due to technical challenges as discussed in Chapter 4.

During the neutralisation reaction hydroxide ions react with available hydrogen ions forming water molecules. The other 'reaction' taking place simultaneously with the neutralisation reaction is the surface disintegration of undissolved $Ca(OH)_2$ solid particles forming hydroxide ions and calcium cations. It can be argued that due to the higher stirrer speed of 1106 rpm (sufficiently higher than the 600 rpm used in the preliminary experiments and even higher that the chemical reaction rate-controlled region of 1000 rpm suggested by Ritchie & Xu (1990) and Bernard *et al.* (2000)), dissolved calcium cations and hydroxide ions are immediately released to the bulk solution. This is valid when we assume that the neutralisation reaction precedes $Ca(OH)_2$ surface disintegration. If the supply of hydroxide ions from the particles surface to the bulk solution is the same as the conversion of hydroxide ions from the bulk to water molecules. We would expect no change in the pH (see Chapter 2).

According to Robinson and Burnham (2001), there are significant differences in dissolution rates of hydrated limes. They argued that the observed rates for commercial hydrated limes could take the minimum of less than 10 seconds to 1 minute for 90% dissolution. This argument is consistent with the obtained results. It can therefore be concluded that the dissolution is very fast, faster than the neutralisation reaction at least in above case. Therefore, as indicated by Robinson and Burnham (2001) and studies such as Connors (1990) and Christian (2004), it can be concluded that the neutralization reactions are very fast, and they are dependent on the solid density and the concentrations of participating acid or base.

5.4.4 The Dissolution rate mechanisms in $Ca(OH)_2$-CH_3COOH system.

The ideal dissolution reaction rate for $Ca(OH)_2$/DI water system away from the equilibrium can be described by Equation 5.16.

$$Ca(OH)_2\,(s) \rightarrow 2OH^-\,(aq, bulk) + Ca^{2+}(aq, bulk) \qquad \ldots: 5.16$$

Equation 5.16 assumes that the formation of intermediate species such as $CaOH^+$ is negligible and it further assumes that the Ca(OH)2/DI water system is in the chemical reaction-controlled

region where the mass-transport influence is overcome. However, in this study, it was shown that the system is relatively closer to the equilibrium, hence the calculated rates are not necessarily the true rates of dissolution but the rate at which the system approach equilibrium as the temperature increases. The dissolution of hydrated lime in deionized water can be broken down as shown from Equation 5.17 to Equation 5.20 (Ritchie & Xu, 1990). The true rate of dissolution can then be determined by slowest of the step from the Equations 5.17 to Equations 5.17. According to Christian (2004), the self-ionization of water and hence water neutralization of hydrated lime is relatively instant when compared to steps below.

$$\mathrm{Ca(OH)_2\ (s) \rightarrow Ca(OH)_2\ (aq) \rightarrow CaOH^+\ (aq, surf.) + OH^-\ (aq, surf.)} \quad \text{...: 5.17}$$

$$\mathrm{CaOH^+\ (aq, surface) \rightarrow OH^-\ (aq, surf.) + Ca^{2+}(aq, surf.)} \quad \text{...: 5.18}$$

$$\mathrm{CaOH^+\ (aq, surface) \rightarrow CaOH^+\ (aq, bulk)} \quad \text{...: 5.19}$$

$$\mathrm{OH^-\ (aq, surf.) + Ca^{2+}(aq, surf.) \rightarrow OH^-\ (aq, bulk) + Ca^{2+}(aq, bulk)} \quad \text{...: 5.20}$$

As pointed out by Giles *et al.* (1993), the dissolution of powdered hydrated lime is consistent with the dissolution of powered quicklime reported by Ritchie & Xu, (1990) and it is mass-transfer controlled at the slower speed (below 250 rpm). Both studies used a rotating disk apparatus and shrinking core model claiming that Equation 5.20 is the slowest step. It must be noted that their model displayed limitations beyond 250 rpm and led to the claim that beyond 250 rpm the system is reaction controlled. This was however not proven by their calculated activation energy which ranged from 13.7 kJ/mol to 15 kJ/mol. The calculated activation energy for this study was more than twice lower, at about 6 kJ/mol. The lower activation value is because the calculated rate is not the true rate of dissolution but the rate at which the system approaches the equilibrium. For the $Ca(OH)_2$/DI water system to be surface reaction rate-controlled, Equation 5.17 and Equation 5.18 must be the slowest step and hence rate-limiting.

Furthermore, feeding $Ca(OH)_2$ as a suspension introduced the likelihood of parallel reactions between the bulk and surface of $Ca(OH)_2$ particles. This means that Equation 5.17 runs parallel to Equation 5.21, and Equation 5.18 runs parallel to Equation 5.22, which pose additional complexities.

$$Ca(OH)_2\ (aq) \rightarrow CaOH^+\ (aq) + OH^-\ (aq) \quad \text{...: 5.21}$$

$$CaOH^+\ (aq) \rightarrow\ Ca^{2+}(aq) + OH^-\ (aq) \quad \text{...: 5.22}$$

Complexities of using acetic acid:

Temperature-dependent $Ca(OH)_2$ dissolution rate experiments were done in acetic acid solutions (HAc). The overall dissolution equation in HAc is as follows:

$$Ca(OH)_2 + 2HAc\ \leftrightarrow\ Ca(Ac)_2\ +\ 2H_2O \quad \text{...: 5.23}$$

Equation 5.23 can be broken down to the steps represent by Equation 5.24 to Equation 5.29. These steps (Equation 5.24 to Equation 5.29) focus on the bulk solution reactions. However, similar to the case of $Ca(OH)_2$ suspension-DI water system, these steps occurs parallely in both the bulk solution and on the surface of the particle. For surface surface reaction-controlled dissolution, the hydrolysis reaction or step (Equation 5.24) may occurs on the diffussion layer, also a proton can react with a solid particle through proton attack or acid attack reaction (Equation 5.30).

$$Ca(OH)_2\ (aq) + H^+\ (aq)\ \leftrightarrow\ CaOH^+\ (aq) + H_2O\ (aq) \quad \text{...: 5.24}$$

$$CaOH^{+}\,(aq) \leftrightarrow Ca^{2+}(aq) + OH^{-}\,(aq) \quad \text{...: 5.25}$$

$$HAc\,(aq) \leftrightarrow Ac^{-}\,(aq) + H^{+}\,(aq) \quad \text{...: 5.26}$$

$$Ca^{2+}(aq) + Ac^{-}\,(aq) \leftrightarrow CaAc^{+}\,(aq) \quad \text{...: 5.27}$$

$$CaAc^{+}\,(aq) + Ac^{-}\,(aq) \leftrightarrow Ca(Ac)_2\,(aq) \quad \text{...: 5.28}$$

$$OH^{-}\,(aq) + H^{+}\,(aq) \leftrightarrow H_2O\,(aq) \quad \text{...: 5.29}$$

$$Ca(OH)_2\,(s) + H^{+}\,(aq, sur) \leftrightarrow CaOH^{+}\,(aq, sur) + H_2O\,(aq, , sur) \quad \text{...: 5.30}$$

The other critical reaction step is the dissociation of HAc (Equation 5.26); HAc is a weak acid hence it partially dissociates forming H^+ and Ac^- ions. This reaction step by proxy controls or influence Equation 5.27 to Equation 5.29. The diffusion of dissolved species from the bulk solution to the particles surface and vice versa adds another layer of complexity.

Limitations on Calcium Data:

Although the calcium concentrations were assayed for the present sets of experiments, there were huge variances in dissolved values measured, similarly to what was identified in Section 5.4.1 for the $Ca(OH)_2$/DI water system, and hence the measured calcium data was not further considered for the rate calculations. The estimation of dissolved calcium data using pH was relatively easy for the $Ca(OH)_2$/DI water system because ideally, in 1L, 1 molar $Ca(OH)_2$ dissolves to form 1 molar calcium ions and 2 moles of hydroxide ions (see Equation 5.16). Also, for this to hold, $CaOH^+$ concentration must be negligible. However, this was not true for for the $Ca(OH)_2$/HAc system because of the partial dissociation of acetic acid. Therefore, the

acetic acid ionization constant was used to estimate calcium concentration in the bulk solution from material balance around the CSTR as elaborated in the following.

Steady State material balance around the slurry CSTR (for liquid phase):

$$\begin{pmatrix}\text{rate of flow}\\ \text{of } j \text{ into}\\ \text{the system}\\ \{moles/time\}\end{pmatrix} = \begin{pmatrix}\text{rate of flow}\\ \text{of } j \text{ out}\\ \text{of}\\ \text{the system}\\ \{moles/time\}\end{pmatrix} - \begin{pmatrix}\text{rate of generation}\\ \text{of } j \text{ by chemical}\\ \text{reaction within}\\ \text{the system}\\ \{moles/time\}\end{pmatrix} \quad \text{...: 5.31}$$

In terms of calcium cations:

$$v_{\text{in}} \cdot [\text{Ca}^{2+}]_{\text{in}} = v_{\text{out}} \cdot [\text{Ca}^{2+}]_{\text{bulk}} - \text{V}(\text{r}_{\text{Ca}^{2+}}) \quad \text{...: 5.32}$$

In terms of protons:

$$v_{\text{in}} \cdot [\text{H}^{+}]_{\text{in}} = v_{\text{out}} \cdot [\text{H}^{+}]_{\text{bulk}} - \text{V}(\text{r}_{\text{H}^{+}}) + v_{\text{out}} \cdot [\text{H}^{+}]_{\text{undessociated}} \quad \text{...: 5.33}$$

Determining the unreacted or undissociated protons, locked up in undissociated acetic acid:

$$\text{K}_{\text{a}}(\text{T}) = \frac{[\text{H}^{+}][\text{Ac}^{-}]}{[\text{HAc}]} = \frac{[\text{H}^{+}][\text{Ac}^{-}]}{[\text{HAc}]_{\text{undessociated}}} \quad \text{...: 5.34}$$

$$[\text{HAc}]_{\text{undessociated}} = [\text{HAc}]_{\text{in}} - [\text{Ac}^{-}] \quad \text{...: 5.35}$$

$$[\text{Ac}^{-}] = \text{K}_{\text{a}} \frac{[\text{HAc}]_{\text{undessociated}}}{[\text{H}^{+}]} \quad \text{...: 5.36}$$

$$[\mathrm{HAc}]_{\mathrm{undessociated}} = [\mathrm{HAc}]_{\mathrm{in}} - \mathrm{K_a}\frac{[\mathrm{HAc}]_{\mathrm{undessociated}}}{[\mathrm{H^+}]} \quad \text{...: 5.37}$$

$$[\mathrm{HAc}]_{\mathrm{undessociated}} = \frac{[\mathrm{HAc}]_{\mathrm{in}}}{1 + \frac{\mathrm{K_a}}{[\mathrm{H^+}]_{\mathrm{bulk}}}} = [\mathrm{H^+}]_{\mathrm{undessociated}} \quad \text{...: 5.38}$$

Therefore, Equation 5.33 becomes Equation 5.40.

$$v_{\mathrm{in}} \cdot [\mathrm{H^+}]_{\mathrm{in}} = v_{\mathrm{out}} \cdot [\mathrm{H^+}]_{\mathrm{bulk}} - \mathrm{V}(\mathrm{r_{H^+}}) + v_{\mathrm{out}}\left(\frac{[\mathrm{AcH}]_{\mathrm{in}}}{1 + \frac{\mathrm{K_a}}{[\mathrm{H^+}]_{\mathrm{bulk}}}}\right) \quad \text{...: 5.39}$$

The rate of calcium generated in terms of proton:

$$\mathrm{r_{H^+,generation}} = -2\mathrm{r_{Ca^{2+}generation}} \quad \text{...: 5.40}$$

Therefore,

$$v_{\mathrm{in}} \cdot [\mathrm{H^+}]_{\mathrm{in}} = v_{\mathrm{out}} \cdot [\mathrm{H^+}]_{\mathrm{bulk}} + 2\mathrm{V}(\mathrm{r_{Ca^{2+}}}) + v_{\mathrm{out}}\left(\frac{[\mathrm{AcH}]_{\mathrm{in}}}{1 + \frac{\mathrm{K_a}}{[\mathrm{H^+}]_{\mathrm{bulk}}}}\right) \quad \text{...: 5.41}$$

Substituting Equation 5.32 in Equation 5.41 and then making calcium concentration in the bulk the subject of the equation, then dividing by the volumetric flow throughout (at steady state, the volumetric flow is constant throughout a reactor; $v_{\mathrm{in}} = v_{\mathrm{out}} = v$), yields

$$[Ca^{2+}]_{bulk} = \frac{1}{2}\left([AcH]_{in} + 2[Ca^{2+}]_{in} - [H^+]_{bulk} - \frac{[AcH]_{in}}{1 + \frac{K_a}{[H^+]_{bulk}}}\right) \quad \text{...: 5.42}$$

To calculate the rate, Equation 5.32 was used, however since the CSTR had two feed stream (steam 1 and steam 2) and one exit stream (stream 3) (See Figure 4.3). The volumetric flow in terms of stream numbers become; $v_{in} = v_1 + v_2 = v_3 = v_{out}$, therefore:

$$v_2 \cdot [Ca^{2+}]_2 = v_3 \cdot [Ca^{2+}]_{bulk} - V(r_{Ca^{2+}}) \quad \text{...: 5.43}$$

$$\frac{v_2}{v_3} \cdot [Ca^{2+}]_2 = [Ca^{2+}]_{bulk} - \frac{V}{v_3} \cdot (r_{Ca^{2+}}) \quad \text{...: 5.44}$$

For, $\tau = \frac{V}{v_3} = \frac{V}{v_{out}}$; $v_{in} = v_1 + v_2 = v_{out}$ also $[Ca^{2+}]_2 = [Ca^{2+}]_{in}$

$$\frac{v_2}{v_3} \cdot [Ca^{2+}]_2 = [Ca^{2+}]_{bulk} - \tau \cdot (r_{Ca^{2+}}) \quad \text{...: 5.45}$$

$$\tau \cdot (r_{Ca^{2+}}) = [Ca^{2+}]_{bulk} - \left(\frac{v_2}{v_3}\right) \cdot [Ca^{2+}]_2 \quad \text{...: 5.46}$$

$$r_{Ca^{2+},gen} = \left(\frac{1}{\tau}\right) \cdot \left([Ca^{2+}]_{bulk} - \frac{v_2}{v_3} \cdot [Ca^{2+}]_{in}\right) \quad \text{...: 5.47}$$

The change in pH as a function of temperature (for the rate determination experiments) was statistically insignificant, this can be seen by the overlapping error bars in Figure 5.32. Therefore, data from the ambient dissolution experiment was used as a comparison.

Table 5-10: Dissolution experiment data for Ca(OH)2/HAc system at ambient temperature of 22°C; used to calculate bulk calcium concentration and hence rate of dissolution.

T | °C	$[HAc]_{in}$ | (mol/L)	Exp. pH	$[Ca^{2+}]_{in}$ | (mol/L)	$[H^{+}]_{out}$ | (mol/L)	$[Ca^{2+}]_{out}$ | (mol/L)	$[HAc]_{out}$ | (mol/L)	r_a, gen | (mol/L. s)	X | (%)
22	0,010	12,12	0,0172	7,59E-13	0,0222	3,25E-20	1,72E-04	96.6
22	0,020	11,83	0,0172	1,48E-12	0,0272	1,24E-19	2,39E-04	97.3
22	0,025	10,84	0,0172	1,45E-11	0,0297	1,18E-17	2,60E-04	97.5
22	0,050	5,14	0,0172	7,24E-06	0,0350	2,96E-06	3,06E-04	97.9
22	0,125	4,38	0,0172	4,17E-05	0,0359	9,81E-05	3,20E-04	97.9
22	0,250	3,91	0,0172	1,23E-04	0,0329	8,55E-04	2,97E-04	97.7
22	0,500	3,51	0,0172	3,09E-04	0,0306	5,39E-03	2,88E-04	97.6

Table 5-11: Dissolution experiments data for Ca(OH)2/HAc system; for 0.02 M HAc, 0.04 M HAc and 0.125 M HAc solutions.

T | °C	$[HAc]_{in}$ | (mol/L)	Exp. pH	$[Ca^{2+}]_{in}$ | (mol/L)	$[H^{+}]_{out}$ | (mol/L)	$[HAc]_{out}$ | (mol/L)	$[Ca^{2+}]_{out}$ | (mol/L)	r_a, gen | (mol/L. s)	X | (%)
25	0,020	4,35	0,0168	4,47E-05	1,15E-04	0,0196	2,40E-04	96.4
25	0,040	4,07	0,0168	8,45E-05	4,08E-04	0,0202	2,64E-04	96.2
25	0,125	2,46	0,0168	3,44E-03	6,64E-01	0,0154	2,02E-04	96.0
34	0,020	4,46	0,0156	3,51E-05	7,68E-05	0,0187	2,29E-04	96.3
36	0,040	3,82	0,0153	1,50E-04	1,35E-03	0,0173	2,25E-04	96.4
35	0,125	2,50	0,0155	3,19E-03	5,93E-01	0,0142	1,86E-04	96.4
44	0,020	4,39	0,0143	4,11E-05	1,05E-04	0,0171	2,09E-04	95.2
44	0,040	3,59	0,0143	2,57E-04	4,08E-03	0,0153	2,02E-04	95.2
44	0,125	2,62	0,0143	2,38E-03	3,44E-01	0,0135	1,75E-04	95.0

In both Table 5-10 and Table 5-11, the reactor content (bulk solution) conditions are assumed to be the same as the exit stream condition (for example $[Ca^{2+}]_{bulk} = [Ca^{2+}]_{out}$), furthermore, $[Ca^{2+}]_{sat} = [Ca^{2+}]_{in}$ since $Ca(OH)_2$ was fed as a suspension.

Further it is noted from Table 5-10 and Table 5-11 that the conversions in the acidic environment are relatively high (≥ 95%). These results are consistent with PSD results that showed that under acid environment most of the particles are dissolved (See Section 5.1.4).

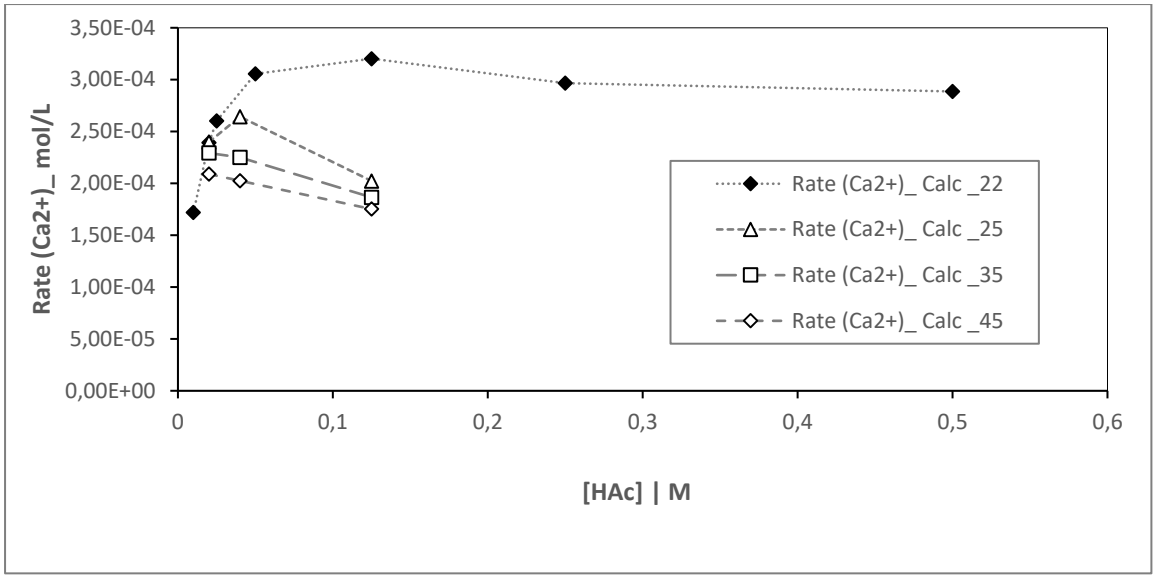

Figure 5.35: Shows the rate of Ca(OH)2 dissolution as a function of inlet acetic acid concentration at 22°C, 25°C, 35°C and 45°C. 22°C was the ambient temperature, 25°C, 35°C and 45°C were controlled using the thermostat and jacketed CSTR of the same size as the one used for ambient temperature condition. The mean residence time was kept constant under 2 minutes.

Figure 5.35 shows the rate of $Ca(OH)_2$ dissolution as a function of inlet acetic acid concentration at 22°C, 25°C, 35°C and 45°C as calculated in Tables 5-10 and 5-11. At 22°C, the dissolution rate increases with the increase in the inlet acetic acid concentration until 0.125 M, beyond which it decreases approaching a steady state value. This is because, beyond 0.125 M, the $Ca(OH)_2$/HAc system reaches a point where acetic acid is in excess, the dissociation of acetic acid seems to have reached equilibrium leading to unchanging dissolution rate value. The increase in dissolution rate below the acetic acid concentration of 0.125 M, is due to the presence of solids, as the solids dissolves rapidly, calcium and hydroxide ions are release quickly to the bulk solution. Similarly, as in 22°C, at 25°C, the dissolution rate increases with the increase in the inlet acetic acid concentration to 0.04 M, then decreases to 0.125 M. This trend shows an earlier and a lower maximum because at higher temperature the dissociation of acetic acid is increased (See the acetic acid ionization constants in Table 5.11), therefore, the interaction between the reactants is enhanced. The dissolution rate trends at 35°C and 45°C has no maximum, at either temperature the dissolution rate decreases with the increase inlet acetic acid concentration. At 45°C, the dissolution rate decreased linearly with the increase in the inlet acetic acid concentration. The same argument of the dissociation of

acetic acid applies; at this point, the rate of dissociation of acetic acid is proportional to the rate of dissolution.

Rate expression development:

From the rate of $Ca(OH)_2$ dissolution expression derived in Section 4.3.2, Equation 5.48 represent the rate of $Ca(OH)_2$ dissolution in the bulk solution of acetic acid.

$$r_{Ca^{2+}} = k_r(T_0)\exp\left\{{}^{E}/_{R}\left(\frac{1}{T_1} - \frac{1}{T_0}\right)\right\}[Ca^{2+}]^{\alpha}[H^{+}]^{\beta} \quad \text{...: 5.48}$$

where T_0 is the reference temperature (25°C), Using the experimental data in Table 5.11 and goal-seek function in Microsoft Excel (see Figure C11 and Figure C12 in Appendix D), $k_r(T_0)$ was determined as 0.0122 s^{-1} and the activation energy (E) is 5.7 kJ mol^{-1}. The order of reaction with respect to calcium ion concentration was found to be 0.93 (which is effectively first-order) and the order of reaction with respect to proton concentration was 0.023 (which is effectively zero-order). This means that the rate of $Ca(OH)_2$ dissolution in acetic acid is independent of pH from 25°C to 44°C and a strong function of calcium concentration. This result is counterintuitive as calcium in solution should inhibit further dissolution of calcium or not have any effect, but not promote the reaction. Since the calcium concentration was indirectly calculated from the solution pH which differed only marginally in all experiments (See Table 5-11), it is likely that the observed reaction order is a result of experimental variability rather than a firm trend.

Conclusions

On PSD analysis

Considering that $Ca(OH)_2$ powder is difficult to handle because of its hygroscopic nature, it was found that using a highly reactive and stable milk-of-lime is a better solution. However, using lime suspension or milk-of-lime has its own limitations in that it is difficult to trace the dissolution of $Ca(OH)_2$ through particle size reduction using conventional methods, such as laser diffraction. It was found that for $Ca(OH)_2$ dissolution, the only way to measure PSD is if SEM images are taken and then PSD and hence specific surface area determined from image analysis, which is a very tedious approach. It was confirmed that the shape of the $Ca(OH)_2$ particles is micro-crystalline hexagonal plate.

On dissolved calcium determination methods

Calcium analysis methods (such as flame spectroscopy, o- cresolphthalein complexone UV/Vis spectrophotometer method and EBT-EDTA – Reverse Titration) are necessary for the determination of dissolution trends. The most reliable results were obtained from ICP-OES. From the results it is seen that both o- cresolphthalein complexone UV/VIS spectrophotometer method and EBT-EDTA – Reverse Titration method can only measure calcium concentrations in calcium solution systems without impurities. It was found that o-cresolphthalein complexone UV/Vis spectrophotometer method can only be applied at low calcium concentrations (1-2 ppm), on the other hand, EBT-EDTA – Reverse Titration method was successful for calcium concentration up to 100 ppm. Therefore, between the two methods, EBT-EDTA – Reverse Titration method was found to be the more favourable one for calcium systems free of magnesium ions (Mg^{2+}), ferric cations (Fe^{3+}) or sulphate ions (SO_4^{2-}). However, neither method is suitable for study of AMD systems where all 3 of these species prevail.

Reaction Rate and rate expression

In conclusion, the dissolution of hydrated lime in deionized water is first order, with dissolution rate constant of 1×10^{-2} s^{-1} and the activation energy of 6436 J mol^{-1}. This indicates that the rate of mass transfer between boundary layer and bulk solution determines the rate of $Ca(OH)_2$

dissolution. Furthermore, for the $Ca(OH)_2$-deionized water system, it was found the rate of dissolution increase with the increase in pH, especially between the pH of 11 and 12. There was no link or pH data point obtained between pH of 11 and the lower pH values. The effect of temperature on the dissolution was statistically insignificant from 25°C to 45°C, which confirms that the dissolution rate is independent of temperature at this range and hence primarily diffusion controlled.

The dissolution rate of hydrated lime was found to increase with the strength of the acid. As partly hypothesised, below the pH of 7 (from pH 5 – 2), the rate of $Ca(OH)_2$ dissolution increases with a decrease in pH, however, the assumption that the dissolution of $Ca(OH)_2$ is chemical-reaction controlled was not proven. The rate expression for the $Ca(OH)_2$-deionized water system also applies to the $Ca(OH)_2$-CH_3COOH systems investigated because these were relatively dilute (0.02M – 0.125M CH_3COOH). The dissolution rate as a function of the specific surface area could not be studied directly, however using the extent of dissolution or conversion, which are essentially proxies for surface area, it was found to be one of the most significant variable for a $Ca(OH)_2$-deionized water system. However, this was insignificant in acidic condition since most of the particles were completely dissolved within the residence times investigated, the conversions for dissolution in acetic acid experiments were all greater or equal to 95%.

A rate expression was developed for the acetic acid data, with similar rate and activation energy as those determined for dissolution in de-ionised water and suggesting a first-order dependency on calcium concentration and zero-order dependency on acid, which appears counterintuitive.

Recommendations

On PSD analysis

The minimum number of particles on which the Image analysis works effectively is 500 or more. It is therefore recommended that a thorough image analysis be conducted with at least 500 particles. Furthermore, it is better to granulate powder (in a CO_2 proofed environment) to a relatively narrow range of more uniformly bigger particle sizes. An alternative approach to varying particle size ranges or wide PSD is to control sizes of $Ca(OH)_2$ formed by controlling the particle size of the limestone during calcination. This is one of the reason most of industrial lime producers and some users choose to produce quicklime and $Ca(OH)_2$ on their operation site. The above suggestions only solve the $Ca(OH)_2$ feed characterization (initial PSD); in order to improve the final PSD accuracy, a reactor content or sample may need to be quenched with relatively denser alcohol other than ethanol or propanol. This may require further testing since recent studies have shown that alcohols do not quench $Ca(OH)_2$ dissolution but react with them instead to form alcohol alkoxides.

On dissolved calcium determination methods

Apart from atomic absorption spectroscopy (AAS) or ICP-OES, o-cresolphthalein complexone UV/VIS spectrophotometer method and EBT-EDTA – Reverse Titration can be improved in order to work better in system with impurities. In a context of lime or $Ca(OH)_2$ or dolomitic limes; magnesium is a common metal therefore it is important to know how to effectively handle it. The EBT-EDTA – Reverse Titration method measures both magnesium and calcium; however, it is possible to cancel magnesium effect on OCPC method as well as in EBT-EDTA – Reverse Titration.

Cancellation of the magnesium effect in the OCPC method (Pollard and Martin (1956) method), can be achieved by using Gitelman's method as cited by Hirsch (1967). The Gitelman method is a modification of Pollard and Martin (1956), which is the method used in this study. Gitelman eliminated the interferences of magnesium by including 8-hydroxquinoline and diethyl amine as a buffer (pH of 12). According to Pointe Scientific, Inc. (1998), Baginski et al (1973) modified the method further by including dimethyl sulfoxide (DMSO) to lower the

dielectric constant of the working reagents and repress ionization of OCPC. On the other hand, the titration results can be improved by combining the method used in this study with the method referenced by HKEdCity (2017). In HKEdCity (2017) method, additional separate titrations are done at higher pH, by adding NaOH solution to precipitate $Mg(OH)_2$ using hydroxynaphthol blue as an indicator.

Dissolution rate expressions

It is recommended that the proposed expression be tested with a more controlled and larger data set; also the dissolution rate of $Ca(OH)_2$ be tested as the function of calcium concentration at steady state and specific surface area directly other than proxies. This model can then be expanded to other variables such as total volume of the pores, size distribution of the pores, particle size, and the degree of agglomeration as suggested by Oates (1998). Oates (1998) reported that by then there were still ongoing developments as attempts of answering questions such as how effective does the $Ca(OH)_2$ surface area correlates with the specific surface area as measured by the BET (Brunauer–Emmett–Teller) technique, total volume of the pores, size distribution of the pores, particle size, and the degree of agglomeration.

An alternative approach on kinetics that will satisfy Oates (1998) suggestion is a laser interferometry technique. As cited by Meenan et al. (2001), a thorough study on dissolution kinetics or dissolution rate can be pursued by using laser interferometry technique. This technique is reported to allow for the topographic map of a crystal face, a study of various crystallization parameters (such as degrees of supersaturation) on liquid inclusion formation, defect formation mechanisms and dislocation site (Meenan, et al., 2001). This technique has been used by Colombani and Bert (2007) to determine kinetic parameters such as rate constant and diffusivity coefficients for gypsum dissolution in water, hence this can be attempted for $Ca(OH)_2$ dissolution.

References

Aube, B., 2005. *The Science of Treating Acid Mine Drainage and Smelter Effluents,* Quebec: EnvirAube. pp. 67-71

Bernard, L., Freche, M., Lacout, J. L. & Biscans, B., 2000. Modeling of the dissolution of calcium hydroxyde in the preparation of hydroxyapatite by neutralization. *Chemical Engineering Science,* Volume 55, pp. 5683-5692.

Bishop, E., 1972. *Indicators: International Series of Monographs in Analytical Chemistry.* 1st ed. Oxford: Pergamon Press. pp. 40-46

Boynton, R. S., 1980. *Chemistry and Technology of Lime and Limestone.* 2nd ed. Totonto: John Wiley and Sons, Inc. pp. 27-32

Burival, Z., 2016. *Calcite - The Master of Shapes,* s.l.: Minerals expert.org.

Carr, R. W., 2007. *Modeling of Chemical Reactions.* 1st ed. Oxford: Elsevier. pp. 17-23

Christian, G. D., 2004. *Analytical Chemistry.* 6th ed. Hoboken: John Wiley and Sons, Inc.. pp. 40-44

Coker, A. K., 2001. *Modeling of Chemical Kinetics and Reactor Design.* 1st ed. Houston: Gulf Publishing Company. pp. 60-65

Colombani, J. & Bert, J., 2007. Halographic Interferometry Study of the Dissolution and Diffusion of Gypsum in Water. *Geochimica et Cosmochimica Acta,* 71(8), pp. 1913-1920.

Connors, K. A., 1990. *Chemical Kinetics: The Study of Reaction Rates in Solution.* 1st ed. New York: VCH Publishers, Inc.pp. 120-128

Cornell, R. M. & Schwertmann, U., 2003. *The Iron Oxides.* 2nd ed. Weinheim: WILEY-VCH Verlag GmnH & Co. KGaA. pp. 87-90

Dokoumetzidis, A. & Macheras, P., 2006. A century of dissolution research: From Noyes and Whitney to the Biopharmaceutics Classification System. *International Journal of Pharmaceutics,* 321(1), pp. 1-11.

Dokoumetzidis, A., Papadopoulou, V., Valsami, G. & Macheras, P., 2008. Development of a reaction-limited model of dissolution: Application to official dissolution tests experiments. *International Journal of Pharmaceutics,* 355(1-2), pp. 114-125.

Dowling, A., O'Dwyer, J. & Adley, C. C., 2015. Lime in the Limelight. *Journal of Cleaner Production,* Volume 92, pp. 13-22.

Dutta, S. & Shirai, T., 1980. Experimental Investigation on a Fast and Exothermic Solid-liquid Reaction System. *Chemical Engineering Science,* 35(1-2), pp. 209-216.

Eshel, G., Levy, G. J., Mingelgrin, U. & Singer, M. J., 2004. Critical Evaluation of the Use of Laser Diffraction. *Soil Science Society of America,* Volume 68, pp. 736-743.

Fogler, H. S., 2006. *Elements of Chemical Reaction Engineering.* 4th ed. Upper Saddle River: Pearson Education, Inc.. pp. 130-136

Furrer, G. & Stumm, W., 1986. The Coordination Chemistry of Weathering: I. Dissolution Kinetics of -Al2O3 and BeO. *Geochimica et Cosmochimica Acta,* 50(9), pp. 1847-1860.

Galan, I., Glasser, F. P., Baza, D. & Andrade, C., 2015. Assessment of the Protective Effect of Carbonation on Portlandite Crystals. *Cement and Concrete Research,* Volume 74, pp. 68-77.

Geller, W., Klapper, H. & Salomons, W., 1998. *Acidic Mining Lakes.* 1st ed. Berlin: Springer-Verlag.

Giles, D. E., Ritchie, I. M. & Xu, B.-A., 1993. The kinetics of dissolution of slaked lime. *Hydrometallurgy,* 32(1), pp. 119-128.

Haider, C., 2004. *Electrodes in Potentiometry,* Herisau: Metrohm Ltd..

Harvey, D., 2000. *Morden Analytical Chemistry.* 1st ed. New York: The McGraw-Hill Companies, Inc.. pp. 17-23

Harvey, D., 2019. *Chemistry LibreText.* [Online] Available at: https://chem.libretexts.org/ [Accessed 10 Januarry 2020].

Ikornikova, N. Y., 1973. Growth Characteristics of Calcite Crystals in Aqueous Solutions of Carbonic Acid. In: A. N. Lobachev, ed. *Crystallization Processes under Hydrothermal Conditions.* Consultants Bureau: New York, pp. 93-112.

Irabien, A., Toquero, A. & Ortiz, M. I., 1989. Kinetic Behaviour of Non-isothermal Lime Hydration. *The Chemical Engineering Journal,* 40(2), pp. 93-99.

Jakobsen, H. A., 2008. *Chemical Reactor Modelling: Multiphase Reactive Flows.* 1st ed. Berlin: Springer-Verlag. pp. 60-63

Johannsen, K. & Rademacher, S., 1999. Modelling the Kinetics of Calcium Hydroxide Dissolution in Water. *Acta Hydrochimica et Hydrobiologica,* 27(2), pp. 72-78.

Johnson, D. B. & Hallberg, K. B., 2005. Acid Mine Drainage Remediation Options: A Review. *Science of the Total Environment,* Volume 338, pp. 3-14.

Johnson, S., 2018. *Advantages & Disadvantages of XRD and XRF.* [Online] Available at: https://sciencing.com/advantages-disadvantages-xrd-xrf-6054766.html [Accessed 16 April 2018].

Kelly, R. N. & Etzler, F. M., 2005. *Donner Technologies: Innovative Particle Characterization; What is Wrong with Laser Diffraction?.* [Online] Available at: http://www.donner-tech.com [Accessed 16 April 2018].

Lawinska, K. & Modrzewski, R., 2017. Analysis of sieve holes blocking in a vibrating screen and a rotary and drum screen. *Physicochemical Problems of Mineral Processing,* 53(2), pp. 812-828.

Levenspiel, O., 1999. *Chemical Reaction Engineering.* 3rd ed. Danvers: John Wiley & Sons.

Lewis, C. J. & Boynton, R. S., 1999. *National Lime Association.* [Online] Available at: https://www.lime.org [Accessed May 2015].

Liu, M., 2016. Mean Age Theory for Quantitative Mixing Analysis. In: S. M. Kresta, A. W. Etchells III, D. S. Dickey & V. A. Atiemo-Obeng, eds. *Advances in Industrial Mixing: A Companion to the Handbook of Industrial Mixing.* Hoboken: John Wiley and Sons, Inc., pp. 21-41.

Lottermoser, B. G., 2010. *Mine Wastes.* 3rd ed. Heidelberg: Springer.

Marsden, J. O. & House, I. C., 2006. *The Chemistry of Gold Extraction.* 2nd ed. Littleton: Society for Mining, Metallurgy, and Exploration, Inc. (SME).

Meenan, P. A., Anderson, S. R. & Klug, D. L., 2001. The Influence of Impurities and Solvents on Crystallization. In: A. S. Myerson, ed. *Handbook of Industrial Crystallization.* 2nd ed. Woburn: Butterworth-Heinemann, pp. 67-100.

Metrohm, 2010. *Metrosensor electrodes,* Herisau: Mehrohm Ltd..

Middle Tennessee State University Chemistry Department, 2015. *Determination of Calcium by Standardized EDTA Solution ,* Murfreesboro: Middle Tennessee State University Chemistry Department.

Minerals.net, 2014. *Minerals.net.* [Online]
Available at: https://www.minerals.net/mineral/pyrrhotite.aspx
[Accessed 6 February 2018].

Mjimba, V., Mujuru, M. & Mutanga, S. S., 2017. The Legacy of Acid Mine Drainage in South Africa. In: S. S. Mutanga & M. Mujuru, eds. *Management and Mitigation of Acid Mine Drainage in South Africa: Input for Mineral Beneficiation in Africa.* Pretoria: Africa Institute of South Africa, pp. 8-26.

Montgomery, D. C. & Runger, G. C., 2003. *Applied Statistics and Probability for Engineers.* 3rd ed. New York: John Wiley & Sons. Inc. pp. 37-50.

Mujuru, M., Mutanga, S. S. & Dyosi, Z., 2017. The Formation of Acid Mine Drainage. In: S. S. Mutanga & M. Mujuru, eds. *Management and Mitigation of Acid Mine Drainage in South Africa: Input for Mineral Beneficiation in Africa.* Pretoria: Africa Institute of South Africa, pp. 27-40.

Naidoo, S., 2017. Overview of AMD in South Africa. In: S. Naidoo, ed. *Acid Mine Drainage in South Africa.* 1st ed. Pretoria: Springer Nature, pp. 1-8.

Oates, J. A. H., 1998. *Lime and Limestone: Chemistry and Technology, Production and Uses.* 1st ed. Weinheim: Wiley-VCH. pp. 67-70.

Patterson, G. K., Paul, E. L., Kresta, S. M. & Etchells III, A. W., 2004. Mixing and Chemical Reactions. In: E. L. Paul, V. A. Atiemo-Obeng & S. M. Kresta, eds. *Handbook of Industrial Mixing: Science and Practice.* Hoboken: John Wiley and Sons, Inc., pp. 755-867.

Perry, D. L., 2011. *Handbook of Inorganic Compounds.* 2nd ed. Boca Raton: CRC Press, Taylor & Francis Group.

Pollard, F. H. & Martin, J. V., 1956. The Spectrophotometric Determination of the Alkaline-earth Metals with Murexide, Eriochrome Black T and with o-Cresolphthalein Complexone. *The Analyst,* 81(963), pp. 348-353.

Puall, B., Macka, M. & Haddad, P. R., 1997. Determination of calcium and magnesium in water samples by high-performance liquid chromatography on a graphitic stationary phase with a mobile phase containing o-cresolphthalein complexone. *Journal of Chromatography A,* 789(1-2), pp. 329-337.

Pub Chem, 2018. *Pub Chem website.* [Online]
Available at: https://pubchem.ncbi.nlm.nih.gov/compound/2735296#section=Top
[Accessed 14 August 2018].

Rancke-Madsen, E., 1972. The History of indicators. In: E. Bishop, ed. *Indicators: International Series of Monographs in Analytical Chemistry.* Oxford: Pergamon Press, pp. 1-2.

Ridgley, N. H., 2016. *Aragonite - The Pearly Carbonate,* Reno: MineralExpert.org.

Ritchie, I. M. & Xu, B.-A., 1990. The kinetics of lime slaking. *Hydrometallurgy,* 23(2-3), pp. 377-396.

Robinson, B. & Burnham, J., 2001. Relative Dissolution Rates of Several Hydrated Limes. *Journal of Environmental Engineering,* 127(6), pp. 565-568.

Shah, S. I. A., Kostiuk, L. W. & Kresta, S. M., 2012. The Effect of Mixing, Reaction Rates, and Stoichiometry on Yield for Mixing Sensitive Reactions-Part I: Model Development. *International Journal of Chemical Engineering,* Volume 2012, pp. 1-16.

Snorek, s. m. et al., 2007. PQRI Recommendations on Particle-Size Analysis of Drug Substances Used in Oral Dosage Forms. *Journal of Pharmaceutical Sciences,* 96(6), pp. 1451-1467.

Souza, D. O. C. & Menegalli, F. C., 2011. Image analysis: Statistical Study of Particle Size Distribution and Shape Characterization. *Powder Technology,* 214(1), pp. 57-63.

Stefanakis, A., Akratos, C. S. & Tsihrintzis, V. A., 2014. *Vertical Flow Constructed Wetlands.* 1st ed. Oxford: Elsevier.

Tadros, M. E., Skalny, J. & Kalyoncu, R. S., 1976. Kinetics of Calcium Hydroxide Crystal Growth from Solution. *Journal of Colloid and Interface Science,* 55(1), pp. 21-24.

The International Network for Acid Prevention, 2014. *The International Network for Acid Prevention Website.* [Online]
Available at: https://www.inap.com.au/acid-drainage/#whatard
[Accessed 06 December 2019].

United Nations, 2017. *Sustainable Development Knowledge Platform.* [Online]
Available at: https://sustainabledevelopment.un.org/sdg6
[Accessed 29 May 2017].

United Nations, 2017. *United Nations Sustainable Development Water and Sanitation.* [Online] Available at: http://www.un.org/sustainabledevelopment/water-and-sanitation/
[Accessed 29 May 2017].

University of Canterbury College of Science, 2008. *Determination of Calcium Ion Concentration ,* ChristChurch: University of Canterbury College of Science.

Vigneau, E., Loisel, C., Devaux, M. F. & Cantoni, P., 2000. Number of Particles for the Determination of Size Distribution from Microscopic Images. *Powder Technology,* 107(3), pp. 243-250.

Wang, J., Keener, T. C., Li, G. & Khang, S.-J., 1998. The Dissolution Rate of Ca(OH)2 in Aqueous Solutions. *Chemical Engineering Communications*, 169(1), pp. 167-184.

Weast, R. C., 1984. *Handbook of Chemistry and Physics.* 64th ed. Boca Raton: CRC Press Inc.. pp. 33-34.

Whittington, B. I., 1996. The chemistry of CaO and Ca(OH)2 relating to Bayer process. *Hydrometallurgy,* 43(1-3), pp. 13-35.

Zinck, J., 2006. *Disposal, Reprocessing and Reuse Option for Acidic Drainage Treatment Sludge.* Lexington, American Society of Mining and Reclamation.

Zinder, B., Furrer, G. & Stumm, W., 1986. The Coordination Chemistry of Weathering: II. Dissolution of Fe(III) oxides. *Geochimica et Cosmochimica Acta,* 50(9), pp. 1861-1869.

Appendix A Dissolution tests in CSTR

Appendix A.1.1 Continuous Stirred Tank Reactor (CSTR) Equations

Kinetic studies for reactions are usually performed in batch and semi- reactor systems. However, if it is desired to control rate of conversion of a reactant or concentration of a product, flow systems or CSTRs are a better option. The starting point for any flow reaction system (reactor design) is the material balance. This proceeds as follows (Levenspiel, 1999):

$$\begin{pmatrix} Rate\ of \\ reactant \\ flow\ into \\ element\ of \\ volume \end{pmatrix} = \begin{pmatrix} Rate\ of \\ reactant \\ flow\ out \\ of\ element \\ of\ volume \end{pmatrix} + \begin{pmatrix} Rate\ of\ reactant \\ loss\ due\ to \\ chemical\ reaction \\ within\ the\ element \\ of\ volume \end{pmatrix} + \begin{pmatrix} Rate\ of \\ accumulation \\ of\ reactant \\ in\ element \\ of\ volume \end{pmatrix} \quad \text{...: A.1}$$

A simplified version of the Equation 8.7 is as follows:

$$\text{Input} = \text{output} + \text{disappearance by reaction} + \text{accumulation} \quad \text{...: A.2}$$

$$F_{A,in} - F_{A,out} + \int_0^V r_A\, dV = \frac{dN_A}{dt} \quad \text{...: A.3}$$

At the steady state; accumulation $= \frac{dN_A}{dt} = 0$; therefore;

$$F_{A0} - F_A = (-r_A)V \quad \text{...: A.4}$$

Substituting $F_{A,in} = v_{in}C_{A,in}$ and $F_{A,out} = v_{out}C_{A,out}$

$$(-r_A) = \frac{v_{in}C_{A,in} - v_{out}C_{A,out}}{V} \quad \text{...: A.5}$$

For cases where, $v_{out} = v_{in}$ then substitute $\tau = \frac{V}{v_{in}} = \frac{V}{v_{out}} = \frac{V}{v}$ in Equation A.5

$$(-r_A) = \left(\frac{1}{\tau}\right)(C_{A,in} - C_{A,out}) \quad \text{...: A.6}$$

Appendix B Dissolved calcium analysis

Table B 1: The effect of Magnesium in EBT-EDTA 1

Ca^{2+} = 100 ppm; Mg^{2+} = 130 ppm	Sample 1	Sample 2	Sample 3
Vol. Ca^{2+} ; mL	25	25	25
Volume EDTA ; mL	15.1	14.65	16.45
Ca^{2+} ; mg, aliquot	5.76	5.42	6.08
Ca^{2+} ; ppm, unknown	230.59	216.74	243.37
Mean Ca^{2+} ; ppm, unknown	**230**		
StdDv	**11**		
StdEr	**6**		

In Table B 1, a similar behaviour as in Table 5-2 is applicable. Therefore, a similar argument as presented in Table 5-2 holds, the only difference is that in this case, the concentration of magnesium used is lower than that in Table 5-2.

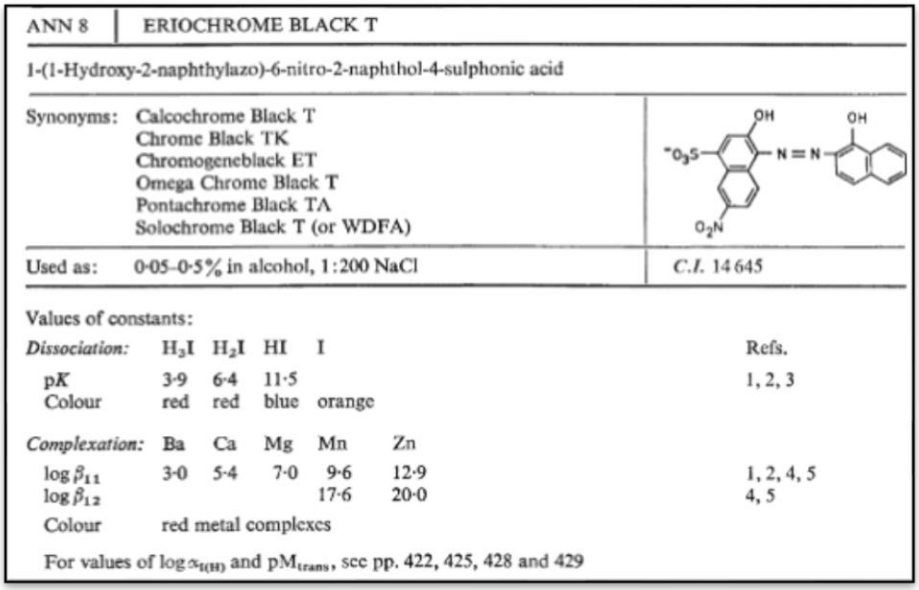

ANN 8 | ERIOCHROME BLACK T

1-(1-Hydroxy-2-naphthylazo)-6-nitro-2-naphthol-4-sulphonic acid

Synonyms: Calcochrome Black T
Chrome Black TK
Chromogeneblack ET
Omega Chrome Black T
Pontachrome Black TA
Solochrome Black T (or WDFA)

Used as: 0·05–0·5% in alcohol, 1:200 NaCl

C.I. 14 645

Values of constants:

Dissociation:	H_3I	H_2I	HI	I		Refs.
p*K*	3·9	6·4	11·5			1, 2, 3
Colour	red	red	blue	orange		
Complexation:	Ba	Ca	Mg	Mn	Zn	
$\log \beta_{11}$	3·0	5·4	7·0	9·6	12·9	1, 2, 4, 5
$\log \beta_{12}$				17·6	20·0	4, 5
Colour	red metal complexes					

For values of $\log \alpha_{I(H)}$ and pM_{trans}, see pp. 422, 425, 428 and 429

Figure C 1: Eriochrome Black T complexation (Bishop, 1972)

Table B 2: The effect of Magnesium in EBT-EDTA 3

Ca^{2+} = 100 ppm; Mg^{2+} = 0.85 ppm	Sample 1	Sample 2	Sample 3
Vol. Ca^{2+} ; mL	25.3	25.3	25.23
Volume EDTA ; mL	8.52	8.12	8.11
Ca^{2+} ; mg, aliqout	3.25	3.00	3.00
Ca^{2+} ; mg, unknown	130	120	120
Mean Ca^{2+} ; mg, unknown	**123**		
StdDv	**5**		
StdEr	**3**		

Table B.2 has a similar effect as observed in Tables B.1 and Table 5-2. However, 123 ± 3 ppm is relatively higher than the expected value of ca. 101 ppm. This same argument is true for Table 5-2 where you expect 120 ppm and get 150 ppm. These results suggest that even though EBT complexes with both Mg and Ca, the complexation is different for each case.

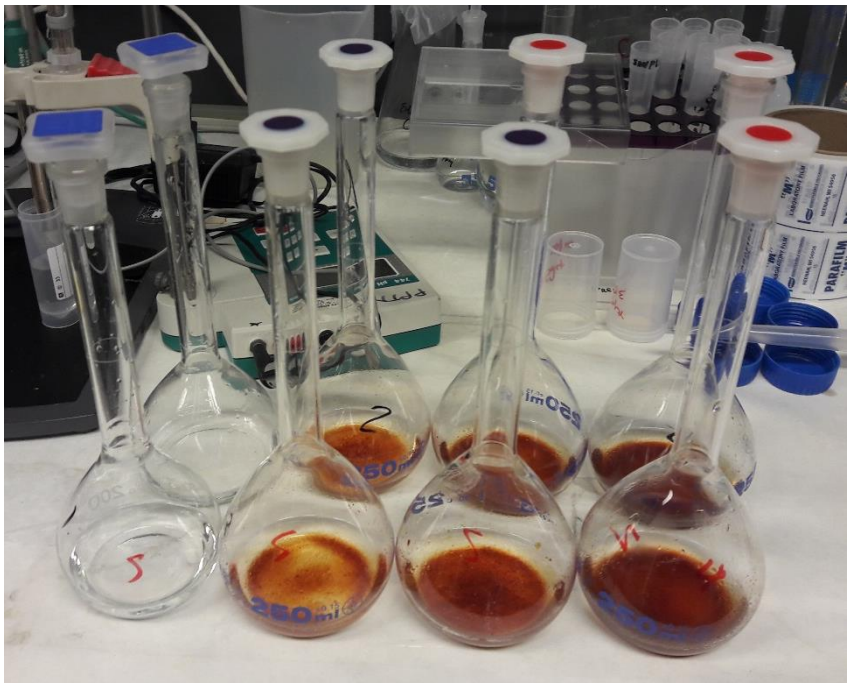

Figure C 2: The effect of ferric ions in OCPC method

Equipment or apparatus ***o-cresolphthalein complexone colorimetric method****:*

1. Volumetric flask (100, 250 and 1 000 mL).
2. JENWAY Model 6405 Spectrophotometer.
3. Plastic cuvettes
4. Eppendorf pipettes (5 and 10 mL)
5. The pH meter
6. Merck Nova 60 Spectroquant
7. Measuring cylinders (50, 100 and 500 mL)

Table B 3: The effect of sulphates in EBT-EDTA 1

Ca^{2+} = 100 ppm; SO_4^{2-} = 0.85 ppm	Sample 1	Sample 2	Sample 3
Vol. Ca^{2+} ; mL	25.29	25.25	25.31
Volume EDTA ; mL	25.31	24.93	24.14
Ca^{2+} ; mg, aliquot	9.66	9.22	8.93
Ca^{2+} ; mg, unknown	386.50	368.83	357.14
Mean Ca^{2+} ; mg, unknown	371		
StdDv	12		
StdEr	7		

Table B 4: The effect of sulphates in EBT-EDTA 2

Ca^{2+} = 100 ppm; SO_4^{2-} = 0.85 ppm	Sample 1	Sample 2	Sample 3
Vol. Ca^{2+} ; mL	25	25	25
Volume EDTA ; mL	9.35	9.45	9.15
Ca^{2+} ; mg, aliquot	3.57	3.50	3.38
Ca^{2+} ; mg, unknown	142.78	139.81	135.37
Mean Ca^{2+} ; mg, unknown	**139**		
StdDv	**3**		
StdEr	**2**		

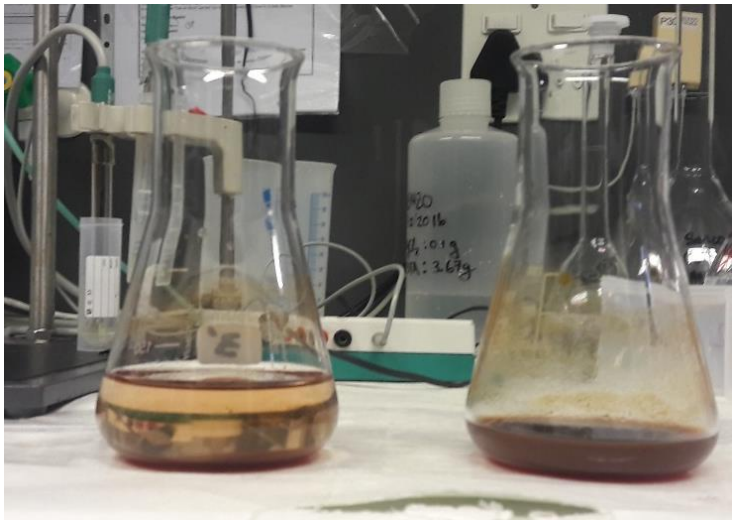

Figure C 3: The effect of ferric ions in EBT-EDTA method

Equipment or apparatus in EDTA-EBT titration method:

1. Volumetric flask (100, 250 and 1 000 mL).

2. Eppendorf pipettes (5 and 10 mL)

3. The pH meter

4. Measuring cylinders (50, 100 and 500 mL)

5. 50 mL burettes

Beer's Law and Multicomponent Samples

The relation between concentration (C) and absorbance (A_i) can be defined in terms of Beer's law as shown by Equation below:

$$A_i = \varepsilon b C \qquad \text{...: B.1}$$

Where, ε is the molar absorptivity with units $\text{cm}^{-1}\text{M}^{-1}$ and b is the thickness of the sample in centimetre (cm). The molar absorptivity is dependent on the wavelength of electromagnetic radiation. For a sample solution with two components X and Y, the total absorbance (A_{tot}) is as follows:

$$A_{tot} = A_X + A_Y = \varepsilon_X b C_X + \varepsilon_Y b C_Y \qquad \text{...: B.2}$$

Appendix C Dissolution tests in CSTR

Appendix C.1.1 Dissolved calcium and steady state pH on reaction rate.

This section serves as an extension of the results chapter, focusing on the outcomes of the dissolution tests.

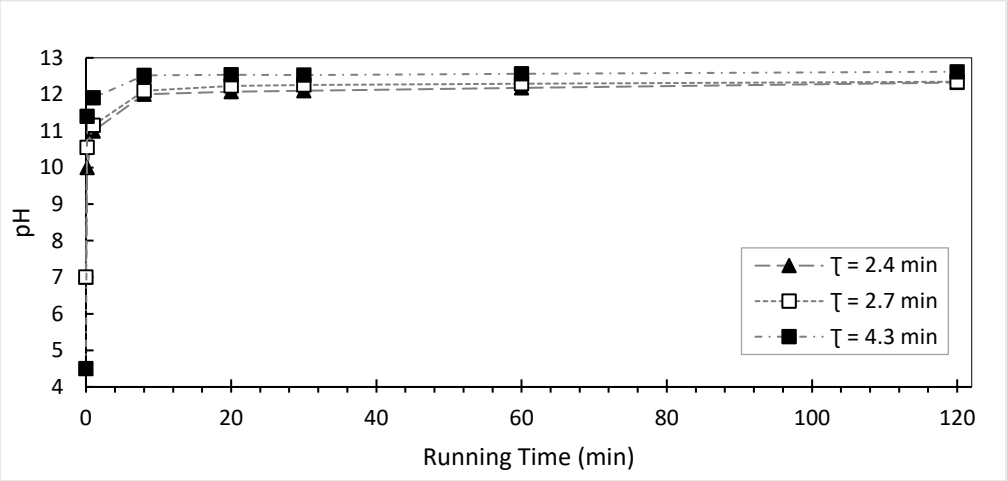

Figure C 4: Effect of residence time on the dissolution of industrial $Ca(OH)_2$ in de-ionized water in the overflow slurry CSTR system; measured at (22 °C and 1 atm).

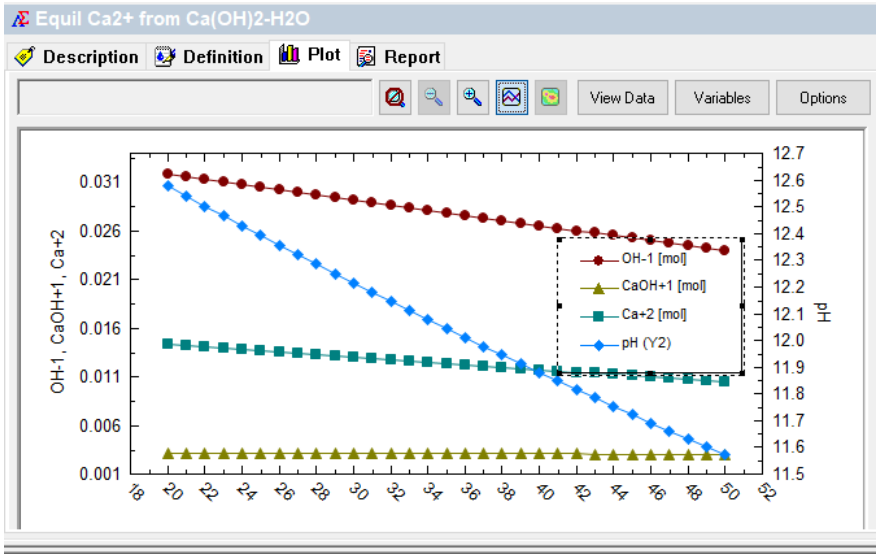

Figure C 5: OLI Ca(OH)2/DI-water equilibrium data

Appendix C.1.2 Residence time on the reaction rate.

This section details the relationship between the number of residence time and steady state pH for a shorter residence time and longer residence time.

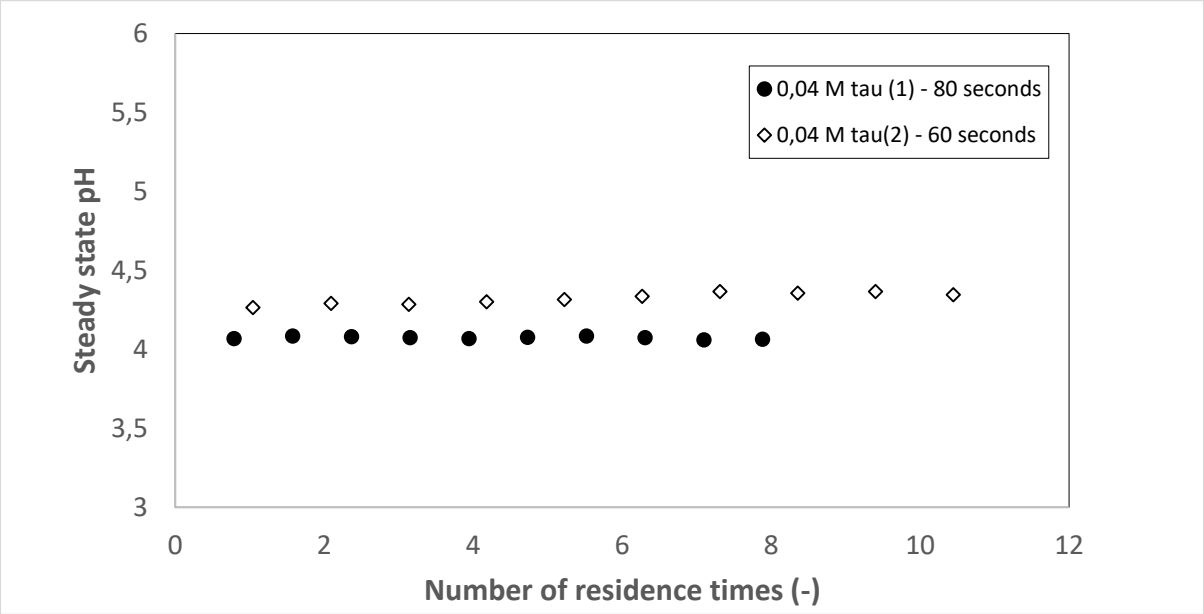

Figure C 6: Effect of residence time in $Ca(OH)_2$ dissolution in 0.04 M CH_3COOH solution at 25 °C.

In Figure C 7, both the longer (80 seconds) and a shorter residence time (60 seconds) system reaches the steady state after about two residence times. For the longer residence time (80 seconds), the steady state pH increases from a starting pH (which is the pH at one residence time) of 4.07 to 4.08.

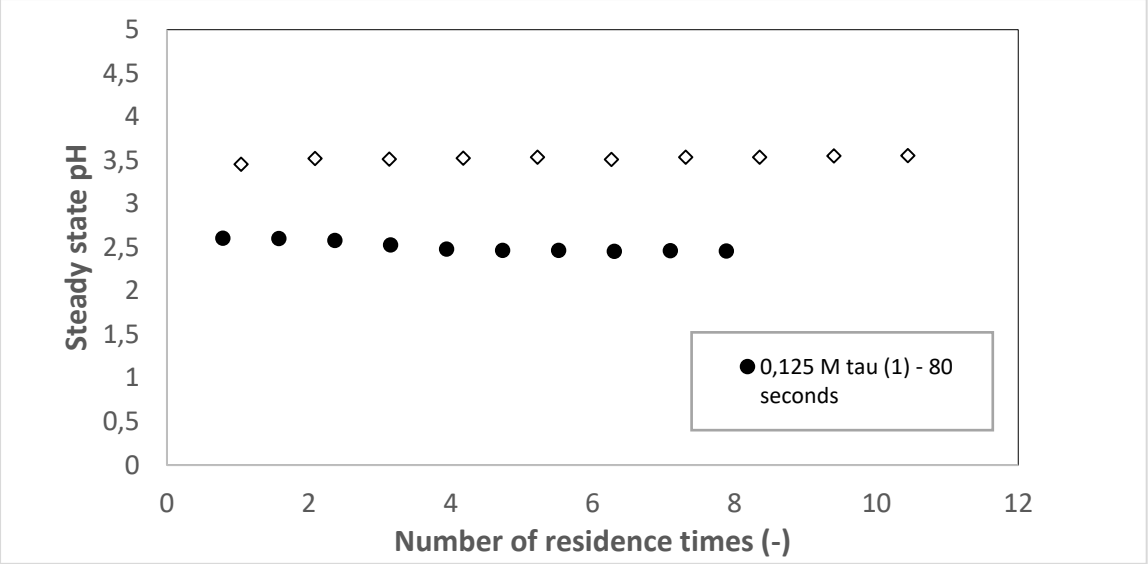

Figure C 8: Effect of residence time in $Ca(OH)_2$ dissolution in 0.125 M CH_3COOH solution at 25 °C.

Similarly as in Figure C 9 , in Figure C 10 both the longer and a shorter residence time system reaches the steady state after about one residence time. It is work noting that about the fifth residence time, the steady state pH seems to decrease slightly from 2.48 to 2.47. It can be argued that the difference of 0.01 is insignificant.

Appendix D Rate expression development

Appendix D.1.1 Determination of the orders of reaction and rate parameters.

T (K)	Rate (Ca2+)_Ca	*k_0_(T)*	[H],blk	[Ca], bulk	a	b	Rate (Ca2+)_*	Delta^2
298,15	0,0002397	0,002255	0,000045	0,019613	0,006617	0,553310	0,000247	4,69E-11
298,15	0,0002642	0,002801	0,000084	0,020230	0,136537	0,276990	0,000258	4,54E-11
298,15	0,0002023	0,003036	0,003441	0,015443	0,253004	0,305344	0,000218	2,40E-10
307,15	0,0002292	0,003412	0,000035	0,018736	0,006949	0,641888	0,000222	5,88E-11
309,15	0,0002251	0,003260	0,000150	0,017273	0,258632	0,074823	0,000210	2,39E-10
308,15	0,0001865	0,003630	0,003187	0,014235	0,169909	0,448629	0,000189	5,42E-12
317,15	0,0002090	0,004031	0,000041	0,017082	0,022056	0,634273	0,000192	2,93E-10
317,15	0,0002024	0,004281	0,000257	0,015352	0,153981	0,388631	0,000181	4,57E-10
317,15	0,0001752	0,004432	0,002380	0,013536	0,175332	0,468647	0,000169	3,36E-11
								1,4E-09

Figure C 11: Determination of the global values of a and b

E	k0	*a*	b
4965,761257	0,01216075	0,022801939	0,933468189

Figure C 12: Global values of ko, a and b

Appendix E Miscellaneous

Appendix E.1.1 Calibration curves for pumps

The calibration curves (Figure C13 to Figure C17) below were used to convert pump's rpm to volumetric flows in ml/s.

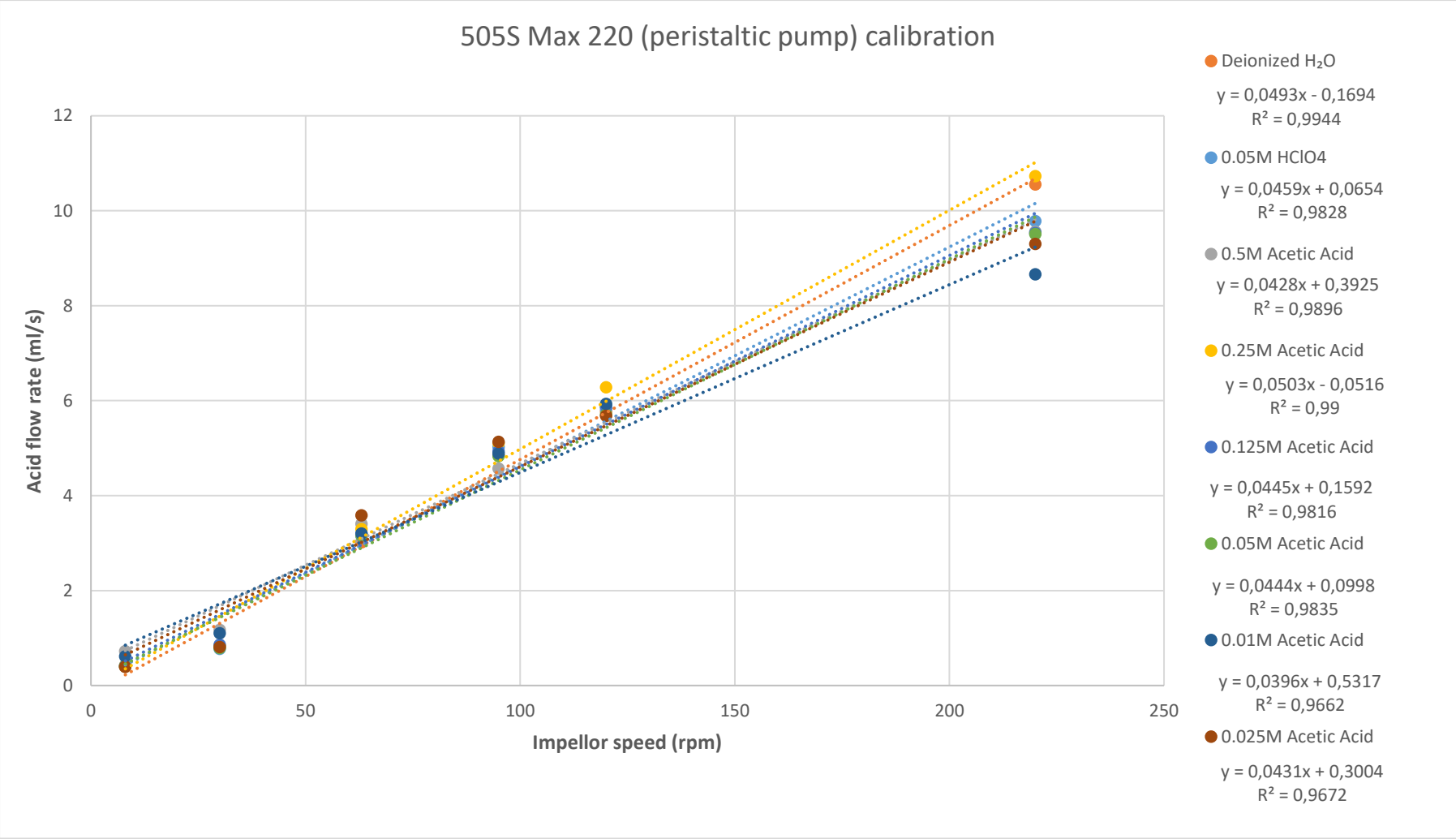

Figure C 13: Calibration curves for CH_3COOH pumps used for CSTR experiments

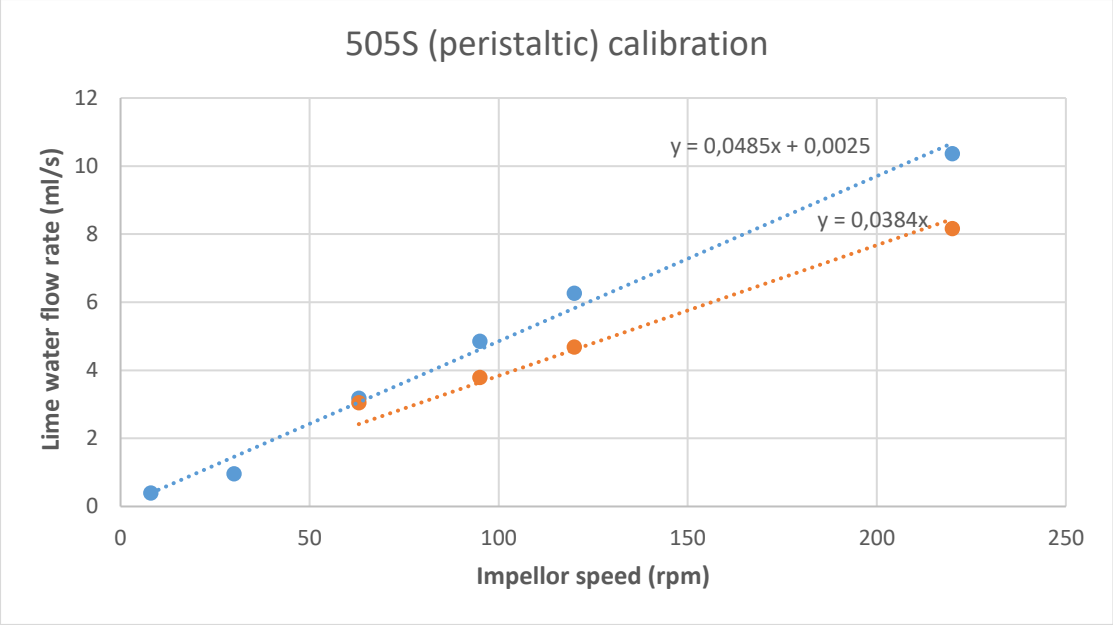

Figure C 14: Calibration curves for limewater used for CSTR experiments

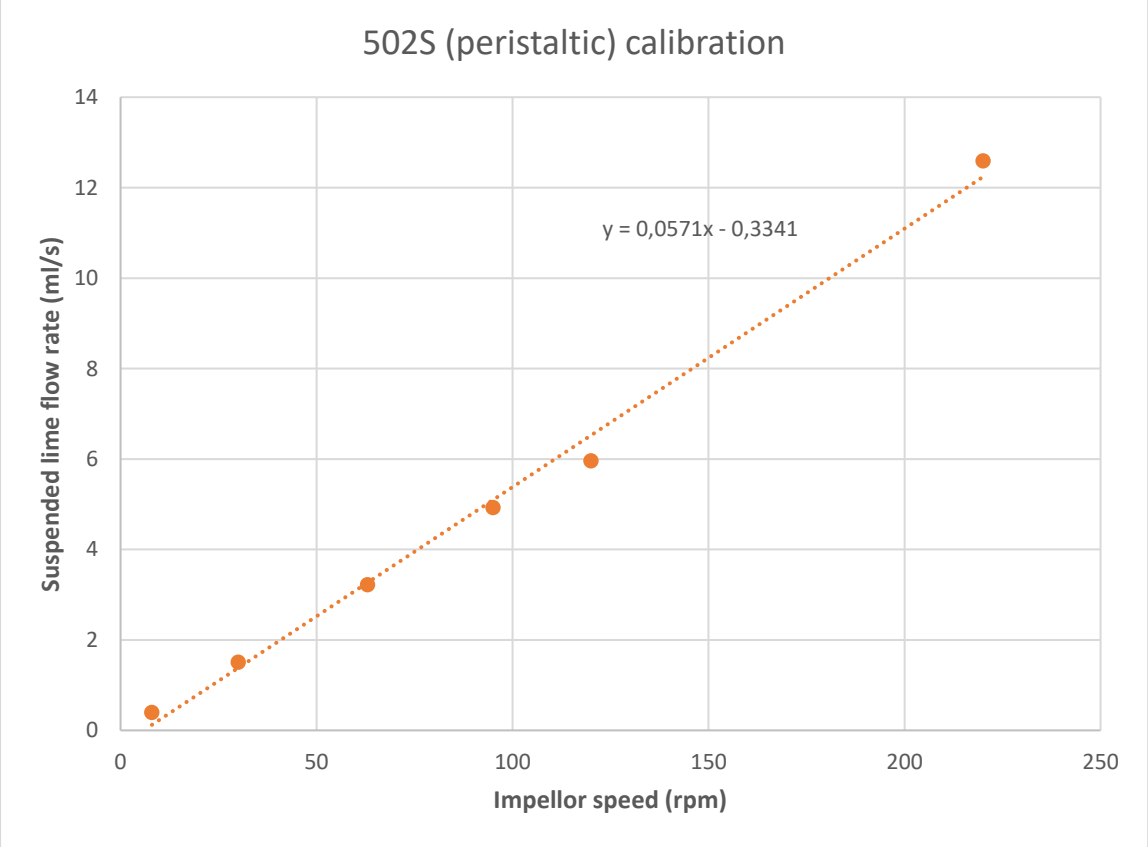

Figure C 15: Calibration curves milk of lime used for CSTR experiments (for 502S peristaltic pump)

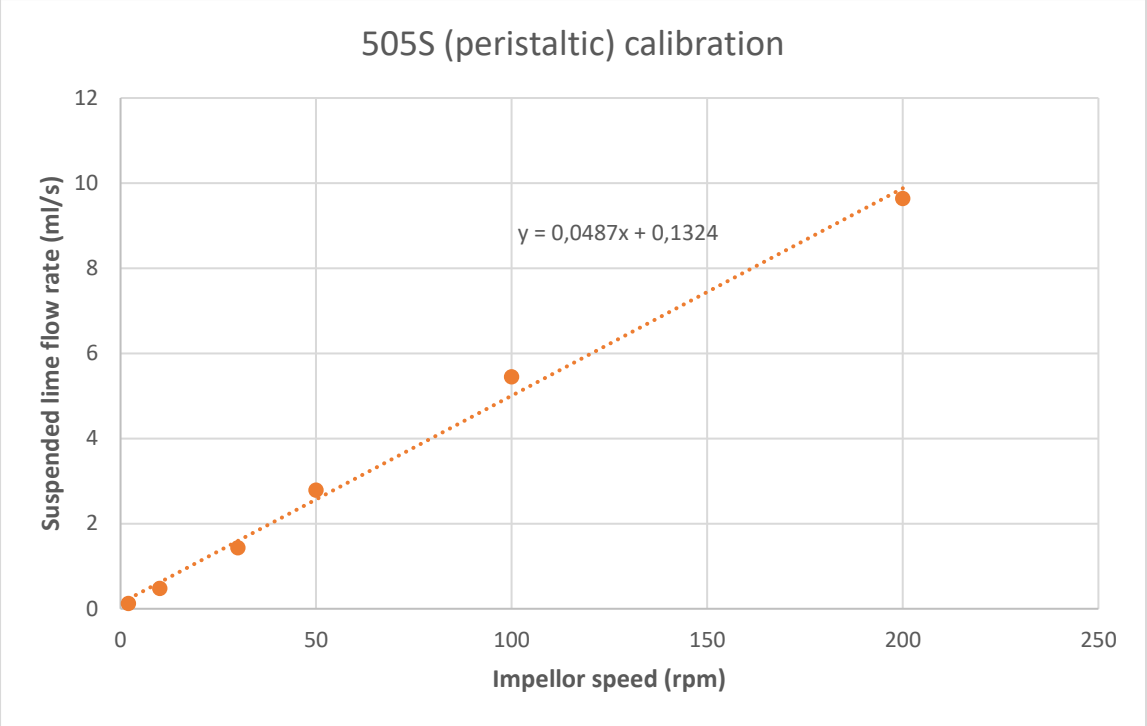

Figure C 16: Calibration curves for milk of lime used for CSTR experiments (for 505S peristaltic pump)

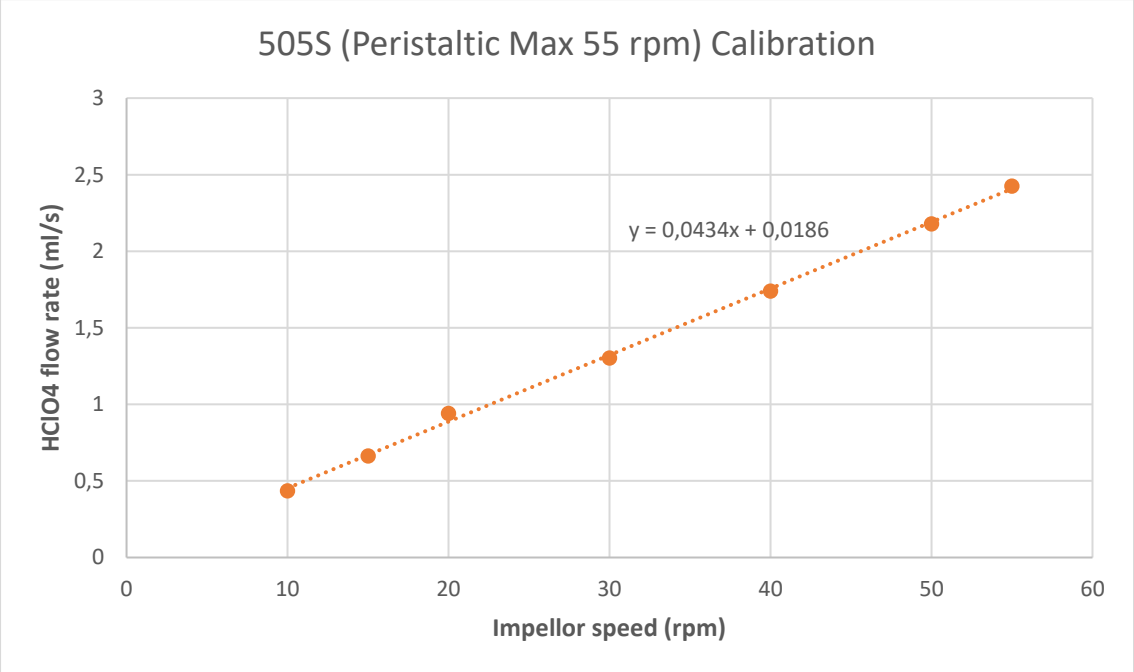

Figure C 17: Calibration curves for perchloric acid pumps used for CSTR experiments